LRP 376/89 May 1989

CONTROL OF THE VERTICAL INSTABILITY IN TOKAMAKS

E.A. Lazarus, J.B. Lister, G.H. Neilson

CONTROL OF THE VERTICAL INSTABILITY IN TOKAMAKS

E.A. LAZARUS*
General Atomics Inc., P.O. Box 85608, San Diego, California,
United States of America
J.B. LISTER
Centre de Recherches en Physique des Plasmas, Association Euratom – Confédération Suisse, Ecole Polytechnique Fédérale de Lausanne, 1015 Lausanne, Switzerland
G.H. NEILSON
Fusion Energy Division, Oak Ridge National Laboratory, Oak Ridge, Tennessee,
United States of America

ABSTRACT. The problem of control of the vertical instability is formulated for a massless filamentary plasma. The massless approximation is justified by an examination of the role of inertia in the control problem. The system is solved using Laplace transform techniques. The linear system is studied to determine the stability boundaries. It is found that the system can be stabilized up to a critical decay index, which is predominantly a function of the geometry of the passive stabilizing shell. A second, smaller critical index, which is a function of the geometry of the control coils, determines the limit of stability in the absence of derivative gain in the control circuit. The system is also studied numerically in order to incorporate the non-linear effects of power supply dynamics. The power supply bandwidth requirement is determined by the open-loop growth rate of the instability. The system is studied for a number of control coil options which are available on the DIII–D tokamak. It is found that many of the coils will not provide adequate stabilization and that the use of inboard coils is advantageous in stabilizing the system up to the critical index. Experiments carried out on DIII–D confirm the appropriateness of the model. Using the results of the model study, we have stabilized DIII–D plasmas with decay indices up to 98% of the critical index. Measurement of the plasma vertical position is also discussed.

---

*On leave from Fusion Energy Division, Oak Ridge National Laboratory, Oak Ridge, Tennessee 37831-8072, USA.

1. INTRODUCTION

The motivation of this work was to improve axi-symmetric stability in the DIII–D tokamak. However, the results are generally applicable to tokamaks requiring quadrupole fields to produce elongated plasmas, resulting in unstable field curvature. The orientation of this work is to avoid the details of loss of stability and to provide instead a formal treatment of the control problem. DIII–D is an excellent choice of device for a general study because of the generality of its poloidal field system, shown in Fig. 1.

In this work, when we refer to any particular coil (e.g. "F7"), we are referring to the anti-symmetric current flowing in the coil pair F7A and F7B, with the sign convention that positive current in the upper coil has the same sense as the plasma current.

The philosophy of this investigation is to develop the simplest possible mathematical model of the problem, namely a filamentary plasma model, and pursue an analysis within the context of this model which incorporates the control algorithms and the power supply characteristics. We model only the vertical part of the control system, avoiding the interaction with the remainder of the poloidal coil set, except for its imposition of the destabilizing quadrupole field. Plasma profiles enter through the quantity $\beta_p + (\ell_i/2)$ in the critical index. We are considering the problem of vertical stability in the presence of a quadrupole field produced by some unspecified set of external coils. The relationship of elongation to vertical stability depends on the plasma profiles and the totality of the shaping field. The appropriateness of this model is determined experimentally, and we report results from experiments on DIII–D which demonstrate that this model provides the information needed to characterize the vertical control problem.

The difficulty in stabilizing the plasma is characterized by the ratio of the decay index, n, [1] to the critical index, n_c, which is determined largely by the vessel geometry. Here we assume that the vacuum vessel is the dominant passive stabilizing element, as is the case on DIII–D. By applying the results of the analysis presented here and making the appropriate modifications in the feedback system, plasmas with n/n_c of –0.98 have been vertically stabilized.

The characterization of the vessel, and of its interaction with the plasma, is a major aspect of the analysis. We employ an eigenmode description of the poloidal distribution

of the toroidal vessel currents. This simplification reduces the problem to analytically manageable dimensions. This eigenmode description of the vessel was used successfully both to analyze control loops for the ISX-B tokamak [2] and, with the massless filament approximation used here, in treating the problem of radial control [3]. As in Ref. [3], we consider a treatment which places major importance on the specification of the dynamic power supply requirements for fulfilling the control function. The cost of the power systems is comparable to the cost of the tokamak; thus, an understanding of the consequences of coil positions and control algorithms needs to be integrated with the initial design of the tokamak.

The vertical problem is easier to treat than the radial one because the plasma inductance is not an explicit function of the vertical position, z. Thus, while the radial control problem is fundamentally non-linear, the vertical control problem is linear and susceptible to an analytic treatment, only becoming non-linear through, for example, exceeding limits in power supplies. Since this analysis depends more critically on the vessel description than the previous work, the eigenmode description is treated in detail in Appendix A. This paper is organized as follows.

Section 2 contains the basic mathematical description of the plasma-vessel system under consideration. A review of the basic description of passive stabilization is a starting point from which we show that the approximation of a massless plasma, or instantaneous force balance, provides a good analytic prediction of the growth rate for any plasma which might plausibly be controlled with an active circuit. Having eliminated two roots in the problem in this manner, we extend the analysis to a system of plasma, passive stabilizer, and active coil. This system is again solved using Laplace transform techniques in Section 3. We study the nature of the stability boundaries of the closed-loop system. We find that there is a second critical index, characteristic of the active coil set, above which there are no stable solutions without velocity feedback in the control loop. The variation of the stable operating window with n/n_c is discussed and we find that it is possible to stabilize plasmas with $|n|/n_c \sim 1$. Time-domain solutions, which allow the inclusion of the non-linear effects of a dynamic power supply model, are also obtained. The physical nature of the problem is discussed in some detail here, with particular attention to the dynamical interaction of the active control circuit with the passive stabilizer.

In Section 4 we optimize system performance and evaluate power supply requirements. In the presence of power supply constraints, imposed by both voltage and slew rate, the circuit equations are no longer linear, and numerical solutions are presented. This leads rather naturally into a wider study of coil choices and the effects of higher-order eigenmodes of the vessel current on the results, in Section 5. Here the physics of the couplings of the plasma–vessel–coil system are explored in greater detail. We find that with certain choices of outboard coils, the range of decay indices over which stable solutions can be found is restricted. Further, we find that a judicious choice of control strategy is required in order to achieve good performance with plausible power supplies.

In Section 6 we report briefly on experimental results which verify the applicability of this model. Using the concepts discussed in this paper, we have stabilized plasmas with $|n|/n_c = 0.98$. These experiments will be reported in detail in Ref. [4].

In Section 7 we evaluate the need for dynamic compensation in the measurement and establish the criteria which need to be met by the plasma–vessel–active coil system in order to neglect such compensation.

Section 8 contains a concluding discussion in which we offer suggestions for the design and control of future tokamaks.

2. THE PLASMA-VESSEL SYSTEM

We begin with a system consisting of a single-filament plasma within a conducting vessel. This problem has been treated previously [5], but we wish to introduce the concept of a critical index and discuss the detailed nature of the open-loop growth rates which are characteristic of the problem. The plasma is described by the total current I_p, the poloidal beta β_p, the internal inductivity ℓ_i, the external inductance L_{ext}, and the nominal major radius X_0. The surrounding passive conductor has a current I_v flowing in an antisymmetric mode (zero net current). The subscript v refers to the stabilizer, and the subscript p refers to the plasma. Later we introduce the subscript a to refer to the active coil.

First, we must obtain the characteristic growth rates of the vertical instability.

2.1. Basics of passive stabilization

The equations to be solved are the vertical force balance equation for the plasma and the circuit equation for the vessel [see Fig. 2(a)]:

$$m_p \frac{d^2 z}{dt^2} = -2\pi X_0 I_p B_r \tag{1}$$

and

$$V_v = L_v \frac{dI_v}{dt} + R_v I_v + \frac{dM_{vp}}{dz}\frac{dz}{dt} I_p = 0 \tag{2}$$

Here we have neglected terms in $\dot{I}_p$, which we shall justify post priori. The vessel inductance is that of the first eigenmode of an expansion of the vessel current in orthogonal modes. In the limit of infinite aspect ratio and a circular cross-section vessel, these modes are $\sin \ell\theta, \ell = 1, 2, 3, ...$, where θ is the poloidal angle. This vessel description is discussed in detail in Appendix A. For the toroid of arbitrary cross-sectional shape, the modes are calculated numerically, with the angle θ defined by sectors of equal arc length, to preserve the orthogonality, and normalized so the L/R time for each mode is correct. M_{vp} is the mutual inductance of the first eigenmode to the plasma, and R_v is the vessel resistance; m_p is the plasma mass. L_v always refers to the self-inductance of the lumped circuit as represented by the first antisymmetric eigenmode.

The second mode has an L/R time a factor of 1.9 lower than the first mode. Furthermore, its coupling to the plasma is very poor, producing only a small radial field. Thus, its role

in the problem will always be minimal and it is therefore neglected. We shall return to this point in a later section. The higher modes decay at still faster rates.

The poloidal dependence of the first three eigenmodes is shown in Fig. 3. Each mode has a higher degree of spatial structure than the previous one, which is the cause of the decreasing L/R times. Table I lists the time constants and the parameter $2M_{\ell p}^2 X_0/\mu_0 L_\ell$, which is a measure of the mode's effectiveness in vertical stabilization, for these modes. Note that the current distribution of the first mode is highly weighted to the outboard side of the vessel. The spatial dependence will be quite important to the control problem, and we shall return to this topic in Section 5. In Fig. 4 we plot the field lines of our filamentary plasma along with the vessel shape used to generate the eigenmodes. As a result of toroidicity, the field lines intersect the vessel predominantly on the outboard side. This is the physical reason why vertical displacement of the plasma couples most strongly to this mode.

The radial field B_r at X_0, the filament location, can be expanded in a Taylor series. The appropriate expansion parameter is the decay index n, defined as

$$n \equiv -\frac{X_0}{B_z}\frac{\partial B_z}{\partial X} \tag{3}$$

An equivalent definition of the decay index, which avoids explicit reference to the plasma characteristics, is

$$n = -2\pi X_0 \left(\frac{\text{quadrupole field amplitude}}{\text{dipole field amplitude}}\right) \tag{4}$$

This expression is more directly applicable to the evaluation of the decay index as a control parameter, since it can be computed directly from the poloidal coil currents.

The vacuum field, B_r has two components: the external field due to the equilibrium field coils that are producing the unstable curvature [Fig. 2(b)], and the restoring field due to currents induced in the surrounding conducting vacuum vessel by the plasma motion.

Assuming stationary fields, $\nabla \times \vec{B} = 0$, and the equilibrium field equation,

$$\begin{aligned} B_r &= B_{r_0} + \frac{\partial B_r}{\partial z} z \\ &= B_{r_0} - \frac{n B_{z_0} z}{X_0} \\ &= \frac{-I_v}{2\pi X_0}\frac{\partial M_{vp}}{\partial z} + \frac{\mu_0 I_p \Gamma n z}{4\pi X_0^2} \end{aligned} \tag{5}$$

where

$$\Gamma \equiv \frac{L_{ext}}{\mu_0 X_0} + \frac{\ell_i}{2} + \beta_p + \frac{1}{2} \tag{6}$$

and B_{z_0} is the equilibrium vertical field at X_0.

Combining Eqs (1) and (3) and using the prime to denote d/dz, we obtain

$$\ddot{z} - \frac{I_v M'_{vp} I_p}{m_p} + \frac{\mu_0 I_p^2 \Gamma n z}{2 m_p X_0} = 0 \tag{7}$$

If we define $\gamma_v \equiv R_v/L_v$, then from Eq. (2)

$$\dot{I}_v + \gamma_v I_v + \frac{M'_{vp} I_p}{L} \dot{z} = 0 \tag{8}$$

Now we Laplace transform this pair of equations by letting $d/dt \rightarrow s$ and define the characteristic frequency,

$$\omega_1^2 \equiv \frac{\mu_0 I_p^2 \Gamma}{2 m_p X_0} \tag{9}$$

and the critical index,

$$n_c \equiv \frac{2 M'^2_{vp} X_0}{\mu_0 \Gamma L_v} \tag{10}$$

Then the indicial equation for the characteristic roots of Eqs (7) and (8) is

$$(s^2 + n\omega_1^2)(s + \gamma_v) + s\omega_1^2 n_c = 0 \tag{11}$$

In the limiting case of no coupling between the plasma and the vessel ($n_c = 0$) the roots are $s = \pm\sqrt{-n}\omega_1$ and $s = -\gamma_v$. The vessel current decays with the L/R time. For $n < 0$, the vertical instability has a characteristic growth rate of several microseconds for typical tokamak parameters.

By inspection, one can see that a transition occurs at $n = -n_c$. For decay indices more negative than $-n_c$, the growth rate of the vertical instability is of order ω_1, typically 10^5 to 10^6 s^{-1}. This critical index is a measure of the maximum field curvature which can be countered by currents induced in the stabilizing shell. For values of $n < -n_c$, the vessel's impedance is so great that the current induced in the vessel by the plasma motion cannot produce sufficient radial field at an adequate rate to provide stability.

Since this equation cannot be factored, numerical solutions are presented in Fig. 5, which shows both the real and imaginary parts. The first root shown (S_1) is the one of

interest to us. The growth rate is positive for all $n < 0$ and grows rapidly for $n \sim -n_c$. The growth rate is independent of both the plasma current and mass. This root becomes stable again for $n < -n_c$; however, one of the other pair of roots becomes unstable. These other roots do depend on both the plasma current and mass and have typical growth rates which are at least an order of magnitude greater than the first root. Thus we see that for $n > -n_c$ the dominant features are those of the electromagnetic system, and the plasma can be maintained provided that an active coil produces a radial field which replaces the vessel field on the appropriate time scale. If the decay index becomes more negative than this value, the plasma is maintained within the vessel only on the inertial time scale.

In summary, there is only one root of interest for control purposes, which is the most dangerous one, for $|n| < -n_c$. The roots which result from the inertial terms have slower growth rates for this condition, but once n reaches its critical value, they have growth rates which preclude stabilization. Thus, we focus on the real part of the root S_1 and find an excellent analytic approximation for it in the massless plasma limit (instantaneous force balance).

With the exception of the discussion of experimental results, we treat Γ as a constant, namely 1.80, leading to $n_c \sim 1.65$. Note, however, that the critical index, which is a measure of the tolerance of the plasma in the vessel to an applied quadrupole field, is dependent on the plasma properties through this term. In addition, the elongation achieved for an applied quadrupole amplitude decreases with increasing ℓ_i. Thus, maximum elongation will be a very strong function of this quantity.

2.2. The approximation of instantaneous force balance

In this limit the only solution is $B_r(z) = 0$. Thus, we set $B_r = 0$ in Eq. (3), solve for z, and differentiate:

$$\dot{z} = \frac{2M'_{vp}X_0}{\mu_0 I_p \Gamma n} \cdot \dot{I}_v \tag{12}$$

Substituting for $\dot{z}$ in Eq. (2), and employing the definition of n_c, we obtain

$$\left(1 + \frac{n_c}{n}\right) \dot{I}_v + \gamma_v I_v = 0 \tag{13}$$

The eigenvalue, which we denote as γ_0, is then

$$\gamma_0 = \frac{-\gamma_v n}{n + n_c} \tag{14}$$

We show this solution in Fig. 6(a). The ratio of this approximation to the first root of Eq. (11), discussed in Section 2.1, is also shown. It can be seen that the analytic form is an excellent approximation to the exact solution. As n becomes increasingly negative, the growth rate gradually increases and thus the frequency response of the active circuit will need to increase in a corresponding fashion.

2.3. The effect of a current ramp

It is straightforward to show that a current ramp can affect the growth rate of the axisymmetric mode if the ramp rate is comparable to γ_v. In Eq. (2) we add the term $M'_{vp} z \dot{I}_p$. Then, defining $\gamma_I \equiv (\dot{I}_p / I_p)$, we find that the analog to Eq. (13) is

$$\left(1 + \frac{n_c}{n}\right) \dot{I}_v + \left(\gamma_v + \frac{n_c}{n} \gamma_I\right) I_v = 0 \tag{15}$$

and the growth rate of the instability is

$$\gamma_0 = \frac{-(\gamma_v n + n_c \gamma_I)}{n + n_c} \tag{16}$$

Thus, $\dot{I}_p$ effects are only of interest for rates of the current ramp which are unlikely to be achieved during the plasma pulse. An exception is during the startup, where these effects are stabilizing and, in any event, the decay index is required to be near zero in order to form a proper null. However, for a fast system of passive stabilization, care should be taken during the current rampdown to keep $\gamma_I \ll \gamma_v$. A linear rampdown of I_p will always lead ultimately to a loss of vertical stability, but an exponential rampdown will not cause this problem.

Note that the growth rate is changed for $n > -n_c$, but the ideal limit remains at $n = -n_c$, since one of the inertial roots will have a positive real part.

3. THE PLASMA–VESSEL–ACTIVE COIL SYSTEM

Having demonstrated that the massless approximation accurately reproduces the dangerous root, we can now use this simplification and expand the problem to include an active coil, intended to provide stability on a longer time scale. The use of this approximation will allow us to work with second-order, rather than fourth-order, differential equations. In this section we accomplish two tasks: first, we add feedback control and solve the closed-loop equations in the frequency domain, and second, we solve the open-loop equations in the time domain. We wish to study the system (Fig. 7) of "the tokamak", the feedback controlling the vertical motion, and the power supply which completes the circuit. The closed-loop linear solutions provide the basis for the feedback design and identify stable operating regions. However, the inclusion of the power supply makes the problem non-linear in that the demand of the feedback circuit will not always be within the compliance of the power supply. We solve this problem by evolving the time domain solutions over time steps which are smaller than any of the characteristic times in the problem. At the end of each time step, we take the solution as the initial conditions for the next step, having reevaluated the voltage demand from the feedback circuit and the power supply response to this demand.

The solutions are algebraically complex, and we have not found any further simplification which would provide a more elegant result. In particular, all the possible couplings between plasma, vessel, and active coil are of the same order and none may be neglected. Thus, we choose a notation which compacts the solution as much as possible.

Generalizing Eqs (5) and (2) and adding a circuit equation for the active coil, we have as a starting point from $B_r = 0$

$$\frac{\mu_0 I_p \Gamma}{2X_0} nz - M'_{vp} I_v - M'_{ap} I_a = 0 \tag{17}$$

along with the circuit equations,

$$L_v \frac{dI_v}{dt} + R_v I_v + M_{av} \frac{dI_a}{dt} + \frac{dM_{vp}}{dz}\frac{dz}{dt} I_p = 0 \tag{18}$$

$$L_a \frac{dI_a}{dt} + R_a I_a + M_{av} \frac{dI_v}{dt} + \frac{dM_{ap}}{dz}\frac{dz}{dt} I_p = V_a \tag{19}$$

$Q \equiv (\mu_0 \Gamma n / 2X_0)$, $\alpha_{v,a} \equiv (M'_{p(v,a)}/L_{v,a})$, $\beta_{v,a} \equiv (M_{av}/L_{v,a})$, $\gamma_{v,a} \equiv (R_{v,a}/L_{v,a})$, and $\delta_{v,a} \equiv (M'_{p(v,a)}/Q)$. Also, we divide through by I_p, and henceforth I_v, I_a, and V_a *are in units of plasma current.*

Using these definitions and differentiating Eq. (17), we obtain

$$\dot{z} - \delta_v \dot{I}_v - \delta_a \dot{I}_a = 0 \tag{20}$$

along with the circuit equations,

$$\alpha_v \dot{z} + \dot{I}_v + \gamma_v I_v + \beta_v \dot{I}_a = 0 \tag{21}$$

$$\alpha_a \dot{z} + \beta_a \dot{I}_v + \dot{I}_a + \gamma_a I_a = \frac{V_a}{L_a} \tag{22}$$

As written, these equations can readily be solved by Laplace transform techniques; in particular, we employ the relation $\mathcal{L}(df/dt) = sF(s) + f(0^+)$.

We differentiate Eq. (17) to avoid an improper fraction in the transfer function or, stated differently, to impose as an initial condition that the force balance Eq. (17) is satisfied. Otherwise the evolution of $z(t)$ is determined only to within an arbitrary constant of integration. Denoting the transformed variables as $\mathcal{L}\,[z(t)] = \mathcal{Z}(s)$, $\mathcal{L}\,[I_v(t)] = \mathcal{I}_v(s)$, $\mathcal{L}\,[I_a(t)] = \mathcal{I}_a(s)$, and $\mathcal{L}\,[V_a(t)] = \mathcal{V}_a(s)$, we Laplace transform this set of determining equations, obtaining

$$\begin{pmatrix} s & -\delta_v s & -\delta_a s \\ \alpha_v s & s+\gamma_v & \beta_v s \\ \alpha_a s & \beta_a s & s+\gamma_a \end{pmatrix} \times \begin{pmatrix} \mathcal{Z}\,(s) \\ \mathcal{I}_v\,(s) \\ \mathcal{I}_a\,(s) \end{pmatrix} = \begin{pmatrix} z_0 - \delta_v I_{v_0} - \delta_a I_{a_0} \\ \alpha_v z_0 + I_{v_0} + \beta_v I_{a_0} \\ \alpha_a z_0 + \beta_a I_{v_0} + I_{a_0} + \mathcal{V}_a\,(s)/L_a \end{pmatrix} \tag{23}$$

The general form of the solution to Eq. (23) is

$$\begin{pmatrix} \mathcal{Z}(s) \\ \mathcal{I}_v(s) \\ \mathcal{I}_a(s) \end{pmatrix} = \vec{\vec{H}}(s) \times \begin{pmatrix} K_z(s) + E_z(s) \\ K_v(s) + E_v(s) \\ K_a(s) + E_a(s) \end{pmatrix} \tag{24}$$

where $\vec{K}(s)$ is the vector of the Laplace transform of the initial conditions, and $\vec{E}(s)$ is the Laplace transform of the excitation. Equation (24) defines the transfer function $\vec{\vec{H}}(s)$, which relates the response of an output variable to both the excitation and initial conditions.

We write the transfer function matrix in the form $\vec{\vec{H}}(s) = \left(\hat{H}(s)/|\vec{\vec{H}}^{-1}(s)|\right)$, where

$$\hat{H}(s) = \begin{pmatrix} s^2(1-\beta_a\beta_v)+s(\gamma_a+\gamma_v)+\gamma_a\gamma_v & s^2(\delta_v - \beta_a\delta_a) + s\gamma_a\delta_v & s^2(\delta_a - \beta_v\delta_v) + s\delta_a\gamma_v \\ s^2(\alpha_a\beta_v - \alpha_v) - s\alpha_v\gamma_a & s^2(1+\alpha_a\delta_a) + s\gamma_a & -s^2(\alpha_v\delta_a + \beta_v) \\ s^2(\alpha_v\beta_a - \alpha_a) - s\alpha_a\gamma_v & -s^2(\alpha_a\delta_v + \beta_a) & s^2(1+\alpha_v\delta_v) + s\gamma_v \end{pmatrix} \tag{25}$$

and the characteristic polynomial, $C(s) \equiv |H^{-1}(s)|$, is

$$\begin{aligned} C(s) &= s^3(1 - \beta_a\beta_v + \alpha_a\delta_a + \alpha_v\delta_v - \alpha_v\beta_a\delta_a - \alpha_a\beta_v\delta_v) \\ &+ s^2(\alpha_a\delta_a\gamma_v + \alpha_v\delta_v\gamma_a + \gamma_a + \gamma_v) \\ &+ s\gamma_a\gamma_v \end{aligned} \tag{26}$$

The characteristic polynomial, $C(s)$, defines the global behavior of the total system, and the matrix elements $\hat{H}_{ij}(s)$ contain the input-output couplings. $C(s)$ has one trivial root ($s = 0$) corresponding to Eq. (20) and two non-zero roots, which we denote γ_1 and γ_2.

From Eq. (26),

$$\gamma_{1,2} = \frac{\gamma_v(1+\alpha_a\delta_a) + \gamma_a(1+\alpha_v\delta_v) \pm \mathcal{R}}{2[(\alpha_a\beta_v - \alpha_v)\delta_v + (\alpha_v\beta_a - \alpha_a)\delta_a + \beta_a\beta_v - 1]} \tag{27}$$

where

$$\begin{aligned} \mathcal{R} &= \{\gamma_v^2(1+\alpha_a\delta_a)^2 + \gamma_a^2(1+\alpha_v\delta_v)^2 2\gamma_a\gamma_v \\ &+ [\delta_v(\alpha_a\alpha_v\delta_a + 2\alpha_a\beta_v - \alpha_v) + \delta_a(2\alpha_v\beta_a - \alpha_a) + 2\beta_a\beta_v - 1]\}^{\frac{1}{2}} \end{aligned} \tag{28}$$

The roots $\gamma_{1,2}$ are real with one root greater than zero. Note that there is a term which scales as γ_v, as found previously, and another which is related to γ_a. We shall return to this point in more detail.

3.1. Adding feedback to the transfer function

We now study the effect of a linear feedback controller on the complete system response. The particular case is intended to approximate the present DIII–D control system, which operates with vertical control provided by the F6 and F7 coils (Fig. 1), which are fed in parallel by independent power supplies but driven from the same controller signal. The relative gains used are 8:1 in favor of the F7 coils. We shall treat the system as if these two antisymmetric coil pairs were actually in series, preserving our second-order system and its relative simplicity.

The unstable open-loop transfer function, $H(s)$, must be stabilized by the addition of a feedback voltage on the active coil. We employ a simple PD (proportional-derivative) position controller, giving a coil voltage prescribed as

$$\frac{V_a(t)}{L_a} = G_z\,[z(t) - z_{ref}(t)] + G_v \frac{d}{dt}\,[z(t) - z_{ref}(t)] \tag{29}$$

It is important to note that a true feedback circuit treats zI_p as the controlled variable; otherwise, the circuit gains would need to be made proportional to the plasma current. This is not explicit in our notation where we have normalized the original equations, dividing through by I_p.

G_z provides the proportional positional feedback and G_v provides derivative positional feedback or velocity feedback. For the moment we neglect the inclusion of integral positional feedback because it will raise the order of the transfer function, whereas the proportional and derivative gains preserve the order. We assume that we will subsequently be able to add an integral feedback term to annul the asymptotic error, using a gain which will not adversely affect the stability, where it is critical.

Equation (23) now becomes

$$\begin{pmatrix} s & -\delta_v s & -\delta_a s \\ \alpha_v s & s+\gamma_v & \beta_v s \\ (\alpha_a - G_v)s - G_z & \beta_a s & s+\gamma_a \end{pmatrix} \times \begin{pmatrix} \mathcal{Z}(s) \\ \mathcal{I}_v(s) \\ \mathcal{I}_a(s) \end{pmatrix} = \begin{pmatrix} z_0 - \delta_v I_{v_0} - \delta_a I_{a_0} \\ \alpha_v z_0 + I_{v_0} + \beta_v I_{a_0} \\ \alpha_a z_0 + \beta_a I_{v_0} + I_{a_0} + (G_z + sG_v)\mathcal{Z}_{ref}(s) \end{pmatrix} \tag{30}$$

The solution for the Laplace transformed variables is still of the form of Eq. (24), except that we now have the closed-loop transfer function shown above. For the present, we assume that the initial conditions are quiescent, $\vec{K}(s) = 0$, and consider only the regulator problem, $z_{ref}(t) = 0$. We restrict our attention to the response to step function excitations of unit amplitude onto the active coil voltage, $\mathcal{V}_a(s) = 1/s$.

With the same notation as previously, with the subscript *cl* denoting the closed-loop system, the characteristic polynomial becomes

$$\begin{aligned} \frac{C_{cl}(s)}{s} &= s^2[1 - \beta_a\beta_v + \delta_v(\alpha_v - \alpha_a\beta_v) \\ &\quad +\delta_a(\alpha_a - \alpha_v\beta_a) - G_v(\delta_a - \delta_v\beta_v)] \\ &+ s^1[\gamma_a + \gamma_v + \delta_v\alpha_v\gamma_a + \\ &\quad \delta_a\alpha_a\gamma_v - G_z(\delta_a - \delta_v\beta_v) - G_v\delta_a\gamma_v] \\ &+ s^0(\gamma_v\gamma_a - G_z\delta_a\gamma_v) \end{aligned} \tag{31}$$

where we have factored out the trivial root due to Eq. (20). We rewrite this as

$$\begin{aligned}\frac{C_{cl}(s)}{s} &= s^2(a_2 - d_1 G_v) \\ &+ s^1(a_1 - d_1 G_z - d_2 G_v) \\ &+ s^0(a_0 - d_2 G_z)\end{aligned} \tag{32}$$

where we have used the notation $C(s)/s = a_2 s^2 + a_1 s + a_0$ for the open-loop characteristic polynomial, Eq. (26).

The effect of positional feedback is therefore seen to be characterized completely by the two coefficients: $d_1 \equiv \delta_a - \delta_v \beta_v$, and $d_2 \equiv \delta_a \gamma_v$. The first term, d_1, is given by

$$d_1 = \frac{M'_{pa}}{Q} - \frac{M'_{pv}}{Q}\frac{M_{av}}{L_v} \tag{33}$$

and simply represents the change in z due to an instantaneous change in the normalized I_a, taking into account the induced change in I_v. The second term, d_2, is given by

$$d_2 = \frac{M'_{pa}}{Q}\frac{R_v}{L_v} \tag{34}$$

This represents the change in z due to a change in the current in the active coil multiplied by the decay rate of the induced vessel currents, and is the rate at which the change in B_r and hence z due to the active current alone will occur.

The closed-loop numerator matrix, $\hat{H}_{cl}(s)$, remains similar to $\hat{H}(s)$, and is given by:

$$\hat{H}_{cl}(s) = \begin{pmatrix} \hat{H}_{11} & \hat{H}_{12} & \hat{H}_{13} \\ \hat{H}_{21} + s^2\beta_v G_v + s\beta_v G_z & \hat{H}_{22} - sG_v\delta_a - G_z\delta_a & \hat{H}_{23} \\ \hat{H}_{31} + s^2 G_v + s(G_z + \gamma_v G_v) + \gamma_v G_z & \hat{H}_{32} - sG_v\delta_v - G_z\delta_v & \hat{H}_{33} \end{pmatrix} \tag{35}$$

Most importantly, the element $\hat{H}_{13}$, which determines the effect of the active coil voltage on the plasma position, remains unchanged by the feedback gain coefficients. All information on the modified vertical motion in the closed-loop system is therefore contained in the denominator.

The roots of the closed-loop denominator are denoted $s_{1,2}$, corresponding to Eq. (27). Since the denominator is quadratic, the necessary and sufficient condition for stability of the closed-loop system is simply the Hurwitz condition, namely, that the polynomial coefficients of $C_{cl}(s)$ all have the same sign. Stable solutions will be oscillatory or overdamped, depending on the choices of G_z and G_v. Rather than specify criteria on the step response and then deduce the applicable choice of G_z and G_v, which may not be realizable, we inspect

the behaviour of the solutions in the G_z:G_v plane. This will also lead us to a better feeling for the effect of the various terms which we shall directly control.

For $C_{cl}(s) = a_2' s^2 + a_1' s + a_0'$, stability requires that

$$\begin{aligned} a_2' &\equiv a_2 - d_1 G_v \lesseqgtr 0 \\ a_1' &\equiv a_1 - d_1 G_z - d_2 G_v \lesseqgtr 0 \\ a_0' &\equiv a_0 - d_2 G_z \lesseqgtr 0 \end{aligned} \tag{36}$$

where either the upper or lower inequalities are simultaneously satisfied.

Although it appears that this second-order system can be stabilized by gains G_z and G_v of both signs, one of these signs is an artifact of the approximation of instantaneous force balance which requires an infinite speed of response to annul any perturbation. This is most easily seen by inspecting the third-order system derived from Eq. (30), with a finite filter time constant on the controller output, $(G_z + sG_v)/(1 + s\tau)$. This leads to a cubic characteristic equation given by

$$\begin{aligned} a_3'' &= a_2 \tau \\ a_2'' &= a_2 - d_1 G_v + a_1 \tau \\ a_1'' &= a_1 - d_1 G_z - d_2 G_v + a_0 \tau \\ a_0'' &= a_0 - d_2 G_z \end{aligned} \tag{37}$$

The Hurwitz criterion applied to these coefficients now becomes restricted to all coefficients having the same sign as a_2, as a necessary but insufficient condition for stability. One of the inequality signs of Eq. (36) disappears.

Using this restricted criterion, we explore the coupled system response as the control gains (G_z, G_v) are varied, Fig. 8. The stability criteria (36) correspond to the straight thick lines A–A ($G_v = a_2/d_1$) and B–B ($G_z = -a_0/d_2$) and the line C–D defined by the axis intersection points $(G_z, G_v) = (0, a_1/d_1)$ and $(a_1/d_2, 0)$. In the particular case shown, the line A–A is a stability criterion which only limits the operating region at extremely high values of G_z, when the line C–D crosses it. The stable region is therefore the lower left part of this figure.

The solutions are stable and oscillatory in Region I, stable and non-oscillatory in Region II, unstable and oscillatory in Region III, and unstable and non-oscillatory elsewhere.

The critical damping boundary is shown by the curved thick line. The oscillation frequency ($\omega = |\mathrm{Im}(s_{1,2})|$) increases either as the stability boundary C–D is approached or as $-G_z$ is increased, and is shown by the solid lines inside Regions I and III. The system responsiveness, given by the most positive root, increases as G_z increases away from the axis B–B, and as $-G_v$ decreases towards the axis C–D, shown by the dashed lines in Regions I and II; ω is positive and continues to increase as we cross the line C–D towards higher values of G_v.

Although the shape of this figure does not vary for different coils and different equilibrium field decay indices, the regions do move and compress, as we shall see. The shape of this G_z:G_v space is not even specific to the tokamak vertical control problem, but is typical of the control of any second-order system.

One feature evident from Fig. 8, which will be used later, is that there is no connection between the overdamped zone and the unstable zone without crossing an oscillatory zone, as long as we keep away from the B–B axis with enough proportional gain.

3.2. Varying the decay index

Varying the equilibrium field decay index and still controlling with the F6 plus F7 coils distorts the G_z:G_v plane as shown in Fig. 9, for $-n$ = 0.4, 1.0, 1.6, corresponding to $-n/n_c$ = 0.24, 0.67, and 0.97.

Stability requires a minimum value of proportional gain G_z (the axis B–B), which varies with the decay index, n, as shown by curve 1 of Fig. 10. This criterion is always easy to satisfy in practice. Stability also requires a minimum value of the derivative feedback coefficient $-G_v$, for a given value of the proportional coefficient G_z, although since the axis C–D is always very flat, this value of G_v is relatively independent of the chosen G_z. As the field decay index increases negatively, the C–D axis moves to more negative values of this minimum derivative feedback gain, as shown by curve 2 of Fig. 10. Critical damping requires an even greater value of $-G_v$, which also increases with negatively increasing field decay index, as shown by curve 3 of Fig. 10.

Curve 2 of Fig. 10 shows that the implementation of a velocity term is essential for stability above a certain field decay index, $n = -0.65$ for the case shown. This value of $-n$ is, in fact, the critical decay index of the active coils, given by

$$n_a \equiv \frac{2M_{ap}'^2 X_0}{\mu_0 \Gamma L_a} \tag{38}$$

It corresponds to the equilibrium field decay index at which the plasma vertical motion would be stabilized by the active coils on their own, without the vessel, and we refer to it as the coil critical decay index by analogy with Eq. (9). Below this value, only proportional gain is required for stability, whereas, for a larger value of decay index, the plasma motion would not induce a large enough EMF in the active coil to provide the necessary restoring force for stability. By adding external derivative control gain, we can excite the active coil with a greater total derivative gain than its own passive response, and we thereby continue to stabilize the plasma motion for greater values of $-n$. The finite vessel time constant allows us to provide this essential derivative control with a bandwidth much lower than the frequency ω_1 in Eq. (9). Once this minimum stabilizing derivative gain has been added, any further increase in the derivative gain will not provide increased stability, but will reduce the system responsiveness.

Figure 11(a) shows the two growth rates and the oscillation frequency of the closed-loop system when we vary the decay index with no derivative control ($G_v = 0$, $G_z = -0.1$), illustrating in a different way the significance of this coil critical index $n = -n_a = -0.65$, beyond which one root is unstable. When derivative control is added, $G_v = -0.002$, the system is stable up to an intermediate value of $n_a < -n < n_c$, Fig. 11(b). When enough derivative gain is added, $G_v = -0.003$, the system is stabilized for all decay indices up to the critical index, Fig. 11(c). This important result — that we can control the vertical plasma motion up to the vessel critical decay index — is true for the F6 plus F7 coils but is not general, as we shall see in Section 5.1.

Curve 4 of Fig. 10 shows the maximum value of $-G_v$ that gives a critically damped response with $|s_1| > 80$, as n is varied with fixed $G_z = -0.15$. The dynamic range of the optimal G_v is over a factor of two, and if we wish to maintain the system responsiveness over the whole range of critical index from the value of $n = 0$ needed at breakdown up to the limit, n_c, then the controller coefficients will have to vary as the field decay index varies.

This could be certainly be carried out under open-loop adaptive control or by controlling the gain coefficients dynamically based on the value of the decay index, which normally varies slowly during the discharge.

If we choose not to vary the control gains as the decay index varies, during plasma shaping towards the vessel limit $n = -n_c$, Figs 9, 10, and 11 illustrate what will happen if the (G_z, G_v) coefficients have been chosen to provide adequate operation for an intermediate decay index, such as $n \sim -n_c/2$. Early in the discharge, at small values of $|n|$, the control will be rather sluggish as the elected G_v will give an excessively overdamped solution for this lower $|n|$, seen in Fig. 11(c). As we increase $|n|$, the system will become more responsive, until it is critically damped at the chosen point. Beyond this, the solution becomes oscillatory with an increasing frequency, given roughly by $\omega \sim (4a_2'a_0' - a_1'^2/2a_2')$.

If the power supplies fail to maintain the oscillatory solution up to $-n = n_c$, we must increase the G_v damping term further, optimizing for the highest achievable values of $-n$, which may well lead to an unacceptably slow response at smaller values of n.

Increasing the G_v damping term not only allows us to reach higher values of $|n|$, but also reduces the maximum voltage in the linear case. As the decay index increases, the maximum voltage requirement to correct a step input to the active coil increases dramatically for G_v = –0.001, Fig. 12. We cannot reach $-n_c$, as we have seen. For G_v = –0.004, which we have shown to be stable up to $-n_c$, the voltage requirement is reduced for all values of n. The effect of keeping the voltage below the linear evolution of the system response is examined in Section 4.

The observations made on the closed-loop system response for the given coil set may be summarized as follows:

- The closed-loop performance has been studied by inspection of the resulting characteristic polynomial.
- There is an open region in the G_z:G_v space in which stable operation can be found, up to a field decay index equal to the vessel critical decay index.
- Above the critical index of the active coils used for vertical control, velocity feedback is essential for closed-loop stability.

- As the decay index varies, a fixed system response requires a significant dynamic variation of the controller coefficients.

- The active coil voltage requirements are reduced significantly by increasing the value of G_v, at the expense of system responsiveness.

3.3. Time-domain solutions

We continue to restrict ourselves to the response to a step in the applied applied voltage ($V_a = 0,\ t \leq 0;\ V_a = V_0,\ t > 0$) for which $\mathcal{L}\ [V_a(t)] = V_0/s$. This allows a time-domain solution suitable for the inclusion of non-linear effects, such as power supply limitations or time dependence of the decay index. With this restriction, there is additional cancellation of a factor s in the response function and we can simplify $\vec{\vec{H}}(s)\cdot[\vec{E}(s)+\vec{K}(s)]$ to the general form

$$\frac{a_t s^2 + b_t s + c_t}{s(s-\gamma_1)(s-\gamma_2)}$$

The inverse transform of this general response function is

$$\frac{a_t\gamma_2^2 + b_t\gamma_2 + c}{\gamma_2^2 - \gamma_1\gamma_2}e^{\gamma_2 t} + \frac{a_t\gamma_1^2 + b_t\gamma_1 + c_t}{\gamma_1^2 - \gamma_1\gamma_2}e^{\gamma_1 t} + \frac{c_t}{\gamma_1\gamma_2} \tag{39}$$

We write these response functions in a vectorized form with coefficients expressed as factors of the initial conditions by defining three vectors corresponding to a_t, b_t, and c_t. We recall that, when using these solutions in the discussion of power supply requirements, our intent is to advance them for short time intervals, appropriate to the bandwidth of the overall system, and then renew these vectors. Thus our generalized coefficients a_t, b_t, and c_t will become, effectively time dependent through this renewal process.

$$\vec{\vec{H}}(s) \times \begin{pmatrix} z_0 - \delta_v I_{v0} - \delta_a I_{a0} \\ \alpha_v z_0 + I_{v0} + \beta_v I_{a0} \\ \alpha_a z_0 + \beta_a I_{v0} + I_{a0} + V_0/sL_a \end{pmatrix} = \vec{\hat{S}}_2 s^2 + \vec{\hat{S}}_1 s + \vec{\hat{S}}_0 \tag{40}$$

The time-domain solutions are

$$\begin{aligned} \begin{pmatrix} z(t) \\ I_v(t) \\ I_a(t) \end{pmatrix} &= \vec{\hat{S}}_2 \left(\frac{\gamma_2^2 e^{\gamma_2 t}}{\gamma_2^2 - \gamma_1\gamma_2} + \frac{\gamma_1^2 e^{\gamma_1 t}}{\gamma_1^2 - \gamma_1\gamma_2} \right) \\ &+ \vec{\hat{S}}_1 \left(\frac{\gamma_2 e^{\gamma_2 t}}{\gamma_2^2 - \gamma_1\gamma_2} + \frac{\gamma_1 e^{\gamma_1 t}}{\gamma_1^2 - \gamma_1\gamma_2} \right) \\ &+ \vec{\hat{S}}_0 \left(\frac{e^{\gamma_2 t}}{\gamma_2^2 - \gamma_1\gamma_2} + \frac{e^{\gamma_1 t}}{\gamma_1^2 - \gamma_1\gamma_2} + \frac{1}{\gamma_1\gamma_2} \right) \end{aligned} \tag{41}$$

where

$$\vec{\hat{S}}_2 = \begin{pmatrix} z_0 \\ I_{v_0} \\ I_{a_0} \end{pmatrix} \tag{42}$$

$$\begin{aligned} \vec{\hat{S}}_1 &= [\delta_v(\alpha_v - \alpha_a\beta_v) + \delta_a(\alpha_a - \alpha_v\beta_a) - \beta_a\beta_v + 1]^{-1} \\ &\quad \times \left\{ \begin{pmatrix} z_0(\alpha_a\delta_a\gamma_v + \alpha_v\delta_v\gamma_a + \gamma_v + \gamma_a) \\ 0 \\ 0 \end{pmatrix} \right. \\ &\quad + \begin{pmatrix} I_{v_0}\gamma_v(\beta_a\delta_a - \delta_v) \\ I_{v_0}\gamma_a(1 + \alpha_v\delta_v) \\ I_{v_0}\gamma_v(\alpha_a\delta_v + \beta_a) \end{pmatrix} \\ &\quad + \begin{pmatrix} I_{a_0}\gamma_a(\beta_v\delta_v - \delta_a) \\ I_{a_0}\gamma_a(\alpha_v\delta_a + \beta_v) \\ I_{a_0}\gamma_v(1 + \alpha_a\delta_a) \end{pmatrix} \\ &\quad \left. + \begin{pmatrix} (\delta_a - \beta_v\delta_v)V_0/L_a \\ -V_0/L_a(\alpha_v\delta_v + \beta_v) \\ V_0/L_a(1 + \alpha_v\delta_v) \end{pmatrix} \right\} \end{aligned} \tag{43}$$

$$\vec{\hat{S}}_0 = \begin{pmatrix} \dfrac{z_0\gamma_a\gamma_v - I_{v_0}\gamma_a\gamma_v\delta_v - I_{a_0}\gamma_a\gamma_v\delta_a + (V_0/L_a)\gamma_v\delta_a}{\delta_v(\alpha_v - \alpha_a\beta_v) + \delta_a(\alpha_a - \alpha_v\beta_a) - \beta_a\beta_v + 1} \\ 0 \\ \dfrac{\gamma_v(V_0/L_a)}{\delta_v(\alpha_v - \alpha_a\beta_v) + \delta_a(\alpha_a - \alpha_v\beta_a) - \beta_a\beta_v + 1} \end{pmatrix} \tag{44}$$

As our examination of the problem develops, it will become necessary to carry out this same calculation for a system of four equations, with two control coils. We leave this to Appendix B.

We close this section with a discussion of the time history of the solution for a particular case. The feedback coefficients are consistent with the optimization discussed above. Our purpose here is to emphasize the physical system being analyzed, in particular the interaction of the plasma with the active coil as mediated by the passive stabilizer. We use this example as the basis for our study of power supply requirements in Section 4.

We take as an initial condition a plasma offset in z by δz, and held in place by the vessel current. These conditions would be the applicable ones for a step perturbation in B_r.

produced by some poloidal coils not active in the vertical control system. (For example, an asymmetric, single-null diverted plasma, programmed for constant elongation, that suffered a change in ℓ_i due to a sawtooth reconnection would experience a step in B_r.) The initial value of applied voltage is zero. Thus $z(0) = \delta z$, $I_v(0) = (n/n_c)\alpha_v \delta z$, $I_a(0) = 0$, and $V_a(0) = 0$. At $t = 0$, $\dot{z}$, $\dot{I}_v$, and $\dot{I}_a$ must all be non-zero for Eqs (17), (18), and (19) to be satisfied. The $\dot{z}$ signal is passed through an RC filter with a time constant of 16 μs since some filtering is required for computational stability.

The system begins its response to the perturbation, trying to return the plasma position to $z = 0$. The trajectory is shown in Fig. 13. In the first instance, the active coil current must hold the plasma in equilibrium at some positive z. Referring to Fig. 2(b) and Eq. (17), one sees that the externally produced radial field experienced by the plasma is negative. Before the vessel current decays and allows the plasma to continue its upward vertical motion, this negative field must be balanced by a positive radial field produced by the active coil; i.e. the current in the coil must be negative. Thus, initially, our control system must apply a negative voltage to the coil and capture the plasma in a new (unstable) equilibrium. In this interval the active coil will induce positive current in the vessel which reduces the vessel's effectiveness in its reaction to the plasma. When the new equilibrium is established at some $z > 0$, with the vessel current having decayed, we now consider restoring the plasma to its initial ($z = 0$) equilibrium. Since a negative velocity is required, from Eq. (20) we require $\dot{I}_a > 0$, and the voltage must turn positive. If we write $V \sim G_z z + G_v \dot{z}$, then both G_z and G_v must be negative.

Note that this motion is also opposed by the vessel, and thus when the plasma has been driven to $z = 0$ there will remain a positive vessel current which will push the plasma upwards again. This positive current, which is induced by the plasma moving down, is reinforced by the current induced by $\dot{I}_a$. It is important to recognize that the vessel does not in any sense restore the plasma position; it only serves to slow any motion of the plasma. Thus, to get from the initial state, $z > 0$, to a final state, $z = 0$, an initial command is required which, in the absence of the vessel, would move the plasma to a still greater z value. Whether the plasma actually moves to a greater z value depends sensitively on the decay index and feedback gain settings.

4. POWER SUPPLY REQUIREMENTS

To evaluate the requirements for maintaining control of the plasma we have performed a non-linear numerical study of the system as expressed in Eq. (41), retaining our series treatment of F6+F7. We choose a simple power supply model as follows. The internal impedance of the supply is anticipated to be negligible compared to that of the active coil. The four-quadrant supply is limited in both voltage and slew rate. The slew time limit, which is defined as the minimum time to effect a change from zero to maximum amplitude (four slew times is one period), is linear, i.e. $\dot{V}$ is only affected when the demand is greater than the allowable slew. When this condition exists, $\dot{V}$ is clamped at the allowed rate. Similarly, the amplitude limit has no effect until the demand exceeds the allowed amplitude. In using this model, we must take care to separate amplitude and bandwidth requirements. Our feedback relation remains

$$\frac{V_a(t)}{L_a} = G_z[z(t) - z_{ref}(t)] + G_v \frac{d}{dt}[z(t) - z_{ref}(t)]$$

Thus a slew limit is reflected through z as an increased voltage demand.

The model power supply response to an oscillatory demand which exceeds both the amplitude and slew limits is shown in Fig. 14.

We determine the maximum required voltage in the absence of any limitation on power supply slew and then use this value as the power supply amplitude while investigating bandwidth requirements. We perform this study under conditions of constant G_z (–0.4) and G_v (–0.005). The values chosen are those suitable for operation at $n \sim -n_c$. While these gains are not optimal for smaller values of n, clearly any single set of gains must include the point of most stringent requirement.

Our model problem is that discussed in Section 3.3, with the plasma initially displaced by δz. The responses at the extremes of n are shown in Fig. 15. There is approximately a factor of two increase in the response time as $|n|$ is decreased from n_c to zero, as discussed previously. These responses are a standard for our experiment in that as limitations are imposed on the power supplies we shall not allow the solutions to move "too far" from these ideal solutions. In particular, we will require that the time required to return the plasma to $z = 0$ is not appreciably changed and that the solution does not become too oscillatory. We do, however, allow one zero-crossing.

We begin by turning off the power supply slew limits and examining the maximum voltage required to return the plasma to $z = 0$ for $0.002 \leq (|n|/n_c) \leq 0.95$. This curve is labelled V_{max} in Fig. 16. Next we turn on the supply with infinite slew time and determine the minimum voltage required to achieve an acceptable solution. This curve is labelled V_{min}^{∞}. Finally, we begin to restrict the slew capability of the power supply and find the minimum slew time which does not perturb the voltage requirement very far from V_{min}^{∞}. This curve is labelled V_{min}.

A typical result with the limited power supply is shown in Fig. 17. The responses $z(t)$ for no supply limitation, for a power supply with infinite slew rate, and for the slew-limited case are displayed. The limitation in amplitude only makes the system response more sluggish, as would a reduction in G_z. However, the bandwidth limitation serves to destabilize the plasma, creating an oscillatory response, as would a reduction in G_v. Thus for vertical control, bandwidth is more critical than amplitude in achieving acceptable performance.

We find that the slew rate must always be greater than γ_v (209 s^{-1}). Furthermore, when the open-loop growth rate Eq. (27) exceeds γ_v, this growth rate corresponds to the minimum slew rate. At this minimum slew time, for $n > n_a$ the voltage requirement V (in Volts) scales approximately as

$$V = \delta z I_p V_0 \exp[-7(n/n_c)], V_0 = 7.5 \times 10^{-4}$$

with δz in meters, I_p in amperes, and V_0 in V/(A·m). The slew requirement at $n = -n_c$ is in excess of 30 V/μs. We note that the typical current maximum in the active coil is about $2 \times 10^{-5} I_p$.

Summarizing these results: the power supply voltage requirement is linear in the plasma displacement, linear in plasma current, but exponential in the decay index. The slew rate requirement is adequately represented by the maximum of the vessel current decay rate and the open-loop growth rate of the unstable mode.

We recall that we have aggressively minimized the requirements here. The power supply requirements at the ideal limit are formidable at best. With these unpromising results in mind and a recognition of the importance of the open-loop growth rate, we seek a more favorable control strategy in Section 5.

5. OPTIMIZATION OF THE CONTROL SYSTEM

5.1. Comparison of the various DIII–D coils

5.1.1. Open-loop growth rate

In Section 3 we studied the closed-loop behaviour of one particular set of coils used for vertical position control on the DIII–D tokamak: the F6 and F7 coils, modelled as if they were fed in series. In Section 4 we concluded that as the decay index approaches the vessel critical decay index, the voltage requirement for the F6 plus F7 coils increases exponentially as $V = V_0 \exp[-7\,(n/n_c)]$, while the slew time requirement is γ_{ol}^{-1}. As a result of this conclusion, we now explore the vertical control capabilities of all the other poloidal field coils in the DIII–D tokamak (Fig. 1) in the hope of doing better.

When we change the poloidal field coil pair used, the shape and character of the G_z:G_v plane stay the same, although the position of the stability and oscillation boundaries move. These changes are due to the different values of L_a, M_{av}, M'_{pa}, and R_a of Eqs (17–19). As a first step, we inspect the open-loop growth rates for the coupled system, using each of the nine antisymmetric coil pairs in turn, with a decay index close to the vessel critical index, $n = -1.64$ $(-n/n_c = 0.99)$. The results are summarized in Table II. We recall that the open-loop growth rate represents the condition where the coil is present, but shorted. The growth rate in the presence of only the vessel is found from Eqs (17–19) by setting R_a to infinity, and is 29,854 s^{-1}. The open-loop growth rate for the F6 plus F7 coils was 17,144 s^{-1}, between the values of the F6 and F7 coils separately. There is a very large range of open-loop growth rates for the separate coils, varying from 1,379 s^{-1} (coil F2) to a barely modified 29,481 s^{-1} (coil F5).

The predictions of relatively poor behavior of the F7 coil alone and good behaviour for the shorted inboard F2 coils are surprising at first sight. The difference is mainly due to the coupling M_{av} between the active coil current and the vessel image current. Specifically, it is the coupling between the active coil current and the first antisymmetric vessel current eigenmode, on which Eqs (17–19) are based, which is important in this calculation. Good coupling between the active coils and the vessel actually drives a destabilizing current in the vessel as the active circuit tries to respond to a plasma displacement. Figure 18 shows the flux distribution of this antisymmetric vessel current mode, in the (R, Z) plane. The

different poloidal coil positions are also indicated. Coil F7 clearly couples best to this current distribution, and coils F1 and F2 are the least coupled. Table II also lists these mutual inductances, M_{av}, for all the coils.

The flux patterns for two coils, the outboard F7 coil and the inboard F2 coil, are shown in Figs 19(a) and 19(b) for stationary active coil currents, that is to say, with no vessel image currents. The field pattern is more favourable for the F7 coil [Fig. 19(a)] than for the F2 coil [Fig. 19(b)], leading to the intuitive choice of the outboard coils for positional control. On the other hand, the induced antisymmetric vessel current resulting from a unit step in the active coil current is

$$I_v = -M_{av}/L_v \tag{45}$$

and also varies from coil to coil. The flux configuration due to the superposition of these two currents is the prompt, or high-frequency, field pattern for the coils, shown in Figs 19(c) and 19(d) for the F7 and the F2 coils, respectively. The exclusion of the prompt F7 coil flux by the first antisymmetric vessel current is almost perfect, and much stronger than for the F2 coil. When we consider only the vessel image currents in this one vessel eigenmode, the prompt shielding of the F2 coil is extremely weak, leading to the marked reduction of the open-loop growth rate seen in Table II. In fact, the stabilizing effect on the growth rate is dominated by the term d_1, Eq. (33), which, as we have already seen, is important when the feedback was introduced, and which represents the prompt radial field on axis.

However, the vessel shell is of course complete, and all prompt flux must be perfectly excluded, as we would find if we were to include all of the higher eigenmodes of the vessel image current distribution. The apparent superiority of the F2 coils in improving the open-loop growth rate is partially due to the incompleteness of the simple three-loop system in modelling the vessel image currents. The F2 coils are almost unshielded by the first antisymmetric mode, Fig. 19(c). To resolve this issue we have evaluated the growth rates from the characteristic polynomial for a system with two vessel modes. Both the second and third antisymmetric modes have been tested, and neither, when combined with the first vessel mode, causes more than a few percent change in the growth rate with the F2 coils. Eventually, we would reach a mode of high enough order to exclude the F2 flux; however, these modes are decaying at ever faster rates, while the plasma is still being restrained by

the first, slowest mode. The control flux from the F2 field coils will always penetrate the vessel on a much shorter time scale than that from the F7 coils, whose strong coupling to the first antisymmetric current mode condemns them to the speed of this slowest vessel mode.

5.1.2. Closed-loop control

In Section 3.2 we found that we could stabilize the vertical plasma motion up to the vessel critical decay index, $n = -n_c$, and that this was true as $(-G_z, -G_v)$ tended to infinity. From Eq. (36), this is clearly not so if $d_1 > 0$. In this case, the coefficient a_2' becomes positive at high G_v, leading to unstable roots. This new criterion, satisfied by the F6 plus F7 coils in Section 3.2, can be written as

$$\frac{M_{pa}'}{M_{av}} > \frac{M_{pv}'}{L_v} = 1.209 \tag{46}$$

Inspecting the individual coil pairs for their values of this coefficient, listed in Table II, we find that coils F1 through F6 satisfy the condition, and the F7, F8 and F9 coils, closest to the first antisymmetric eigenmode current distribution, do not.

The maximum decay index achievable is shown in Fig. 20 as a function of the velocity feedback gain times the coil inductance, $G_v L_a$, for the F7, F2, and F9 coils. The F2 coils reach $-n = n_c$ at a minimum value of $G_v L_a$ and continue to provide stable control as the derivative gain is increased further. Coil F7 reaches $-n = 0.9\ n_c$, after which more derivative gain becomes destabilizing. The F9 coils have a still lower value of this criterion and cannot reach values of $-n$ higher than $0.82\ n_c$.

5.2. Fast/slow hybrid control

The results derived in Section 5.1 led us to conceive a new way of approaching vertical position control on the DIII–D tokamak. The F7 coils, presently dominant in the vertical position control, provide the best rigidity of the plasma position for a given active coil current, but are unable to control the radial field on axis on a fast enough time scale to reach the vessel limit. The F2 coils, on the other hand, are at least a factor of 3 faster at producing a radial field on axis, but do not produce a large homogeneous radial field for defining the steady position. The proposed improvement is to mix the position controller signals between

both the F2 and F7 coils, weighting the F2 coil predominantly with derivative feedback gain. We expect this fast/slow hybrid control to improve the positional control as the decay index is increased and the open-loop growth rate increases. The open-loop growth rates for the F7 coils only, the F2 coils only, and the hybrid are compared in Fig. 21.

5.3. Power requirements for the hybrid control system

We wish to compare the power required for this hybrid system to the results obtained with the F6+F7 coils. The Laplace transformed equations, Eqs (17–19), have been extended to include two active coils (Appendix B). We retain only the first vessel current eigenmode, having established that the second and third antisymmetric modes still have a negligible effect on the open-loop growth rates.

As we have presented the hybrid system, steady-state solutions exist when the vessel current has decayed, but coil currents remain in the fast (inboard) and slow (outboard) coils which provide net zero radial field on axis. We shall eliminate such solutions by placing a high-pass filter in the control loop which drives the fast (F2) coils. Using a time constant of $10 \times \tau_v$, these coils are allowed to react to the plasma on the appropriate time scale, but in steady state the applied voltage will decay to zero. This has an added advantage in that the measurement system is itself sensitive to the fields produced by the coils. No matter how good the compensation for these effects, there will always be a difference in the measured position if the currents producing the radial field are moved from one coil to another. Here we have a system which will have a unique relation of the measured and actual positions in the steady state.

Additionally, since we place a premium on higher-frequency power, we will intercept the derivative signal to the slow (F7) coils with a low-pass filter with a time constant of τ_v. Thus, we can still provide derivative gain with the slow coils and avoid the destabilizing effects which occur if the bandwidth is not limited. That is, we filter the signal to avoid the creation of a flux pattern inside the vessel similar to that shown in Fig. 19(c). This allows us to minimize the power to the fast coils at the expense of somewhat higher requirements for the slow coils. The version of a hybrid control system used in these calculations of power requirements is shown schematically in Fig. 22.

We have not done a formal study of the stability of the linear system equation, Eq. (B.58), in the space G_{z_s}:G_{v_s}:G_{z_f}:G_{v_f}. This would be a complex process and, from the preceding discussion of the circuit modifications needed for optimum solutions, we would still have to modify the gains calculated there. We have studied some restricted aspects of this solution space. In particular, we find that there are stable solutions with only proportional gain on the coils. These solutions show a very fast response and require larger power supply bandwidth than those with derivative gain. For this reason we do not pursue them; they are mentioned here because this feature is discussed in the experimental results.

To quantify the improvement provided by the hybrid system, we have repeated the evaluation of power supply requirements of Section 4 at $n/n_c = -0.99$. We take as the figure of merit for power supply utilization the product $V^{max}I^{max}(dV/dt)^{max}$, which contains both power and slew rate demands on the power supplies and is roughly their cost scaling. When comparing this result to that for the F6 + F7 coils we have divided the voltage for the latter case by two, accounting for our series modelling. The results are shown in Table III. $V^{max}I^{max}(dV/dt)^{max}$, which is a rough measure of power supply cost, is reduced by a factor of 225. The power consumption is nearly halved. Given the fact that the tokamak power systems typically cost more than the tokamak itself, such a gain for a bit of control circuitry is not to be ignored. We find that the amplitude requirement is reduced by nearly an order of magnitude. The bandwidth requirement is reduced by approximately 20 in accordance with the change in the open-loop growth rates shown in Table II. The power supplies needed for this control scheme are quite reasonable by the standards of present fusion experiments. Because the operating point in the four-dimensional gain space has not been optimized, further reduction in the power supply requirements may be possible.

For the hybrid system, there is not a serious bandwidth requirement for the F7 coils which position the plasma. These only need a response time comparable to the vessel L/R time of 5 ms. However, we find again that the slew requirement for the fast part of the system is the open-loop growth rate. The reduction in this growth rate is the critical factor in reduced power supply demands.

6. EXPERIMENTAL CONFIRMATION

We summarize the results of recent vertical control experiments on DIII–D. The full details of these experiments will be reported in Ref. [4]. We began with the observation that plasmas with decay indices of about –0.95 were lost vertically, while the critical index for the vessel is about 1.6. It was found that the amplitude of the G_v term in the control loop was sufficiently small that reversing its sign did not result in a disruption. Thus, this value of $n = -0.95$ represents n_a. We calculate that for our model configuration of F6+F7, $n_a = -0.65$. The reason for the discrepancy is that the equilibrium control is based on flux projection. If the plasma moves vertically, all the poloidal coils contribute a restoring force as they sense the vertical imbalance in flux. This effective reduction in the impedance of all the coils to antisymmetric current flow raises the value of n_a.

The system response to a series of step inputs was studied for different decay indices and control gains. The validity of the magnetically measured position was checked against a differencing of soft X–ray horizontal chords. A typical response is shown in Fig. 23. It can be seen that as the decay index slowly increases the decay of the oscillatory behaviour becomes slower.

We summarize here the main experimental results.

- The main character of the G_z:G_v plane, Fig. 8, has been verified.
- The influence of the decay index, Fig. 9, has also been demonstrated up to the vessel critical decay index. That is, as n increases, increased derivative gain is required for stability at constant proportional gain.
- The destabilizing effect of the current rampdown has been observed [Eq. (16)]. (The open triangle in Fig. 24)
- The faster response of the plasma to an excitation of the F2 coils has been experimentally verified.
- A formal system identification of the dynamic closed-loop system has been performed. The DIII–D vertical control is dominantly a second order system, as in Eqs (17–19). We observe overdamped, stable oscillatory, and unstable oscillatory responses.

- The vessel critical decay index was not reached even at high G_v with only the F7 coils used for control, as in Fig. 20. This is shown by the solid line in Fig. 24.

- When velocity gain was added to the F2 coils as well as to the F7 coils, the maximum achieved decay index approached the calculated vessel limit for these particular plasmas, shown as circled asterisks in Fig. 24. This series of measurements was carried out the day after a vacuum leak when the plasma was very dirty. Thus ℓ_i was about 1.5, much larger than normal, accounting for the low value of $n_c = 1.3$ and the relatively low elongation ($\kappa \sim 2.2$) obtained in these unfavorable conditions.

- As the decay index approached the vessel limit, the controller voltage output increased significantly, as discussed in Section 4.

- Proportional gain applied to the F2 coils is stabilizing. (The open circle on Fig. 24)

7. MEASUREMENT OF Z

The closed-loop Eq. (30) was derived in terms of the plasma position $z(t)$ and a corrector given by the (G_z, G_v) control gains. This presupposes that we are able to instantaneously measure $z(t)$, the height of the current centroid, under all conditions.

Actual measurements of $z(t)$ are carried out on the DIII-D tokamak using a linear combination of flux loop and magnetic field signals. The signals obtained from these coils are, however, also sensitive to all other currents, mainly the poloidal field coil currents and the induced currents in the vacuum vessel. Since the total signal will be the linear sum of these two additional effects, we can write

$$z_{obs}(t) = z(t) + C_v I_v(t) + C_a I_a(t) \tag{47}$$

where we have normalized with respect to I_p as before. Except for the relatively fast skin effect, there are no dynamic terms. Poloidal field coils other than the one we are considering can contribute, and vessel eigenmode currents other than the first one may contribute, depending on the detection loop and coil placement. The signs of C_a and C_v are negative and positive, respectively, if we measure $Z_{obs}(t)$ by outboard flux loops only. For more complex measurements, C_a and C_v must be evaluated for the specific geometry.

One approach to this problem is to back off all the C_a terms electronically, using the measured $I_a(t)$ signals, and to back off the $C_v(t)$ term using a reconstructed value of $I_v(t)$. We examine the effect on the closed-loop system stability of not performing this compensation at all, or of doing it imperfectly.

Since the corrector acts on $z_{obs}(t)$ rather than on $z(t)$, the closed-loop system is modified, and the left-hand matrix in Eq. (30) now becomes

$$\begin{pmatrix} s & -\delta_v s & -\delta_a s \\ \alpha_v s & s + \gamma_v & \beta_v s \\ (\alpha_a - G_v)s - G_z & (\beta_a - C_v G_v)s - C_v G_z & (1 - G_v C_a)s + (\gamma_a - G_z C_a) \end{pmatrix} \tag{48}$$

The resulting characteristic polynomial, analogous to Eq. (31), is

$$\begin{aligned}\frac{C_{cl}(s)}{s} &= s^2[1-\beta_a\beta_v+\delta_v(\alpha_v-\alpha_a\beta_v)\\ &\quad +\delta_a(\alpha_a-\alpha_v\beta_a)-G_v(\delta_a-\delta_v\beta_v)\\ &\quad -C_a(\alpha_v\delta_v+1)G_v+C_v(\alpha_v\delta_a+\beta_v)G_v]\\ &+ s^1[\gamma_a+\gamma_v+\delta_v\alpha_v\gamma_a\\ &\quad +\delta_a\alpha_a\gamma_v-G_z(\delta_a-\delta_v\beta_v)-G_v\delta_a\delta_v\\ &\quad -C_a(\alpha_v\delta_v+1)G_v+C_v(\alpha_v\delta_a+\beta_v)G_v-C_a\gamma_vG_v] \qquad (49)\\ &+ s^0(\gamma_v\gamma_a-G_z\delta_a\gamma_v-C_a\gamma_vG_v)\end{aligned}$$

which we rewrite by analogy with Eq. (32) as

$$\begin{aligned}\frac{C_{cl}(s)}{s} &= s^2(a_2-d_1G_v-e_1G_vC_a+e_2G_vC_v)\\ &+ s^1(a_1-d_1G_z-d_2G_v-e_1G_zC_a+e_2G_zC_v-e_3C_aG_v) \qquad (50)\\ &+ s^0(a_0-d_2G_z-e_3C_aG_z)\end{aligned}$$

where the new coefficients are $e_1=\alpha_v\delta_v+1$, $e_2=\alpha_v\delta_a+\beta_v$, and $e_3=\gamma_v$.

The stability criterion is then that the coefficients of this polynomial have the same sign as a_2, as before. We can inspect these modified criteria to develop some intuition for the effect of a lack of compensation on the closed-loop system stability. Most simply, the stability of the s^0 term increases, since the coil current increases the response, effectively increasing $-G_z$. The oscillation frequency will therefore be increased. The s^2 term is slightly destabilized by $e_1<0$, corresponding to the effectively increased proportional gain, and by $e_2<0$, corresponding to the vessel current "hiding" the displacement. As a result, the velocity term will have to be increased in magnitude slightly to compensate these terms. Only if $-e_2C_v>+d_1$ will such compensation not be possible.

The term linear in s is more complicated and affects the sloping line C–D of Fig. 8 which defines our effective stability boundary. There the terms $-e_3C_aG_v$, $+e_2C_vG_z$ and $-e_1C_aG_z$, will all be destabilizing. We have already seen that the a_1 term is compensated by an increase in G_v, which is still possible provided that $+e_3C_a<d_2$.

With these simple considerations, we have demonstrated that a stable (G_z:G_v) control setting can be found, provided that $-e_3C_a<-d_2$ and $+e_2C_v<-d_1$. Otherwise, dynamic compensation will still allow a practical control system.

Although this conclusion is not particularly general, one important feature must be noted. The choice of optimum placement of detection coils will always be complex, involving the dynamics of the vessel image currents. Furthermore, the apparent coil critical index, n_a, will vary with the detector coil placement. We will, in general, be forced to use G_v partly to stabilize against the effect of the vessel currents, in the position measurement itself, on the closed-loop response. Thus, we will find particular detection coil locations which will create a requirement for more or less velocity gain in order to obtain stable system behaviour.

8. CONCLUDING DISCUSSION

A simple model has been developed for the control of axisymmetric instabilities in tokamaks. We begin with the proposition that a single-filament model of the plasma is adequate for the study of the control problem. We then demonstrate that the massless plasma approximation describes the plasma-vessel interaction on the control time scale, and plasma inertia plays a negligible role. The ultimate justification for this model is its agreement with experimental results. A single filament is a successful descriptor for the control problem because even highly elongated plasmas look similar to a filament at the vessel wall, where controlling measurements are made. To illustrate this, we show a highly elongated equilibrium in Fig. 25. (We have not yet produced this equilibrium in the experiment.) For this case, ℓ_i is 0.65, indicating that the current profile is quite broad. Along with the equilibrium flux contours, we show the plasma contribution alone. This should be compared to the flux contours of Fig. 4. While there is some difference near the axis, along the vessel wall the change is quite small. Thus, the effect of high elongation is more in the effect of the external field on the measurement of plasma position than in the dynamics of the interaction between the vessel and the plasma motion.

The equations are solved using only one eigenmode of the antisymmetric vessel current distribution. It is a simple consequence of toroidicity that this mode will be excited predominantly by the vessel-plasma interaction. A strong motivation for using such an eigenmode expansion of the vessel current is the time ordering of these modes. Each subsequent mode has a finer spatial scale than the next lower mode and, therefore, a faster decay. These simplifications allow us to add the required active control circuit and continue with a second-order system. Again, the experimental observation that the system exhibits second-order behavior is compelling evidence for the suitability of this approach.

While we have studied two higher-order modes, we did not pursue this investigation to the point of establishing which eigenmodes will interact with the F2 coils. Inclusion of the $\ell = 2$ or $\ell = 3$ vessel eigenmode along with $\ell = 1$ and the F2 coils changes $\gamma_{\alpha l}$ by only a few percent. We did not identify the mode number which interacts strongly with the F2 coils. The experimental results confirm that the mode number is high enough to have little effect on the control problem. In separate work [6], the higher-order modes have been examined.

It is found that the F2 coils couple most strongly to the $\ell = 6$ mode which decays with an L/R time of 0.98 ms, compared with 4.78 ms for the $\ell = 1$ mode.

We find that the critical index of the active coil represents the decay index above which the system is unstable in the absence of derivative gain. However, with the appropriate choice of coils and gain settings, it is feasible to operate up to the vessel critical index.

Perhaps the most interesting result is the difference in system response with different choices of control coils. While inboard coils slow the open-loop growth rate by more than a factor of 20 relative to the vessel alone, many of the coils on DIII–D have negligible effect on this growth rate. That is, the destabilizing effect that results from their interaction with the vessel is nearly as strong as the stabilizing effect of producing a radial field within the vessel. While these results might well be mitigated by strong coupling of the plasma to other regions of the vessel as the plasma makes large excursions and is deformed, this does not seem to us to be an attractive feature for a control system. One wishes to control the plasma with only small excursions from the reference position. From our calculations for DIII–D, it appears that reasonable control without inboard coils would be quite difficult. The F7, F8, and F9 pairs do not allow us to reach the critical index, and even the F5 coils, which are quite close to the center column, are undesirable in that γ_{ol} is quite large. It is unfortunate that such valuable space is required for vertical control, although these coils do not necessarily carry large equilibrium currents. We have not examined the use of the F6 coils alone in any detail. It can be seen from Fig. 3 that their interaction with the second and third eigenmodes will be stronger than that of the F2 coils. Their location will make them much more sensitive to the details of the vessel geometry than inboard coils, but as outboard coils are moved closer to the midplane they become more effective. However, as with the comparison of the F1 and F2 coils, moving the coils too close to the midplane will reduce their effectiveness.

Power supply requirements for control have been studied in detail. The principal result is that the power supply slew rate is approximately the open-loop growth rate. This is seen to be the most critical feature of the power system, in that a lack of bandwidth is equivalent to a reduction in the derivative gain, which is the stabilizing term. The required voltage scales exponentially with the decay index but linearly with the plasma current and the position measurement resolution. The choice of coils and the control strategy have a

marked effect on the power requirements. It is quite possible to find coils on DIII-D, such as the F5 pair, with which a formal treatment indicates that the plasma can be stabilized up to the ideal limit, but for which the power supply requirements are not realistic.

Experimentally, in DIII–D the value of n_a is approximately 0.94, somewhat above our predicted value of 0.65. The reason for this discrepancy is partly the flux control used to shape the plasma. This acts as if proportional control for vertical stability were explicitly provided to all the coils, since the programming demands a symmetric flux pattern (or a specified asymmetry). This has the effect of reducing circuit impedance to antisymmetric current flow if the plasma moves vertically. Additionally, simply the inductive coupling of the plasma to these coils will act passively to suppress the growth rate. In fact, we have calculated that were the impedance of all these 18 coils to antisymmetric current reduced to zero, n_a would be about 1.55, quite comparable to n_c.

One might consider that this is a sufficient control system for a tokamak, in that DIII–D operates routinely with $\kappa \sim 2$. However, the large value of n_a is attributable to surrounding the plasma with 18 poloidal field coils driven by individual power supplies. Were the coils moved further from the plasma or driven symmetrically in up-down pairs, n_a would be decreased. Further, the elongation per unit quadrupole lessens with increasing aspect ratio and future devices are likely to have aspect ratios greater than the 2.5 value of DIII–D. Thus it is unlikely that $\kappa \sim 2$ will be achieved quite so readily.

While the equations describing the system are, in principal, straightfoward, the algebra is somewhat tedious. The solutions are not intuitively obvious as presented, but are trivially evaluated numerically. We have provided considerable detail in the hope that they will be used in the design of future tokamaks which have high elongation as an experimental goal. It is the nature of the tokamak that all the circuit elements are closely coupled to the plasma, or else they would not be there. As a consequence, all coils are closely coupled to each other and to the vessel. Other than the obvious decomposition into odd and even functions of z, which allows us to eliminate the remainder of the poloidal coil set from the problem, we were not able to simplify further.

ACKNOWLEDGEMENTS

Two of the authors (E.A.L. and J.B.L.) thank Ron Stambaugh, Tony Taylor, and the DIII–D physics staff for their hospitality during their detachment at General Atomics. All of us are indebted to Arnie Kellman, who bore the primary responsibility for providing discharges with suitably large decay indices, and two of us (E.A.L. and G.H.N.) gratefully acknowledge the continued support of John Sheffield, and are indebted to D.W. Swain for useful suggestions concerning the treatment of the vacuum vessel.

The work described was partly funded by EURATOM, the Ecole Polytechnique Fédérale de Lausanne and the Fonds National Suisse de la Recherche Scientifique. The research was sponsored by the Office of Fusion Energy, U.S. Department of Energy, under contracts DE-AC03-89ER51114 and DE-AC05-84OR21400.

Appendix A.
EIGENMODE REPRESENTATION OF THE VACUUM VESSEL

In order to incorporate the effects of the vacuum vessel into the equilibrium analysis, a lumped-circuit representation is required. One option is to use a large number of parallel filaments and to treat each one as a separate circuit coupled to the plasma, active coils, and all the other filaments. However, this makes the problem rather unwieldy because of the large number of coupled equations that result. The approach taken here is to first analyze the vacuum vessel by itself in terms of the normal toroidal-current modes. The normal modes turn out to be eigenmodes of an integral operator with a symmetric kernel. Each eigenmode can be represented by an RL circuit decoupled from the others by virtue of orthogonality, but inductively coupled to the plasma and active coils (Fig. 26). The eigenvalues are just the R/L decay rates for the corresponding circuits. As is characteristic of Sturm-Liouville problems such as this, the decay rate increases and the coupling to the plasma weakens with increasing eigenmode order, providing a double justification for neglecting all but the lower-order modes. For most purposes, in fact, only one mode need be retained, thus reducing the vacuum vessel representation to a single circuit in the equilibrium control analysis.

We approximate the vacuum vessel as an axisymmetric toroid whose cross section is that of the actual vessel being modeled. The vessel wall thickness, t_v, is assumed to be small compared to characteristic minor dimensions, so the wall can be regarded as a sheet with a surface conductivity $\sigma_v = \sigma t_v$, where σ is the bulk conductivity of the material. The vessel (Fig. 27) is thus defined by the contour of its wall in a toroidal plane (X, Z), which is described parametrically by the functions $X_v(s)$, $Z_v(s)$, and $\sigma_v(s)$. The parameter s, where $0 \le s \le s_0$, is the arc length along the closed contour (such that the points $s = 0$ and $s = s_0$ coincide), and $\sigma_v(s)$ is allowed to vary along the contour.

For an arbitrary toroidal surface current distribution $K(s)$, the poloidal flux linked at a toroidal ring through point s is

$$\psi(s) = 2\pi\mu_0 \int_0^{s_0} ds' G(s,s') K(s') \tag{A.1}$$

where the symmetric kernel $G(s,s')$ is the Green's function,

$$G(s,s') = \frac{X(s)X(s')\left[(2-x^2)K(x) - 2E(x)\right]}{\pi x^2 \{[X(s)+X(s')]^2 + [Z(s)-Z(s')]^2\}^{1/2}} \tag{A.2}$$

$$x^2 = \frac{4X(s)X(s')}{[X(s)+X(s')]^2+[Z(s)-Z(s')]^2} \tag{A.3}$$

and K and E are complete elliptic integrals.

For the normal modes problem, in which the vessel is considered in isolation from other sources, the local current is related to the local flux by Ohm's law:

$$\frac{2\pi X(s)}{\sigma_v(s)}K(s) = -\dot{\psi}(s) \tag{A.4}$$

An eigenmode ℓ of the system is characterized by a *distributed* mode current $K_\ell(s)$, but will be represented by a lumped circuit carrying a current I_ℓ, which we relate to the surface current by

$$K_\ell(s) = \frac{I_\ell}{s_0}k_\ell(s) \tag{A.5}$$

where $k_\ell(s)$ is a dimensionless eigenfunction. The mode decays as exp $(-\gamma_\ell t)$, so Eqs (A.1) and (A.4) combine to yield the integral equation,

$$\gamma_\ell \int_0^{s_0} ds' G(s,s')k_\ell(s') = \frac{X(s)}{\mu_0\sigma_v(s)}k_\ell(s) \tag{A.6}$$

for which the decay rate γ_ℓ is the eigenvalue. Because of the symmetry of $G(s,s')$, any two modes m and ℓ $(m \neq \ell)$ will satisfy the orthogonality condition

$$\int_0^{s_0} ds \frac{X(s)}{\mu_0\sigma_v(s)}k_m(s)k_\ell(s) = 0 \tag{A.7}$$

The normalization condition (i.e. for $m = \ell$) is

$$\int_0^{s_0} ds \frac{X(s)}{\mu_0\sigma_v(s)}\left(k_\ell(s)\right)^2 = \frac{X_0 s_0}{\mu_0\sigma_{v0}} \tag{A.8}$$

where X_0 and σ_{v0} are arbitrary but characteristic values of X and σ_v for the vessel.

We can now derive expressions for the circuit parameters that represent the eigenmode ℓ. The mutual inductance $M_{c\ell}$ between the mode and a coil c located at (X_c, Z_c) (e.g. the plasma, or one coil of the active control windings) can be derived by combining Eqs. (A.1) and (A.5) [since $\psi(X_c, Z_c) = M_{c\ell}I_\ell$]:

$$M_{c\ell} = \frac{2\pi\mu_0}{s_0}\int_0^{s_0} ds' G(c,s')k_\ell(s') \tag{A.9}$$

where $G(c, s')$ is defined by replacing $[X(s), Z(s)]$ by (X_c, Z_c) in the definition of the Green's function [Eq. (A.2)]. The mutual inductance between two distinct modes m and ℓ is

$$M_{m\ell} = \frac{2\pi\mu_0}{s_0^2} \int_0^{s_0} ds\ k_m(s) \int_0^{s_0} ds' G(s, s') k_\ell(s') = 0 \tag{A.10}$$

which vanishes by orthogonality [Eq. (A.7)]. The self-inductance of a mode ℓ is

$$\begin{aligned} L_\ell &= \frac{2\pi\mu_0}{s_0^2} \int_0^{s_0} ds\ k_\ell(s) \int_0^{s_0} ds' G(s, s') k_\ell(s') \\ &= \frac{2\pi X_0}{s_0 \sigma_v \gamma_\ell} \end{aligned} \tag{A.11}$$

and the resistance is $\gamma_\ell L_\ell$:

$$R_\ell = \frac{2\pi X_0}{s_0 \sigma_v} \tag{A.12}$$

which, interestingly, is independent of mode number.

We note that the evaluation of Eqs (A.10) and (A.11) by numerical integration is complicated by the logarithmic singularity of $G(s, s')$ at $s' = s$ [or $x^2 = 1$, referring to Eq. (A.3)]. We treat this by using an approximation for G when s' is close to s, such that $1 - x^2 \ll 1$:

$$G(s, s') \approx \frac{X(s)}{2\pi} \left[\ln 8X(s) - 2 - \frac{1}{2} \ln(s - s')^2 \right] \tag{A.13}$$

This can be integrated analytically, allowing us to approximate the contribution to the contour integral over s' from an interval $(s, s + \delta s)$ near the singularity:

$$\int_s^{s+\delta s} ds' G(s, s') k_\ell(s') \approx \delta s \frac{X(s) k_\ell(s)}{2\pi} \left[\ln \frac{8X(s)}{|\delta s|} - 1 \right] \tag{A.14}$$

The integration over the remainder of the contour is treated by simple numerical integration methods, such as the trapezoidal rule.

The eigenfunctions and eigenvalues of the problem are found by starting with a trial function $k_{t0}(s)$, and successively applying an integral operator proportional to $\mathcal{G}$ to it (where $\mathcal{G}k(s) = \int_0^{s_0} ds' G(s, s') k(s')$). This works because any arbitrary trial function is expandable in the eigenfunctions of the operator $\mathcal{G}$, namely the k_ℓ:

$$k_{t0}(s) = \sum_{n=0}^{\infty} C_\ell k_\ell(s) \tag{A.15}$$

The expansion coefficients C_ℓ are unknown at this point. We operate on k_{t0} a large number of times N with the operator $[\mu_0\sigma_v(s)/X(s)]\mathcal{G}$ to obtain the lowest eigenfunction:

$$k_{tN} = \frac{\mu_0\sigma_v(s)}{X(s)}\mathcal{G}k_{tN-1} = \left[\frac{\mu_0\sigma_v(s)}{X(s)}\right]^N \mathcal{G}^N k_{t0}(s) = \sum_{n=0}^{\infty} \frac{C_\ell}{\gamma_\ell^N} k_\ell(s) \tag{A.16}$$

For large N, the series in Eq. (A.16) will be dominated by the mode with the smallest γ_ℓ, i.e. the lowest-order mode, so that $k_{tN}(s)$ will cease to change with increasing N, except for a multiplicative factor. We use this as the convergence criterion. Once k_{tN} has converged in this manner, we use Eq. (A.8) to find the factor needed to convert it to a properly normalized $k_0(s)$ and use Eq. (A.6) to determine the eigenvalue:

$$\gamma_0 = \left[\int_0^{s_0} ds\; k_0(s)\mathcal{G}k_0(s)\right]^{-1} \tag{A.17}$$

Finding one of the higher-order ($\ell \geq 1$) eigenfunctions requires that all the lower-order ones be found first and filtered out of the initial trial function. The coefficients of known eigenfunctions in Eq. (A.15) can be found by making use of the orthogonality [Eq. (A.7)] and normalization [Eq. (A.8)] conditions,

$$C_\ell = \left(\frac{X_0 s_0}{\mu_0\sigma_{v0}}\right)^{-1} \int_0^{s_0} ds \frac{X(s)}{\mu_0\sigma_v(s)} k_\ell(s) k_{t0}(s) \tag{A.18}$$

To find the ℓth eigenfunction, then, we first find the coefficients of modes 0 through $\ell - 1$ for our trial function, and then generate a modified trial function that has mode ℓ as its lowest-order mode:

$$k_{t'0}(s) = k_{t0}(s) - \sum_{\ell'=0}^{\ell-1} C_{\ell'} k_{\ell'(s)} \tag{A.19}$$

If we apply the operator as before, starting with this *modified* trial function, then $k_\ell(s)$ will in principle emerge as the surviving term. In practice, however, numerical errors cause lower-order terms to reappear, and these would eventually dominate so that the procedure would once again lead to $k_0(s)$. To prevent this from occurring, the lower-order eigenfunctions are filtered out as explained above from each $k_{t'N}(s)$ before continuing the sequence.

In the case of an up-down symmetric vacuum vessel, such as that of Doublet III–D, the eigenmodes are of two types: up-down symmetric and antisymmetric. Only the antisymmetric modes are excited by vertical plasma displacements, so the others can be neglected for purposes of this paper. The antisymmetric modes are selected by starting with an antisymmetric trial function and enforcing antisymmetry periodically to keep the symmetric

modes from entering due to numerical errors. The eigenfunctions for the first three anti-symmetric eigenmodes (numbered $\ell = 0$, 1, and 2, as though the symmetric ones did not exist) are plotted in Fig. 3 of the text. Table I lists the time constants and the parameter $2M_{\ell p}^{\prime 2} X_0/\mu_0 L_\ell$, which is a measure of the mode's effectiveness in vertical stabilization.

Appendix B.
THE HYBRID SYSTEM

As in Section 2 we begin with the open-loop system. We replace the subscript a with s (slow) and f (fast) and extend the definitions of Section 2: $Q \equiv (\mu_0 \Gamma n/2X_0)$, $\alpha_{[v,s,f]} \equiv (M'_{p[v,s,f]}/L_{v,s,f})$, $\beta_{[s,f]} \equiv (M_{[s,f]v}/L[s,f])$, $\gamma_{[v,s,f]} \equiv (R_{[v,s,f]}/L_{[v,s,f]})$, $\delta_{[v,s,f]} \equiv (M'_{p[v,s,f]}/Q)$; we add the definitions $\epsilon_s \equiv (M_{s,f}/L_s)$, $\epsilon_f \equiv (M_{s,f}/L_f)$, $\nu_s \equiv (M_{s,v}/L_v)$, $\nu_f \equiv (M_{f,v}/L_v)$, reducing all coefficients to a single number. The set of equations to be solved is

$$\begin{pmatrix} s & -\delta_v s & -\delta_s s & -\delta_f s \\ \alpha_v s & s+\gamma_v & \nu_s s & \nu_f s \\ \alpha_s s & \beta_s s & s+\gamma_s & \epsilon_s s \\ \alpha_f s & \beta_f s & \epsilon_f s & \gamma_f + s \end{pmatrix} \times \begin{pmatrix} \mathcal{Z}(s) \\ \mathcal{I}_v(s) \\ \mathcal{I}_s(s) \\ \mathcal{I}_f(s) \end{pmatrix} = \tag{B.1}$$

$$\begin{pmatrix} z_0 - \delta_v I_{v_0} - \delta_s I_{s_0} - \delta_f I_{f_0} \\ \alpha_v z_0 + I_{v_0} + \nu_s I_{s_0} + \nu_f I_{f_0} \\ \alpha_s z_0 + \beta_s I_{v_0} + I_{s_0} + \epsilon_s I_{f_0} + \mathcal{V}_s(s)/L_s \\ \alpha_f z_0 + \beta_f I_{v_0} + \epsilon_f I_{s_0} + I_{f_0} \mathcal{V}_f(s)/L_f \end{pmatrix}$$

Inverting the matrix $\vec{\vec{H}}^{-1}$ and extracting the characteristic polynomial, we have

$$\vec{\vec{\hat{H}}}(s) = s^3 \times \vec{\vec{\hat{H}}}^{(3)}(s) + s^2 \times \vec{\vec{\hat{H}}}^{(2)}(s) \tag{B.2}$$

$$+ s \times \begin{pmatrix} (\gamma_s+\gamma_f)\gamma_v + \gamma_f\gamma_s & \delta_v\gamma_f\gamma_s & \delta_s\gamma_f\gamma_v & \delta_f\gamma_s\gamma_v \\ -\alpha_v\gamma_f\gamma_s & \gamma_f\gamma_s & 0 & 0 \\ -\alpha_s\gamma_f\gamma_v & 0 & \gamma_f\gamma_v & 0 \\ -\alpha_f\gamma_s\gamma_v & 0 & 0 & \gamma_s\gamma_v \end{pmatrix}$$

$$+ \begin{pmatrix} \gamma_f\gamma_s\gamma_v & 0 & 0 & 0 \\ 0 & 0 & 0 & 0 \\ 0 & 0 & 0 & 0 \\ 0 & 0 & 0 & 0 \end{pmatrix}$$

where $\vec{\vec{\hat{H}}}^{(3)}(s)$ and $\vec{\vec{\hat{H}}}^{(2)}(s)$ are

$$\hat{H}^{(3)}_{1,1} = (\beta_f\epsilon_s - \beta_s)\nu_s + (\beta_s\epsilon_f - \beta_f)\nu_f - \epsilon_f\epsilon_s + 1 \tag{B.3}$$

$$\hat{H}^{(3)}_{2,1} = (\alpha_s - \alpha_f\epsilon_s)\nu_s + (\alpha_f - \alpha_s\epsilon_f)\nu_f + \alpha_v\epsilon_f\epsilon_s - \alpha_v \tag{B.4}$$

$$\hat{H}^{(3)}_{3,1} = (\alpha_s\beta_f - \alpha_f\beta_s)\nu_f + (\alpha_f - \alpha_v\beta_f)\epsilon_s + \alpha_v\beta_s - \alpha_s \tag{B.5}$$

$$\hat{H}^{(3)}_{4,1} = (\alpha_f\beta_s - \alpha_s\beta_f)\nu_s + (\alpha_s - \alpha_v\beta_s)\epsilon_f + \alpha_v\beta_f - \alpha_f \tag{B.6}$$

$$\hat{H}^{(3)}_{1,2} = (\beta_f\delta_s - \delta_v\epsilon_f)\epsilon_s + \beta_s\delta_f\epsilon_f + \delta_v - \beta_s\delta_s - \beta_f\delta_f \tag{B.7}$$

$$\hat{H}^{(3)}_{2,2} = (-\epsilon_f - \alpha_f\delta_s)\epsilon_s - \alpha_s\delta_f\epsilon_f + \alpha_s\delta_s + \alpha_f\delta_f + 1 \tag{B.8}$$

$$\hat{H}^{(3)}_{3,2} = (\alpha_f\delta_v + \beta_f)\epsilon_s - \alpha_s\delta_v + (\alpha_s\beta_f - \alpha_f\beta_s)\delta_f - \beta_s \tag{B.9}$$

$$\hat{H}^{(3)}_{4,2} = (\alpha_s\delta_v + \beta_s)\epsilon_f - \alpha_f\delta_v + (\alpha_f\beta_s - \alpha_s\beta_f)\delta_s - \beta_f \tag{B.10}$$

$$\hat{H}^{(3)}_{1,3} = (\beta_f\delta_f - \delta_v)\nu_s + (\delta_v\epsilon_f - \beta_f\delta_s)\nu_f - \delta_f\epsilon_f + \delta_s \tag{B.11}$$

$$\hat{H}^{(3)}_{2,3} = (-\alpha_f\delta_f - 1)\nu_s + (\epsilon_f + \alpha_f\delta_s)\nu_f + \alpha_v\delta_f\epsilon_f - \alpha_v\delta_s \tag{B.12}$$

$$\hat{H}^{(3)}_{3,3} = (-\alpha_f\delta_v - \beta_f)\nu_f + \alpha_v\delta_v + (\alpha_f - \alpha_v\beta_f)\delta_f + 1 \tag{B.13}$$

$$\hat{H}^{(3)}_{4,3} = (\alpha_f\delta_v + \beta_f)\nu_s + (-\alpha_v\delta_v - 1)\epsilon_f + (\alpha_v\beta_f - \alpha_f)\delta_s \tag{B.14}$$

$$\hat{H}^{(3)}_{1,4} = (\delta_v\epsilon_s - \beta_s\delta_f)\nu_s + (\beta_s\delta_s - \delta_v)\nu_f - \delta_s\epsilon_s + \delta_f \tag{B.15}$$

$$\hat{H}^{(3)}_{2,4} = (\epsilon_s + \alpha_s\delta_f)\nu_s + (-\alpha_s\delta_s - 1)\nu_f + \alpha_v\delta_s\epsilon_s - \alpha_v\delta_f \tag{B.16}$$

$$\hat{H}^{(3)}_{3,4} = (\alpha_s\delta_v + \beta_s)\nu_f + (-\alpha_v\delta_v - 1)\epsilon_s + (\alpha_v\beta_s - \alpha_s)\delta_f \tag{B.17}$$

$$\hat{H}^{(3)}_{4,4} = (-\alpha_s\delta_v - \beta_s)\nu_s + \alpha_v\delta_v + (\alpha_s - \alpha_v\beta_s)\delta_s + 1 \tag{B.18}$$

$$\hat{H}^{(2)}_{1,1} = -\beta_s\gamma_f\nu_s - \beta_f\gamma_s\nu_f + (1 - \epsilon_f\epsilon_s)\gamma_v + \gamma_s + \gamma_f \tag{B.19}$$

$$\hat{H}^{(2)}_{2,1} = \alpha_s\gamma_f\nu_s + \alpha_f\gamma_s\nu_f - \alpha_v\gamma_s - \alpha_v\gamma_f \tag{B.20}$$

$$\hat{H}^{(2)}_{3,1} = (\alpha_f\epsilon_s - \alpha_s)\gamma_v + (\alpha_v\beta_s - \alpha_s)\gamma_f \tag{B.21}$$

$$\hat{H}^{(2)}_{4,1} = (\alpha_s\epsilon_f - \alpha_f)\gamma_v + (\alpha_v\beta_f - \alpha_f)\gamma_s \tag{B.22}$$

$$\hat{H}^{(2)}_{1,2} = (\delta_v - \beta_f\delta_f)\gamma_s + (\delta_v - \beta_s\delta_s)\gamma_f \tag{B.23}$$

$$\hat{H}^{(2)}_{2,2} = (\alpha_f\delta_f + 1)\gamma_s + (\alpha_s\delta_s + 1)\gamma_f \tag{B.24}$$

$$\hat{H}^{(2)}_{3,2} = (-\alpha_s\delta_v - \beta_s)\gamma_f \tag{B.25}$$

$$\hat{H}^{(2)}_{4,2} = (-\alpha_f\delta_v - \beta_f)\gamma_s \tag{B.26}$$

$$\hat{H}^{(2)}_{1,3} = -\delta_v\gamma_f\nu_s + (\delta_s - \delta_f\epsilon_f)\gamma_v + \delta_s\gamma_f \tag{B.27}$$

$$\hat{H}^{(2)}_{2,3} = -\gamma_f \nu_s - \alpha_v \delta_s \gamma_f \tag{B.28}$$

$$\hat{H}^{(2)}_{3,3} = (\alpha_f \delta_f + 1)\gamma_v + (\alpha_v \delta_v + 1)\gamma_f \tag{B.29}$$

$$\hat{H}^{(2)}_{4,3} = (-\epsilon_f - \alpha_f \delta_s)\gamma_v \tag{B.30}$$

$$\hat{H}^{(2)}_{1,4} = -\delta_v \gamma_s \nu_f + (\delta_f - \delta_s \epsilon_s)\gamma_v + \delta_f \gamma_s \tag{B.31}$$

$$\hat{H}^{(2)}_{2,4} = -\gamma_s \nu_f - \alpha_v \delta_f \gamma_s \tag{B.32}$$

$$\hat{H}^{(2)}_{3,4} = (-\epsilon_s - \alpha_s \delta_f)\gamma_v \tag{B.33}$$

$$\hat{H}^{(2)}_{4,4} = (\alpha_s \delta_s + 1)\gamma_v + (\alpha_v \delta_v + 1)\gamma_s \tag{B.34}$$

The characteristic polynomial for this system is

$$\begin{aligned}
C(s) \;=\; & \\
& s^4\{[(\alpha_f \delta_v + \beta_f)\epsilon_s - \alpha_s \delta_v + (\alpha_s \beta_f - \alpha_f \beta_s)\delta_f - \beta_s]\nu_s \\
& + [(\alpha_s \delta_v + \beta_s)\epsilon_f - \alpha_f \delta_v + (\alpha_f \beta_s - \alpha_s \beta_f)\delta_s - \beta_f]\nu_f \\
& + [(-\alpha_v \delta_v - 1)\epsilon_f + (\alpha_v \beta_f - \alpha_f)\delta_s]\epsilon_s + (\alpha_v \beta_s - \alpha_s)\delta_f \epsilon_f + \alpha_v \delta_v \\
& + (\alpha_s - \alpha_v \beta_s)\delta_s + (\alpha_f - \alpha_v \beta_f)\delta_f + 1\} \\
+ \;& s^3\{(-\alpha_s \delta_v - \beta_s)\gamma_f \nu_s + (-\alpha_f \delta_v - \beta_f)\gamma_s \nu_f \\
& + [(-\epsilon_f - \alpha_f \delta_s)\epsilon_s - \alpha_s \delta_f \epsilon_f + \alpha_s \delta_s + \alpha_f \delta_f + 1]\gamma_v \\
& + [\alpha_v \delta_v + (\alpha_f - \alpha_v \beta_f)\delta_f + 1]\gamma_s + [\alpha_v \delta_v + (\alpha_s - \alpha_v \beta_s)\delta_s + 1]\gamma_f\} \\
+ \;& s^2\{[(\alpha_f \delta_f + 1)\gamma_s + (\alpha_s \delta_s + 1)\gamma_f]\gamma_v \\
& + (\alpha_v \delta_v + 1)\gamma_f \gamma_s\} \\
+ \;& s^1(\gamma_f \gamma_s \gamma_v)
\end{aligned} \tag{B.35}$$

Factoring out the trivial root, and denoting the remaining roots of $C(s)$ as $s_{[1,2,3]}$, we arrive at the time domain solutions for the system in vectorized form:

$$\begin{aligned}
\begin{pmatrix} z(t) \\ I_v(t) \\ I_s(t) \\ I_f(t) \end{pmatrix} &= \vec{S}_3 \left[\frac{(s_2 - s_1)s_3^2 e^{s_3 t} + (s_1 s_2^2 - s_2^2 s_3)e^{s_2 t} + (s_1^2 s_3 - s1^2 s_2)e^{s_1 t}}{(s_2 - s_1)s_3^2 + (s_1^2 - s_2^2)s_3 + s_1 s_2^2 - s_1^2 s_2} \right] \\
&+ \vec{S}_2 \left[\frac{(s_2 - s_1)s_3 e^{s_3 t} + (s_1 s_2 - s_2 s_3)e^{s_2 t} + (s_1 s_3 - s_1 s_2)e^{s_1 t}}{(s_2 - s_1)s_3^2 + (s_1^2 - s_2^2)s_3 + s_1 s_2^2 - s_1^2 s_2} \right] \\
&+ \vec{S}_1 \left[\frac{(s_2 - s_1)e^{s_3 t} + (s_1 - s_3)e^{s_2 t} + (s_3 - s_2)e^{s_1 t}}{(s_2 - s_1)s_3^2 + (s_1^2 - s_2^2)s_3 + s_1 s_2^2 - s_1^2 s_2} \right] \\
&+ \vec{S}_0 \left[\frac{(s_1 s_2^2 - s_1^2 s_2)e^{s_3 t} + (s_1^2 s_3 - s_1 s_3^2)e^{s_2 t} + (s_2 s_3^2 - s_2^2 s_3)e^{s_1 t}}{(s_1 s_2^2 - s_1^2 s_2)s_3^3 + (s_1^3 s_2 - s_1 s_2^3)s_3^2 + (s_1^2 s_2^3 - s_1^3 s_2^2)s_3} \right] \\
&+ \vec{S}_0 \left[\frac{(s_1 - s_2)s_3^2 + (s_2^2 - s_1^2)s_3 - s_1 s_2^2 + s_1^2 s_2}{(s_1 s_2^2 - s_1^2 s_2)s_3^3 + (s_1^3 s_2 - s_1 s_2^3)s_3^2 + (s_1^2 s_2^3 - s_1^3 s_2^2)s_3} \right]
\end{aligned} \tag{B.36}$$

Defining

$$\begin{aligned}
\ell_e &\equiv [(\alpha_f \delta_v + \beta_f)\epsilon_s - \alpha_s \delta_v + (\alpha_s \beta_f - \alpha_f \beta_s)\delta_f - \beta_s]\nu_s \\
&+ [(\alpha_s \delta_v + \beta_s)\epsilon_f - \alpha_f \delta_v + (\alpha_f \beta_s - \alpha_s \beta_f)\delta_s - \beta_f]\nu_f \\
&+ [(-\alpha_v \delta_v - 1)\epsilon_f + (\alpha_v \beta_f - \alpha_f)\delta_s]\epsilon_s \\
&+ (\alpha_v \beta_s - \alpha_s)\delta_f \epsilon_f + \alpha_v \delta_v \\
&+ (\alpha_s - \alpha_v \beta_s)\delta_s + (\alpha_f - \alpha_v \beta_f)\delta_f + 1
\end{aligned} \tag{B.37}$$

the solution vectors are

$$\vec{S}_3 = \begin{pmatrix} z_0 \\ I_{v_0} \\ I_{s_0} \\ I_{f_0} \end{pmatrix} \tag{B.38}$$

$$\vec{\tilde{S}}_2(1) = -\frac{1}{\ell_e} \times \tag{B.39}$$

$$\left(\begin{array}{c}
\{(\alpha_s\delta_v + \beta_s)\gamma_f\nu_s + (\alpha_f\delta_v + \beta_f)\gamma_s\nu_f + [(\epsilon_f + \alpha_f\delta_s)\epsilon_s \\
+ \alpha_s\delta_f\epsilon_f - \alpha_s ds - \alpha_f\delta_f - 1]\gamma_v + [-\alpha_v\delta_v + (\alpha_v\beta_f - \alpha_f)\delta_f - 1]\gamma_s \\
+ [-\alpha_v\delta_v + (\alpha_v\beta_s - \alpha_s)\delta_s - 1]\gamma_f\}z_0 \\
+ [(\beta_f\delta_s - \delta_v\epsilon_f)\epsilon_s + \beta_s\delta_f\epsilon_f + \delta_v - \beta_s\delta_s - \beta_f\delta_f]\gamma_v I_{v_0} \\
+ [(\beta_f\delta_f - \delta_v)\gamma_s\nu_s + (\delta_v\epsilon_f - \beta_f\delta_s)\gamma_s\nu_f + (\delta_s - \delta_f\epsilon_f)\gamma_s]I_{s_0} \\
+ [(\delta_v\epsilon_s - \beta_s\delta_f)\gamma_f\nu_s + (\beta_s\delta_s - \delta_v)\gamma_f\nu_f + (\delta_f - \delta_s\epsilon_s)\gamma_f]I_{f_0} \\
+ [-\frac{V_f}{L_f}\delta_v\epsilon_s + \alpha_v s\delta_v + (\frac{V_f}{L_f}\beta_s - \frac{V_s}{L_s}\beta_f)\delta_f]\nu_s \\
+ [-\frac{V_s}{L_s}\delta_v\epsilon_f + \frac{V_f}{L_f}\delta_v + (\frac{V_s}{L_s}\beta_f - \frac{V_f}{L_f}\beta_s)\delta_s]\nu_f \\
+ \frac{V_f}{L_f}\delta_s\epsilon_s + \frac{V_s}{L_s}\delta_f\epsilon_f - \frac{V_s}{L_s}\delta_s - \frac{V_f}{L_f}\delta_f \\
\\
\{(\alpha_s\delta_v + \beta_s)\gamma_f\nu_s + (\alpha_f\delta_v + \beta_f)\gamma_s\nu_f + [-\alpha_v\delta_v + (\alpha_v\beta_f \\
- \alpha_f)\delta_f - 1]\gamma_s + [-\alpha_v\delta_v + (\alpha_v\beta_s - \alpha_s)\delta_s - 1]\gamma_f\}I_{v_0} \\
+ [(-\alpha_f\delta_f - 1)\gamma_s\nu_s + (\epsilon_f + \alpha_f\delta_s)\gamma_s\nu_f + (\alpha_v\delta_f\epsilon_f - \alpha_v\delta_s)\gamma_s]I_{s_0} \\
+ [(\epsilon_s + \alpha_s\delta_f)\gamma_f\nu_s + (-\alpha_s\delta_s - 1)\gamma_f\nu_f + (\alpha_v\delta_s\epsilon_s - \alpha_v\delta_f)\gamma_f]I_{f_0} \\
+] - \frac{V_f}{L_f}\epsilon_s + (\alpha_f\frac{V_s}{L_s} - \alpha_s\frac{V_f}{L_f})\delta_f + \frac{V_s}{L_s}]\nu_s \\
+ [-\frac{V_s}{L_s}\epsilon_f + (\alpha_s\frac{V_f}{L_f} - \alpha_f\frac{V_s}{L_s})\delta_s + \frac{V_f}{L_f}]\nu_f \\
- \alpha_v\frac{V_f}{L_f}\delta_s\epsilon_s - \alpha_v\frac{V_s}{L_s}\delta_f\epsilon_f + av\frac{V_s}{L_s}\delta_s + \alpha_v\frac{V_f}{L_f}\delta_f \\
\\
[(\alpha_f\delta_v + \beta_f)\epsilon_s - \alpha_s\delta_v + (\alpha_s\beta_f - \alpha_f\beta_s)\delta_f - \beta_s]\gamma_v I_{v_0} \\
+ \{(\alpha_s\delta_v + \beta_s)\gamma_f\nu_s + [(\epsilon_f + \alpha_f\delta_s)\epsilon_s + \alpha_s\delta_f\epsilon_f \\
-\alpha_s\delta_s - \alpha_f\delta_f - 1]\gamma_v + [-\alpha_v\delta_v + (\alpha_v\beta_s - \alpha_s)\delta_s - 1]\gamma_f\}I_{s_0} \\
+ \{(\alpha_s\delta_v + \beta_s)\gamma_f\nu_f + [(-\alpha_v\delta_v - 1)\epsilon_s + (\alpha_v\beta_s - \alpha_s)\delta_f]\gamma_f\}I_{f_0} \\
+ \left[\left(\alpha_f\frac{V_s}{L_s} - \alpha_s\frac{V_f}{L_f}\right)\delta_v - \frac{V_f}{L_f}\beta_s + \frac{V_s}{L_s}\beta_f\right]\nu_f \\
+ \left(\alpha_v\frac{V_f}{L_f}\delta_v + \frac{V_f}{L_f}\right)\epsilon_s - \alpha_v\frac{V_s}{L_s}\delta_v \\
+ (-\alpha_v\frac{V_f}{L_f}\beta_s + \alpha_v\frac{V_s}{L_s}\beta_f - \alpha_f\frac{V_s}{L_s} + \alpha_s\frac{V_f}{L_f})\delta_f - \frac{V_s}{L_s} \\
\\
[(\alpha_s\delta_v + \beta_s)\epsilon_f - \alpha_f\delta_v + (\alpha_f\beta_s - \alpha_s\beta_f)\delta_s - \beta_f]\gamma_v I_{v_0} \\
+ \{(\alpha_f\delta_v + \beta_f)\gamma_s\nu_s + [(-\alpha_v\delta_v - 1)\epsilon_f + (\alpha_v\beta_f - \alpha_f)\delta_s]\gamma_s\}I_{s_0} \\
+ \{(\alpha_f\delta_v + \beta_f)\gamma_s\nu_f + [(ef + \alpha_f\delta_s)\epsilon_s + \alpha_s\delta_f\epsilon_f - \alpha_s\delta_s - \alpha_f\delta_f - 1]\gamma_v \\
+ [-\alpha_v\delta_v + (\alpha_v\beta_f - \alpha_f)\delta_f - 1]\gamma_s\}I_{f_0} \\
+ \left[\left(\alpha_s\frac{V_f}{L_f} - \alpha_f\frac{V_s}{L_s}\right)\delta_v + \frac{V_f}{L_f}\beta_s - \frac{V_s}{L_s}\beta_f\right]\nu_s + \left(\alpha_v\frac{V_s}{L_s}\delta_v + \frac{V_s}{L_s}\right)\epsilon_f \\
-\alpha_v\frac{V_f}{L_f}\delta_v + \left(\alpha_v\frac{V_f}{L_f}\beta_s - \alpha_v\frac{V_s}{L_s}\beta_f + \alpha_f\frac{V_s}{L_s} - \alpha_s\frac{V_f}{L_f}\right)\delta_s - \frac{V_f}{L_f}
\end{array} \right)$$

$$\vec{\tilde{S}}_1 = \frac{1}{\ell_e} \times \tag{B.40}$$

$$\begin{pmatrix}
\{[(\alpha_f\delta_f+1)\gamma_s+(\alpha_s\delta_s+1)\gamma_f]\gamma_v+(\alpha_v\delta_v+1)\gamma_f\gamma_s\}z_0 \\
+[(\beta_f\delta_f-\delta_v)\gamma_s+(\beta_s\delta_s-\delta_v)\gamma_f]\gamma_v I_{v_0} \\
+[\delta_v\gamma_f\gamma_s\nu_s+(\delta_f\epsilon_f-\delta_s)\gamma_s\gamma_v-\delta_s\gamma_f\gamma_s]I_{s_0} \\
+[\delta_v\gamma_f\gamma_s\nu_f+(\delta_s\epsilon_s-\delta_f)\gamma_f\gamma_v-\delta_f\gamma_f\gamma_s]I_{f_0} \\
+\left(-\frac{V_f}{L_f}\delta_s\epsilon_s-\frac{V_s}{L_s}\delta_f\epsilon_f+\frac{V_s}{L_s}\delta_s+\frac{V_f}{L_f}\delta_f\right)\gamma_v-\frac{V_f}{L_f}\delta_v\gamma_s\nu_f \\
+\frac{V_f}{L_f}\delta_f\gamma_s+\frac{V_s}{L_s}\delta_s\gamma_f-\frac{V_s}{L_s}\delta_v\gamma_f\nu_s \\
\\
(\alpha_v\delta_v+1)\gamma_f\gamma_s I_{v_0}+(\gamma_f\gamma_s\nu_s+\alpha_v\delta_s\gamma_f\gamma_s)I_{s_0} \\
+(\gamma_f\gamma_s\nu_f+\alpha_v\delta_f\gamma_f\gamma_s)I_{f_0} \\
-\frac{V_s}{L_s}\gamma_f\nu_s-\frac{V_f}{L_f}\gamma_s\nu_f-\alpha_v\frac{V_f}{L_f}\delta_f\gamma_s-\alpha_v\frac{V_s}{L_s}\delta_s\gamma_f \\
\\
(\alpha_s\delta_v+\beta_s)\gamma_f\gamma_v I_{v_0}+(\alpha_s\delta_s+1)\gamma_f\gamma_v I_{s_0}+(\epsilon_s+\alpha_s\delta_f)\gamma_f\gamma_v I_{f_0} \\
+\left[\left(\alpha_f\frac{V_s}{L_s}-\alpha_s\frac{V_f}{L_f}\right)\delta_f+\frac{V_s}{L_s}\right]\gamma_v+\left(\alpha_v\frac{V_s}{L_s}\delta_v+\frac{V_s}{L_s}\right)\gamma_f-\frac{V_f}{L_f}\epsilon_s \\
\\
(\alpha_f\delta_v+\beta_f)\gamma_s\gamma_v I_{v_0}+(\epsilon_f+\alpha_f\delta_s)\gamma_s\gamma_v I_{s_0}+(\alpha_f\delta_f+1)\gamma_s\gamma_v I_{f_0} \\
++\left[\left(\alpha_s\frac{V_f}{L_f}-\alpha_f\frac{V_s}{L_s}\right)\delta_s+\frac{V_f}{L_f}\right]\gamma_v+\left(\alpha_v\frac{V_f}{L_f}\delta_v+\frac{V_f}{L_f}\right)\gamma_s-\frac{V_s}{L_s}\epsilon_f
\end{pmatrix}$$

$$\vec{\tilde{S}}_0 = \frac{1}{\ell_e} \times \tag{B.41}$$

$$\begin{pmatrix}
\gamma_f\gamma_s\gamma_v z_0-\delta_v\gamma_f\gamma_s\gamma_v I_{v_0}-\delta_s\gamma_f\gamma_s\gamma_v I_{s_0}-\delta_f\gamma_f\gamma_s\gamma_v I_{f_0} \\
+\left(\frac{V_f}{L_f}\delta_f\gamma_s+\frac{V_s}{L_s}\delta_s\gamma_f\right)\gamma_v \\
\\
0 \\
\\
\frac{V_s}{L_s}\gamma_f\gamma_v \\
\\
\frac{V_f}{L_f}\gamma_s\gamma_v \\
\\
\end{pmatrix}$$

We now proceed to obtain the closed-loop characteristic polynomial and transfer function. Here there are proportional and derivative gains for both active circuits. Thus,

$$\vec{\vec{H}}_{cl}^{-1} = \begin{pmatrix}
s & -\delta_v s & -\delta_s s & -\delta_f s \\
\alpha_v s & s+\gamma_v & \nu_s s & \nu_f s \\
-G_{v_s}s+\alpha_s s-G_{z_s} & \beta_s s & s+\gamma_s & \epsilon_s s \\
-G_{v_f}s+\alpha_f s-G_{z_f} & \beta_f s & \epsilon_f s & s+\gamma_f
\end{pmatrix} \tag{B.42}$$

We express the reduced transfer matrix in terms of its value relative to the open-loop system by defining

$$\vec{\vec{D}} \equiv \vec{\vec{H}}_{cl} - \vec{\vec{H}} \tag{B.43}$$

Then

$$D_{1,1} = D_{1,2} = D_{1,3} = D_{1,4} = 0 \tag{B.44}$$

$$\begin{aligned} D_{2,1} &= s^3[(\epsilon_s G_{v_f} - G_{v_s})\nu_s + (\epsilon_f G_{v_s} - G_{v_f})\nu_f] \\ &+ s^2[(-G_{z_s} + \epsilon_s G_{z_f} - \gamma_f G_{v_s})\nu_s + (\epsilon_f G_{z_s} - G_{z_f} - \gamma_s G_{v_f})\nu_f] \\ &+ s(-\gamma_f G_{z_s}\nu_s - \gamma_s G_{z_f}\nu_f) \end{aligned} \tag{B.45}$$

$$\begin{aligned} D_{2,2} &= s^3[(\delta_f\epsilon_f - \delta_s)G_{v_s} + (\delta_s\epsilon_s - \delta_f)G_{v_f}] \\ &+ s^2[(\delta_f\epsilon_f - \delta_s)G_{z_s} + (\delta_s\epsilon_s - \delta_f)G_{z_f} - \delta_s\gamma_f G_{v_s} - \delta_f\gamma_s G_{v_f}] \\ &+ s(-\delta_s\gamma_f G_{z_s} - \delta_f\gamma_s G_{z_f}) \end{aligned} \tag{B.46}$$

$$\begin{aligned} D_{2,3} &= s^3(\delta_f G_{v_f}\nu_s - \delta_s G_{v_f}\nu_f) \\ &+ s^2(\delta_f G_{z_f}\nu_s - \delta_s G_{z_f}\nu_f) \end{aligned} \tag{B.47}$$

$$\begin{aligned} D_{2,4} &= s^3(\delta_s G_{v_s}\nu_f - \delta_f G_{v_s}\nu_s) \\ &+ s^2(\delta_s G_{z_s}\nu_f - \delta_f G_{z_s}\nu_s) \end{aligned} \tag{B.48}$$

$$\begin{aligned} D_{3,1} &= s^3[(\beta_s G_{v_f} - \beta_f G_{v_s})\nu_f + G_{v_s} - \epsilon_s G_{v_f}] \\ &+ s^2[(\beta_s G_{z_f} - \beta_f G_{z_s})\nu_f + G_{z_s} - \epsilon_s G_{z_f} \\ &\quad + (\gamma_v + \gamma_f)G_{v_s} - \epsilon_s\gamma_v G_{v_f}] \\ &+ s[(\gamma_v + \gamma_f)G_{z_s} - \epsilon_s\gamma_v G_{z_f} + \gamma_f\gamma_v G_{v_s}] + \gamma_f\gamma_v G_{z_s} \end{aligned} \tag{B.49}$$

$$\begin{aligned} D_{3,1} &= s^3[(\beta_s G_{v_f} - \beta_f G_{v_s})\nu_f + G_{v_s} - \epsilon_s G_{v_f}] \\ &+ s^2[(\beta_s G_{z_f} - \beta_f G_{z_s})\nu_f + G_{z_s} - \epsilon_s G_{z_f} \\ &\quad + (\gamma_v + \gamma_f)G_{v_s} - \epsilon_s\gamma_v G_{v_f}] \\ &+ s[(\gamma_v + \gamma_f)G_{z_s} - \epsilon_s\gamma_v G_{z_f} + \gamma_f\gamma_v G_{v_s}] + \gamma_f\gamma_v G_{z_s} \end{aligned} \tag{B.50}$$

$$
\begin{aligned}
D_{3,2} &= s^3[(\delta_v - \beta_f\delta_f)G_{v_s} + (\beta_s\delta_f - \delta_v\epsilon_s)G_{v_f}] \\
&+ s^2[(\delta_v - \beta_f\delta_f)G_{z_s} + (\beta_s\delta_f - \delta_v\epsilon_s)G_{z_f} + \delta_v\gamma_f G_{v_s}] \\
&+ s\delta_v\gamma_f G_{z_s} \qquad \text{(B.51)}
\end{aligned}
$$

$$
\begin{aligned}
D_{3,3} &= s^3(\delta_v G_{v_f}\nu_f - \delta_f G_{v_f}) \\
&+ s^2(\delta_v G_{z_f}\nu_f - \delta_f G_{z_f} - \delta_f\gamma_v G_{v_f}) \\
&- s\delta_f\gamma_v G_{z_f} \qquad \text{(B.52)}
\end{aligned}
$$

$$
\begin{aligned}
D_{3,4} &= s^3(\delta_f G_{v_s} - \delta_v G_{v_s}\nu_f) \\
&+ s^2(-\delta_v G_{z_s}\nu_f + \delta_f G_{z_s} + \delta_f\gamma_v G_{v_s}) \\
&+ s\delta_f\gamma_v G_{z_s} \qquad \text{(B.53)}
\end{aligned}
$$

$$
\begin{aligned}
D_{4,1} &= s^3[(\beta_f G_{v_s} - \beta_s G_{v_f})\nu_s - \epsilon_f G_{v_s} + G_{v_f}] \\
&+ s^2[(\beta_f G_{z_s} - \beta_s G_{z_f})\nu_s - \epsilon_f G_{z_s} + G_{z_f} \\
&\quad - \epsilon_f\gamma_v G_{v_s} + (\gamma_v + \gamma_s)G_{v_f}] \\
&+ s[-\epsilon_f\gamma_v G_{z_s} + (\gamma_v + \gamma_s)G_{z_f} + \gamma_s\gamma_v G_{v_f}] + \gamma_s\gamma_v G_{z_f} \qquad \text{(B.54)}
\end{aligned}
$$

$$
\begin{aligned}
D_{4,2} &= s^3[(\beta_f\delta_s - \delta_v\epsilon_f)G_{v_s} + (\delta_v - \beta_s\delta_s)G_{v_f}] \\
&+ s^2[(\beta_f\delta_s - \delta_v\epsilon_f)G_{z_s} + (\delta_v - \beta_s\delta_s)G_{z_f} + \delta_v\gamma_s G_{v_f}] \\
&+ s\delta_v\gamma_s G_{z_f} \qquad \text{(B.55)}
\end{aligned}
$$

$$
\begin{aligned}
D_{4,3} &= s^3(\delta_s G_{v_f} - \delta_v G_{v_f}\nu_s) \\
&+ s^2(-\delta_v G_{z_f}\nu_s + \delta_s G_{z_f} + \delta_s\gamma_v G_{v_f}) \\
&+ s\delta_s\gamma_v G_{z_f} \qquad \text{(B.56)}
\end{aligned}
$$

$$
\begin{aligned}
D_{4,4} &= s^3(\delta_v G_{v_s}\nu_s - \delta_s G_{v_s}) \\
&+ s^2(\delta_v G_{z_s}\nu_s - \delta_s G_{z_s} - \delta_s\gamma_v G_{v_s}) \\
&- s\delta_s\gamma_v G_{z_s} \qquad \text{(B.57)}
\end{aligned}
$$

The elements $\hat{H}_{1,3}$ and $\hat{H}_{1,4}$ are unchanged in the closed-loop system, as expected from the results of Section 3. The closed-loop characteristic polynomial is

$$
\begin{aligned}
\frac{C_{cl}(s)}{s} = \quad & \\
& s^3\{[(\delta_v - \beta_f\delta_f)G_{v_s} + (\beta_s\delta_f - \delta_v\epsilon_s)G_{v_f} + (\alpha_f\delta_v + \beta_f)\epsilon_s - \alpha_s\delta_v \\
& + (\alpha_s\beta_f - \alpha_f\beta_s)\delta_f - \beta_s]\nu_s + [(\beta_f\delta_s - \delta_v\epsilon_f)G_{v_s} + (\delta_v - \beta_s\delta_s)G_{v_f} \\
& + (\alpha_s\delta_v + \beta_s)\epsilon_f - \alpha_f\delta_v + (\alpha_f\beta_s - \alpha_s\beta_f)\delta_s - \beta_f]\nu_f \\
& + (\delta_f\epsilon_f - \delta_s)G_{v_s} + (\delta_s\epsilon_s - \delta_f)G_{v_f} + [(-\alpha_v\delta_v - 1)\epsilon_f \\
& + (\alpha_v\beta_f - \alpha_f)\delta_s]\epsilon_s + (\alpha_v\beta_s - \alpha_s)\delta_f\epsilon_f + \alpha_v\delta_v \\
& + (\alpha_s - \alpha_v\beta_s)\delta_s + (\alpha_f - \alpha_v\beta_f)\delta_f + 1\} \\
+ \quad & s^2\{[(\delta_v - \beta_f\delta_f)G_{z_s} + (\beta_s\delta_f - \delta_v\epsilon_s)G_{z_f} + \delta_v\gamma_f G_{v_s} + (-\alpha_s\delta_v - \beta_s)\gamma_f]\nu_s \\
& + [(\beta_f\delta_s - \delta_v\epsilon_f)G_{z_s} + (\delta_v - \beta_s\delta_s)G_{z_f} + \delta_v\gamma_s G_{v_f} + (-\alpha_f\delta_v - \beta_f)\gamma_s]\nu_f \\
& + (\delta_f\epsilon_f - \delta_s)G_{z_s} + (\delta_s\epsilon_s - \delta_f)G_{z_f} + [(\delta_f\epsilon_f - \delta_s)\gamma_v - \delta_s\gamma_f]G_{v_s} \\
& + [(\delta_s\epsilon_s - \delta_f)\gamma_v - \delta_f\gamma_s]G_{v_f} \\
& + [(-\epsilon_f - \alpha_f\delta_s)\epsilon_s - \alpha_s\delta_f\epsilon_f + \alpha_s\delta_s + \alpha_f\delta_f + 1]\gamma_v \\
& + [\alpha_v\delta_v + (\alpha_f - \alpha_v\beta_f)\delta_f + 1]\gamma_s + [\alpha_v\delta_v + (\alpha_s - \alpha_v\beta_s)\delta_s + 1]\gamma_f\} \\
+ \quad & s^1\{\delta_v\gamma_f G_{z_s}\nu_s + \delta_v\gamma_s G_{z_f}\nu_f + [(\delta_f\epsilon_f - \delta_s)\gamma_v - \delta_s\gamma_f]G_{z_s} \\
& + [(\delta_s\epsilon_s - \delta_f)\gamma_v - \delta_f\gamma_s]G_{z_f} - \delta_s\gamma_f\gamma_v G_{v_s} - \delta_f\gamma_s\gamma_v G_{v_f} \\
& + [(\alpha_f\delta_f + 1)\gamma_s + (\alpha_s\delta_s + 1)\gamma_f]\gamma_v + (\alpha_v\delta_v + 1)\gamma_f\gamma_s\} \\
+ \quad & s^0(-\delta_s\gamma_f\gamma_v G_{z_s} - \delta_f\gamma_s\gamma_v G_{z_f} + \gamma_f\gamma_s\gamma_v)
\end{aligned}
\tag{B.58}
$$

REFERENCES

[1] MUKHOVATOV, V.S., SHAFRANOV, D., Nucl. Fusion **11** (1971) 605.

[2] NEILSON, G.H., DYER, G.R., EDMONDS, P.H., Nucl. Fusion **24** (1984) 1291.

[3] LAZARUS, E.A., NEILSON, G.H., Nucl. Fusion **27** (1987) 383.

[4] LISTER, J.B., LAZARUS, E.A., MORET, J.M., et al., to be submitted to Nucl. Fusion.

[5] JARDIN, S.C., LARRABEE, D.A., Nucl. Fusion **22** (1982) 1095.

[6] LEUER, J.A., General Atomics, personal communication, 1988.

LIST OF FIGURES

FIG. 17. Response for a typical case limited by power supply. For this case, $n = -1.32$, $n_c = 1.65$, $n_a = 0.65$, $G_z = -0.4$, *and* $G_v = -0.005$. *Shown are (a) the plasma position, (b) the vessel current, (c) the active coil current, and (d) the applied voltage. Along with the actual plasma position, the plasma positions which would occur with no amplitude and slew limits are shown in (a).*

FIG. 18. Flux contours of the antisymmetric vessel current in the (R, Z) *plane.*

FIG. 19. Flux contours for stationary active coil currents in (a) the F7 coil and (b) the F2 coil, and flux contours following an instantaneous jump in the active coil current when the induced vessel current is added in (c) the F7 coil and (d) the F2 coil.

FIG. 20. Maximum decay index achievable as a function of G_v $(G_z = -0.1)$.

FIG. 21. Open-loop growth rate versus $-n/n_c$. *With (a) the F7 coils only, (b) the F2 coils only, and (c) the hybrid system.*

FIG. 22. Block diagram of hybrid vertical control system as modelled in calculation of power supply requirements.

FIG. 23. System response for an underdamped case controlled with the F6+F7 coils.

FIG. 24. Maximum values of $-n$ *reached during decay index ramps terminating in a loss of vertical control disruption, with and without the use of the F2 coils.*

FIG. 25. (a) A highly elongated $(\kappa = 3)$ *plasma within the DIII-D vessel. (b) The intersection of the plasma field with the vacuum vessel.*

FIG. 26. A circuit representation of the vacuum vessel eigenmodes $(\ell = 1, 2, 3, ...)$, *with the plasma and active coils.*

FIG. 27. Parametric description of a vacuum vessel with arbitrary cross-section for eigenmode analysis.

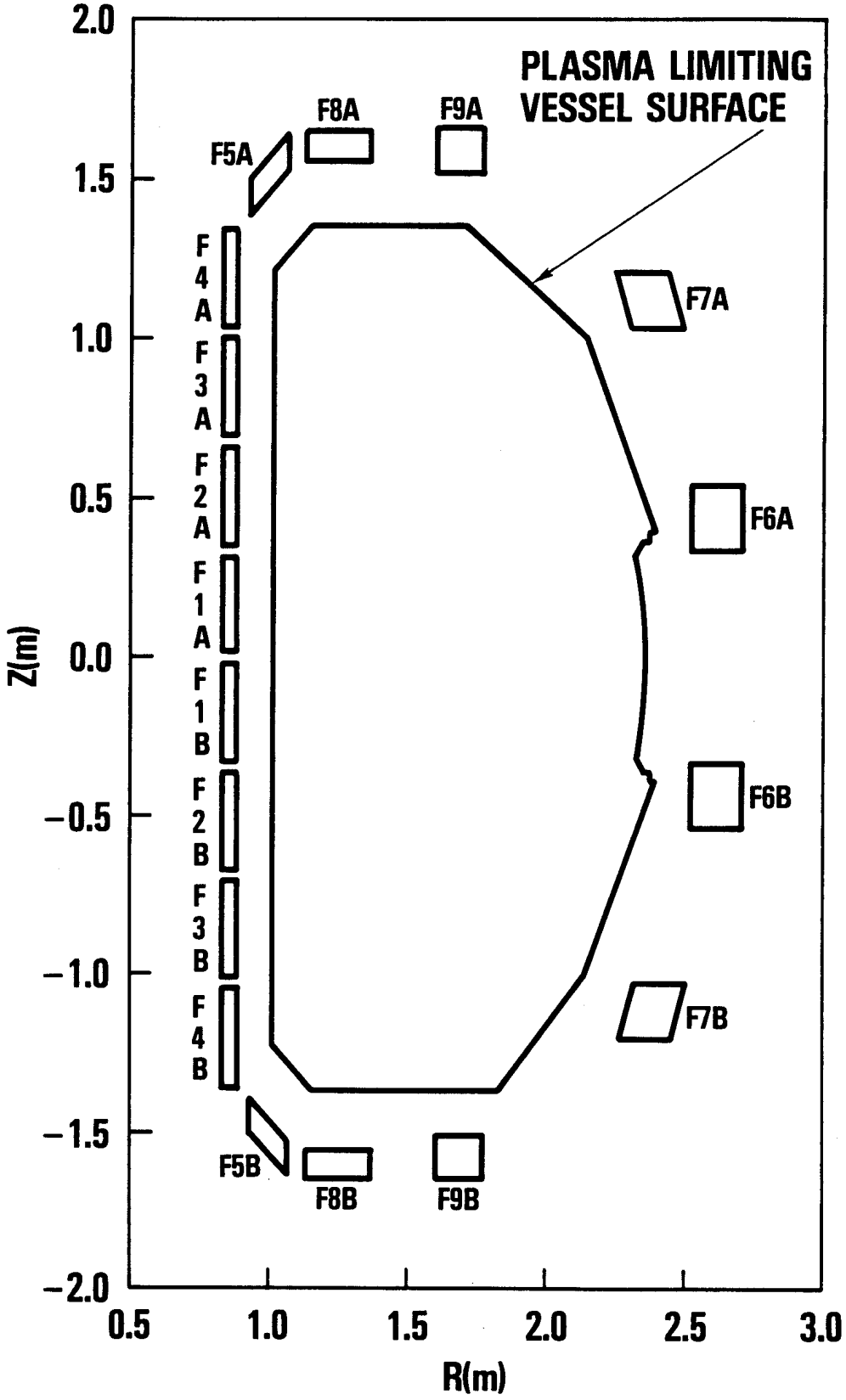

LAZARUS, et al. Fig. 1

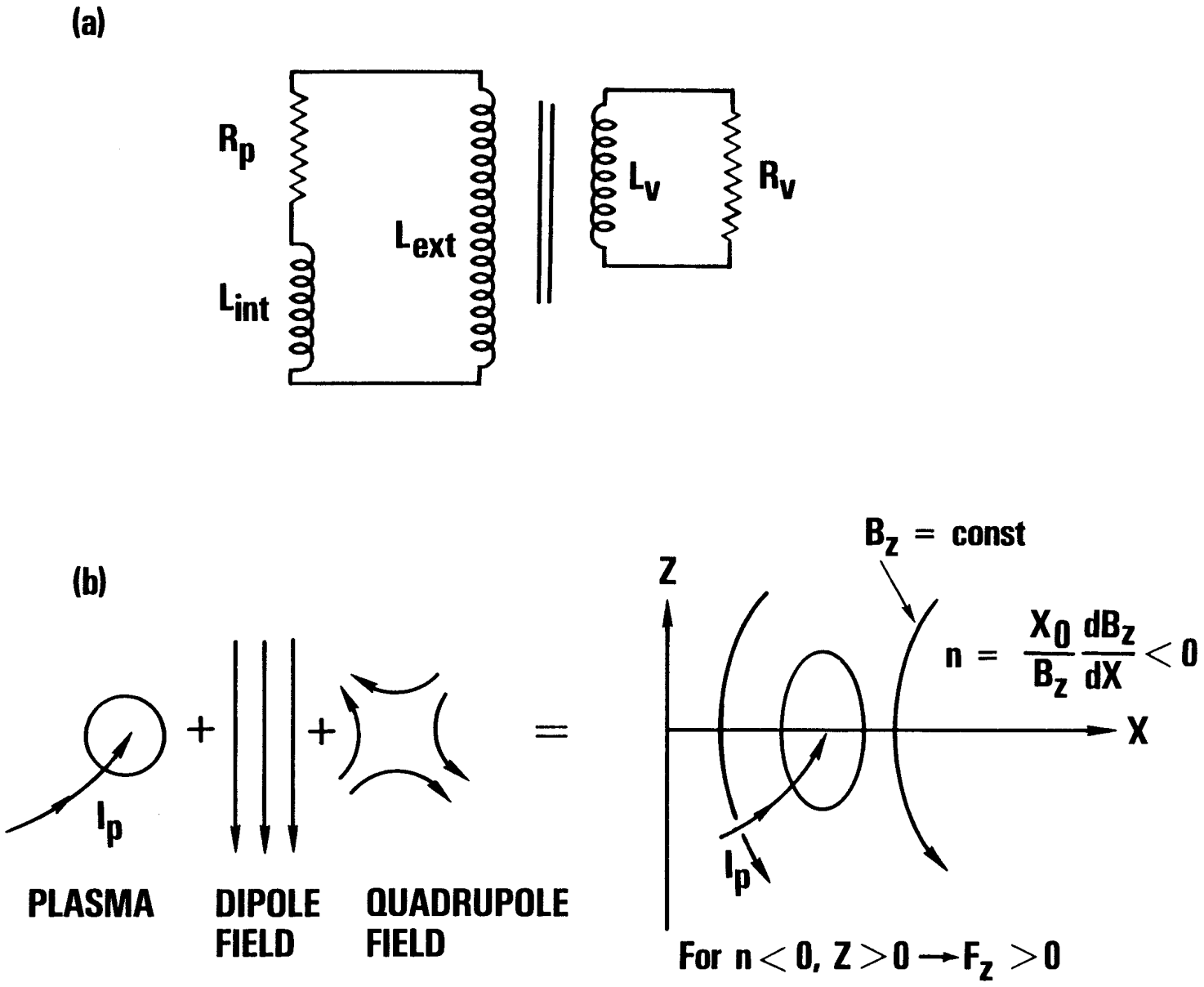

LAZARUS, et al.

Fig. 2

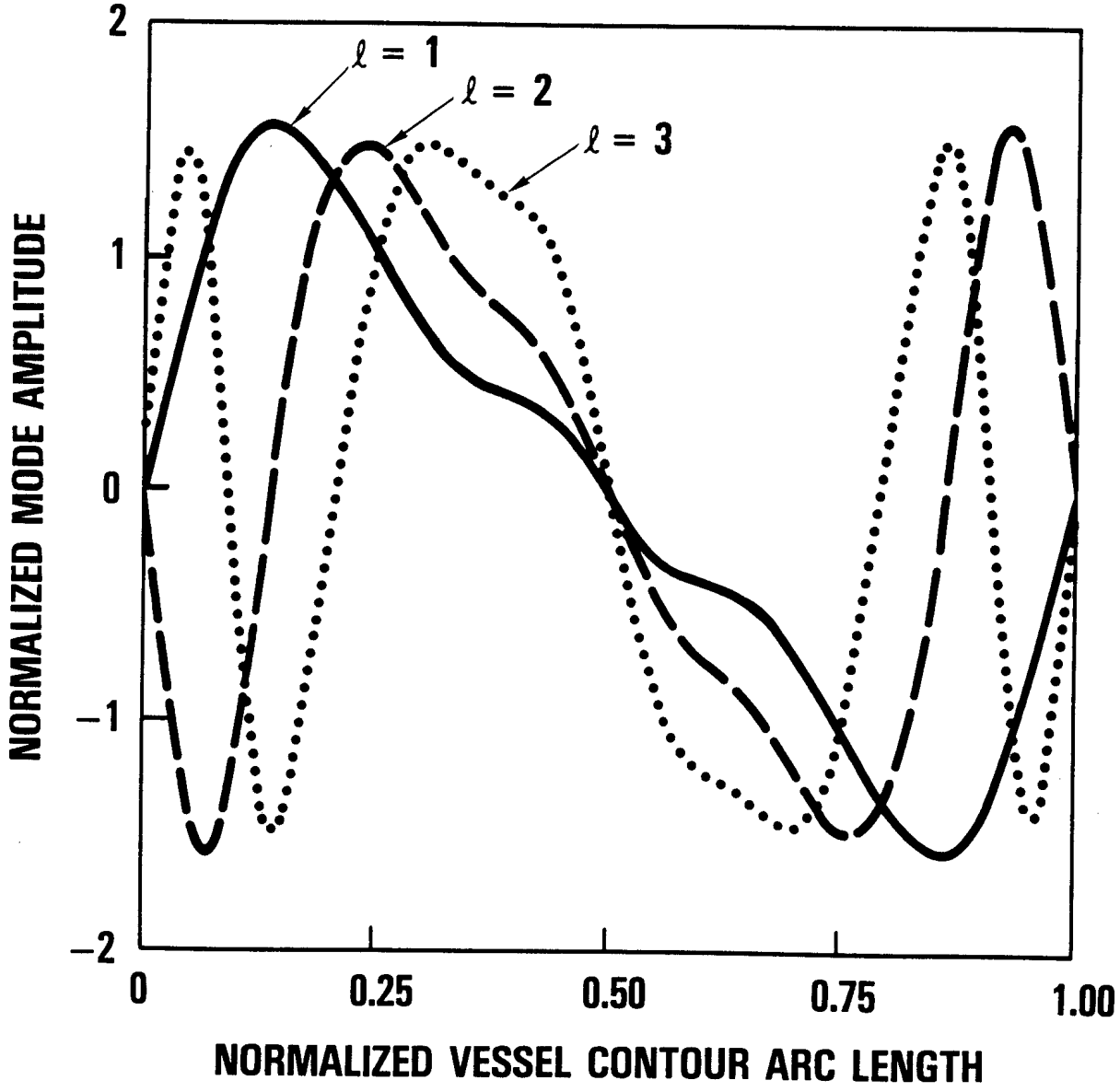

LAZARUS, et al. Fig. 3

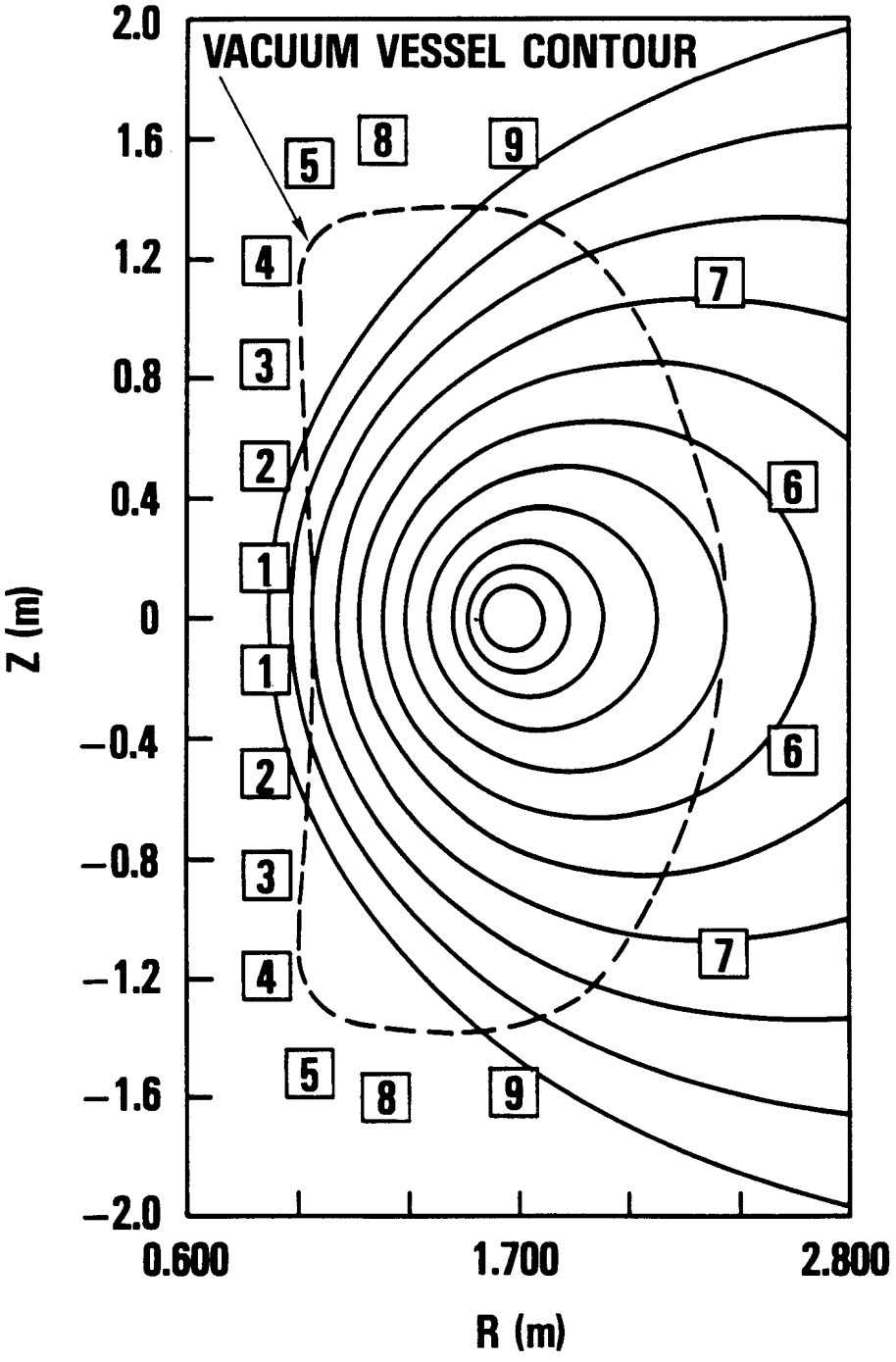

LAZARUS, et al. **Fig. 4**

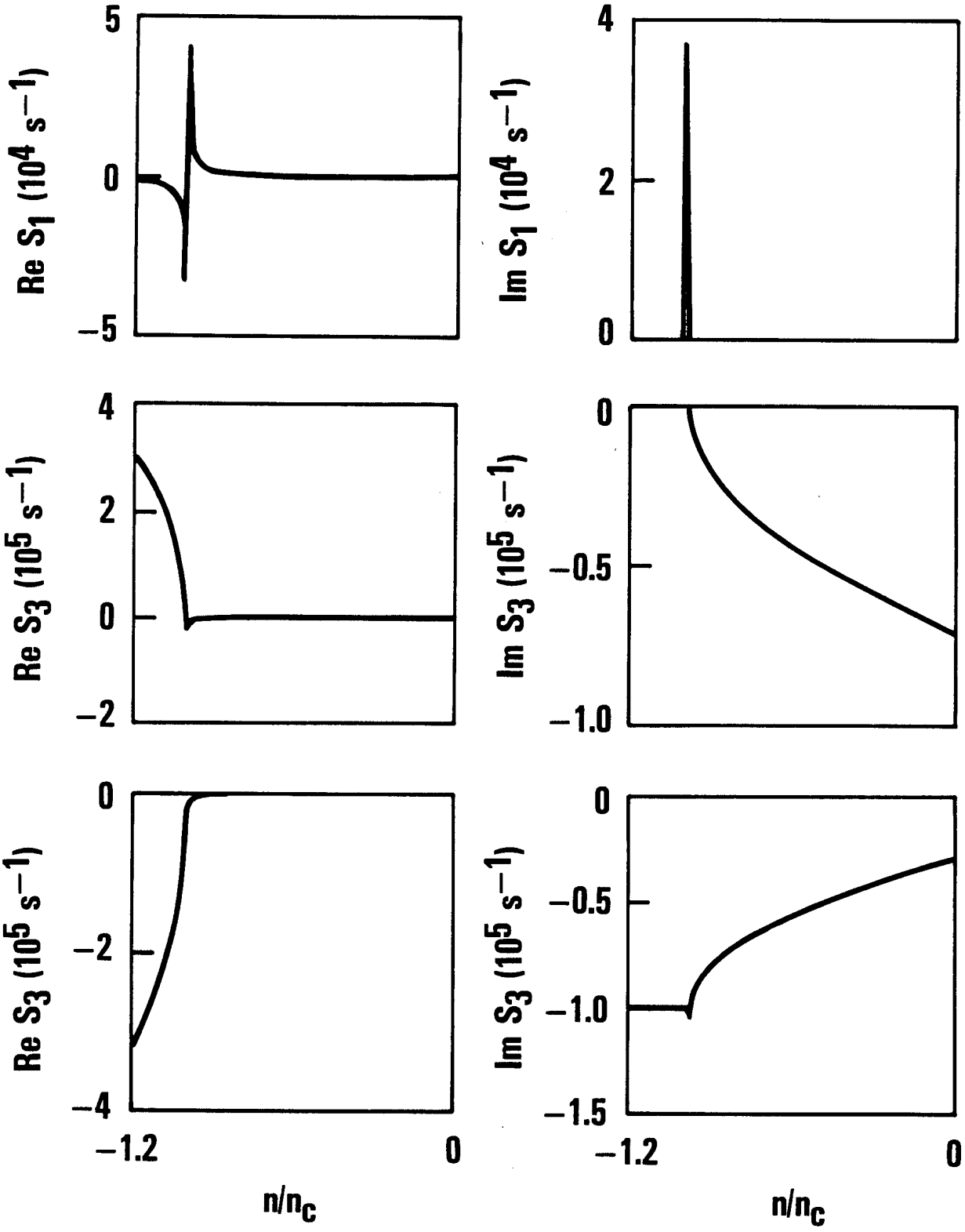

LAZARUS, et al. Fig. 5

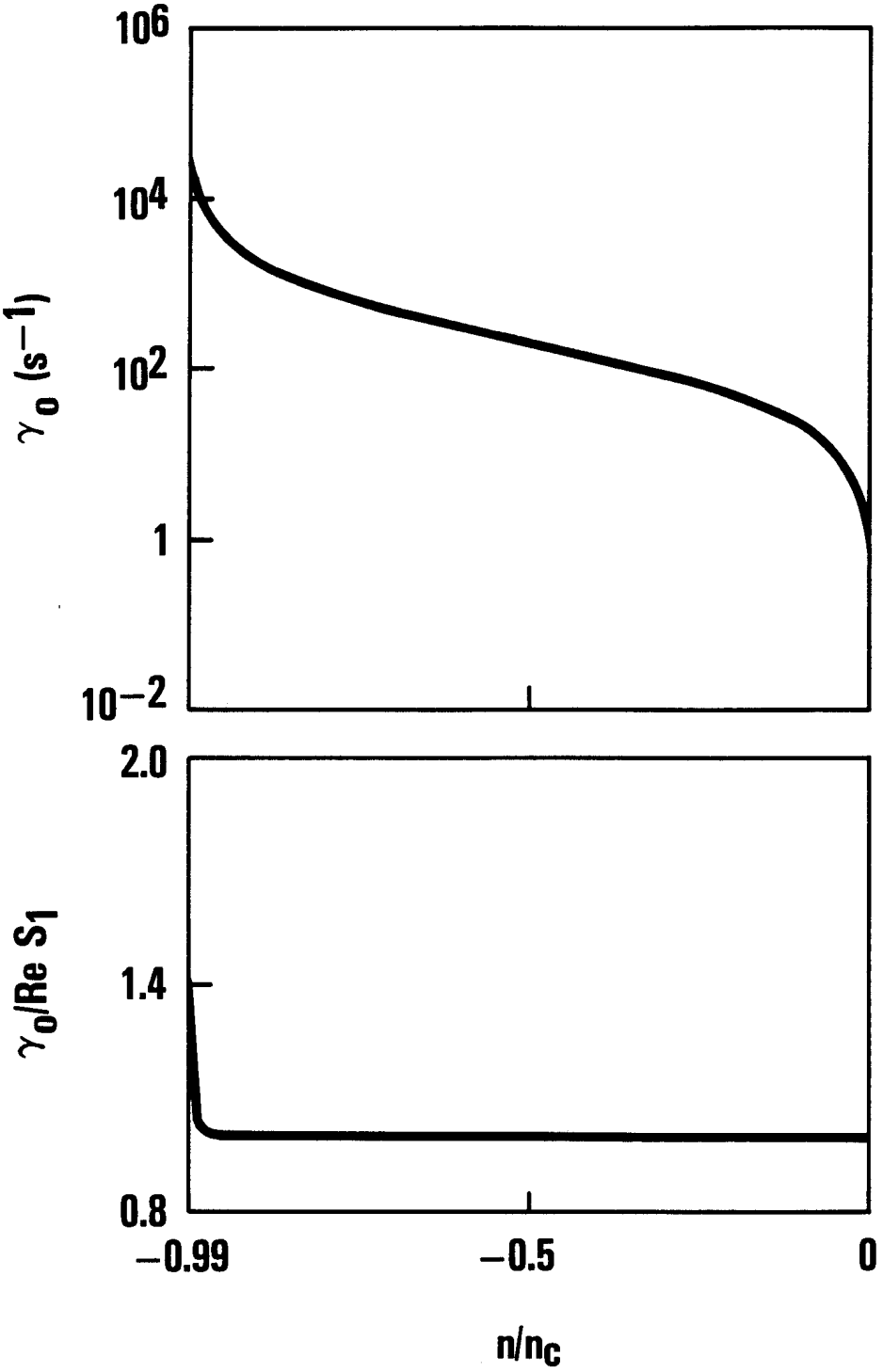

LAZARUS, et al. Fig. 6

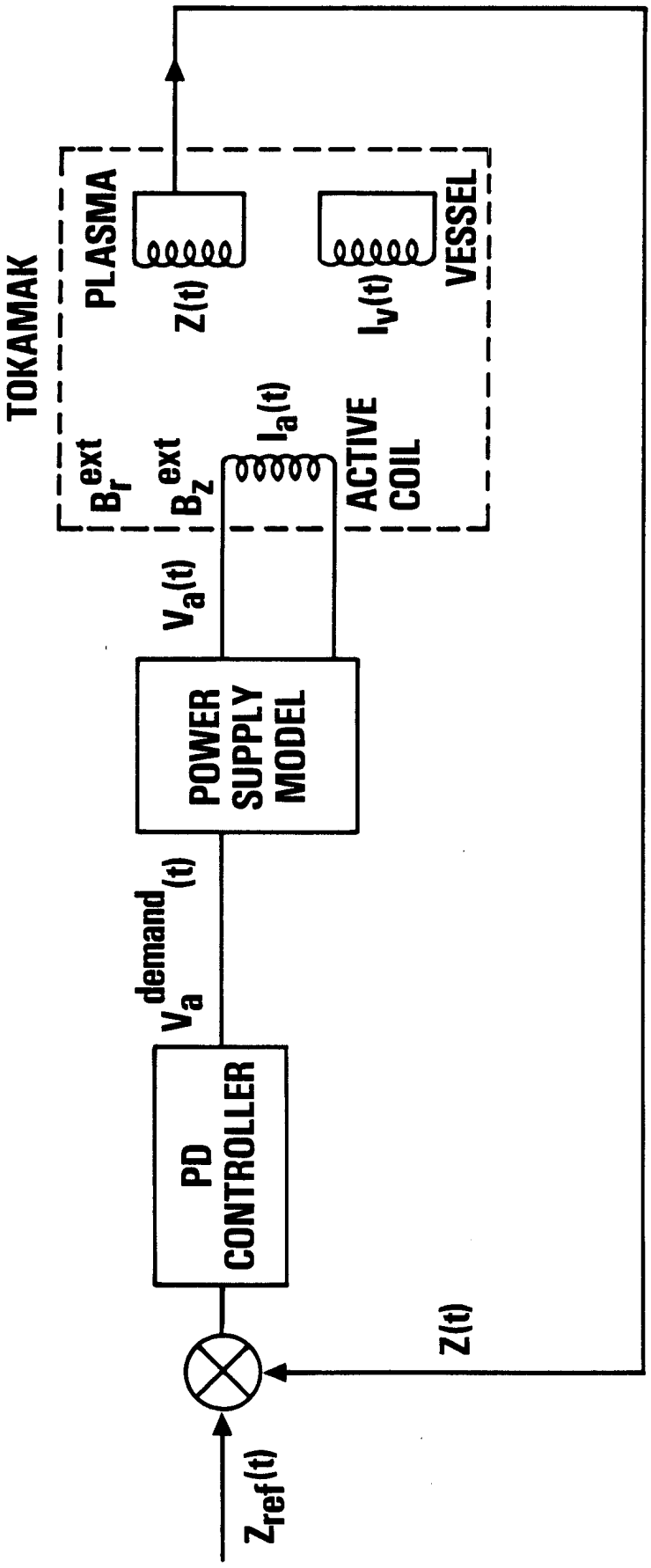

LAZARUS, et al. Fig. 7

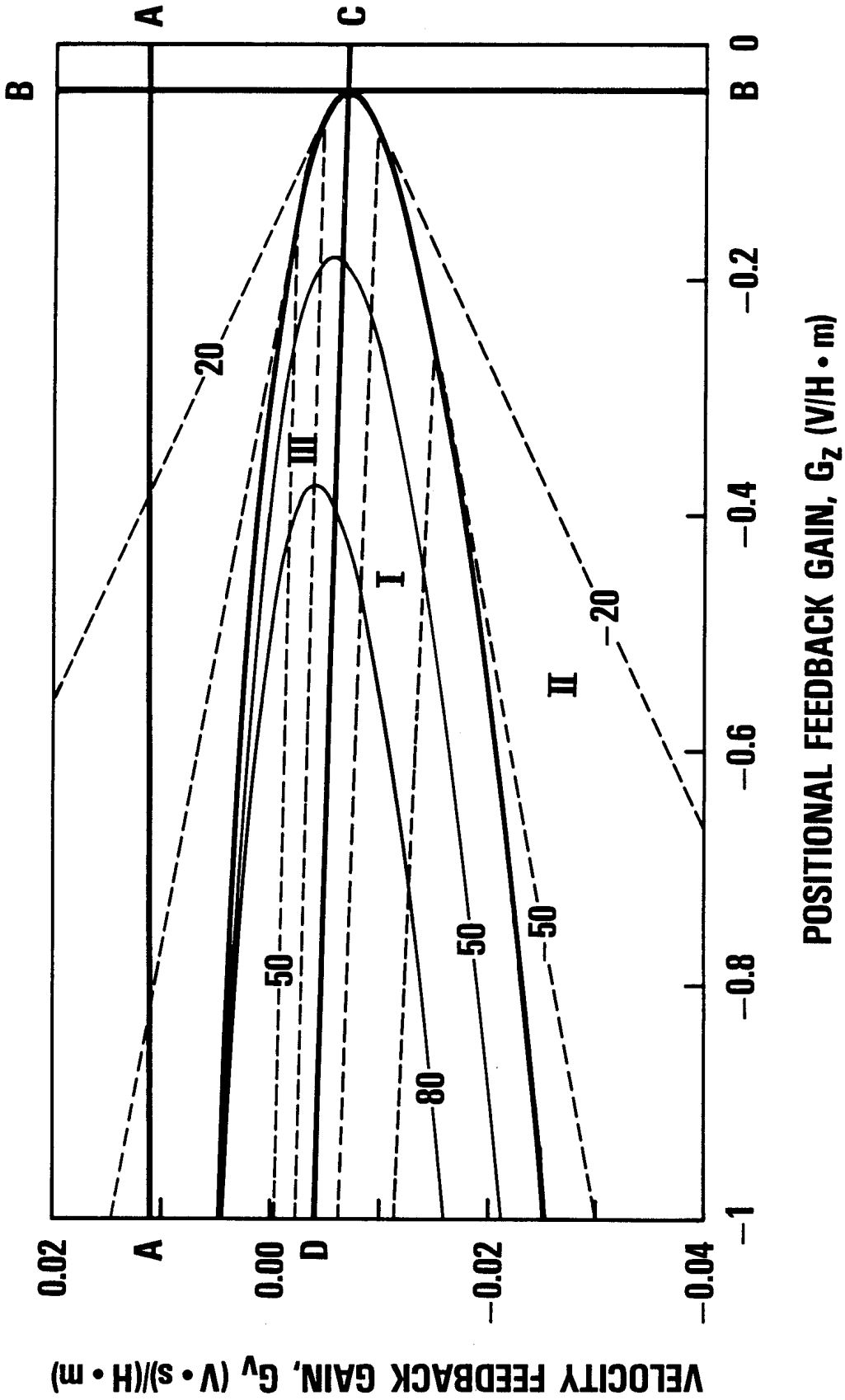

LAZARUS, et al. Fig. 8

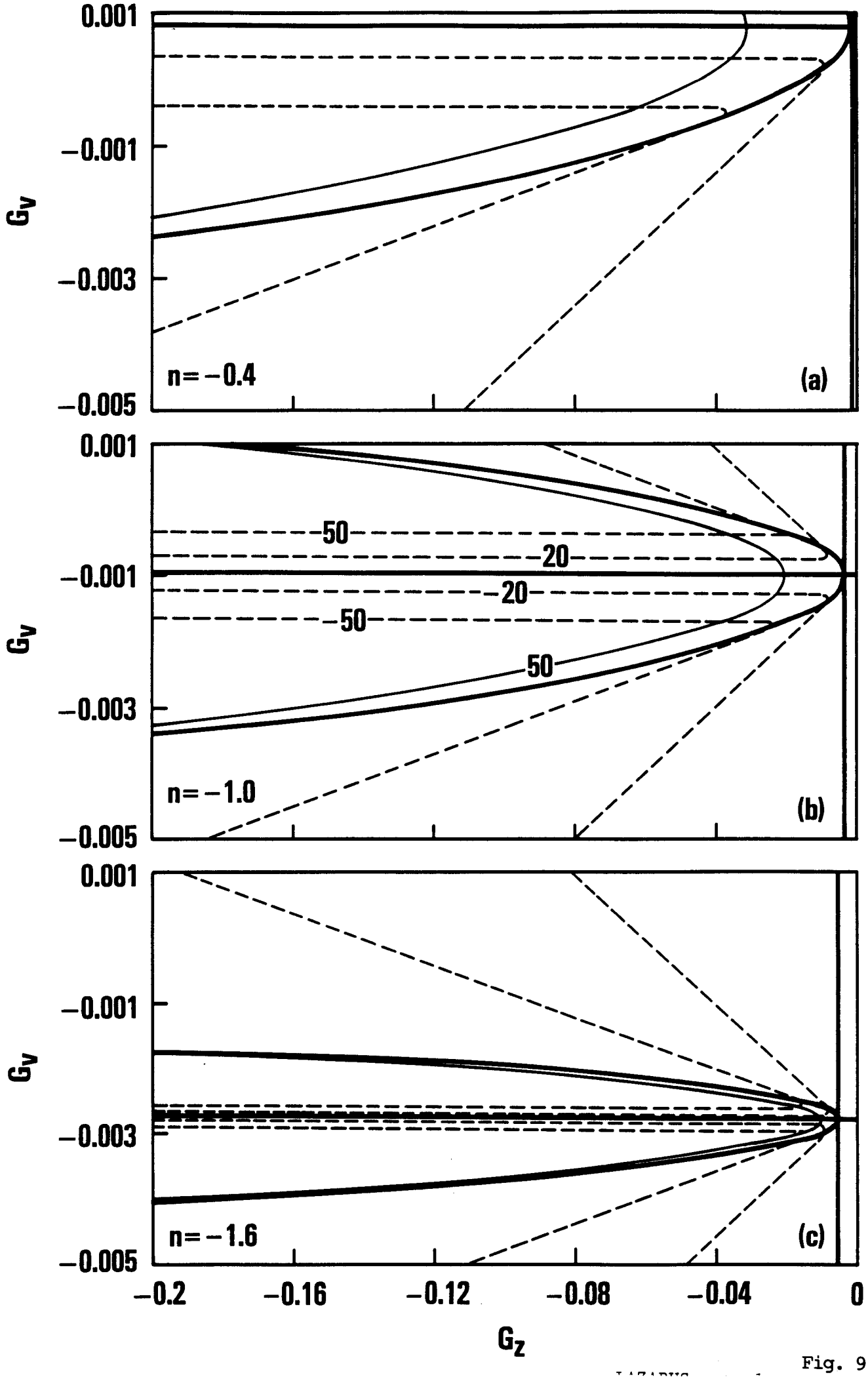
0.001
−0.001
−0.003
−0.005
G_V
n=−0.4
(a)
50
20
20
50
50
n=−1.0
(b)
n=−1.6
(c)
−0.2
−0.16
−0.12
−0.08
−0.04
0
G_Z

Fig. 9

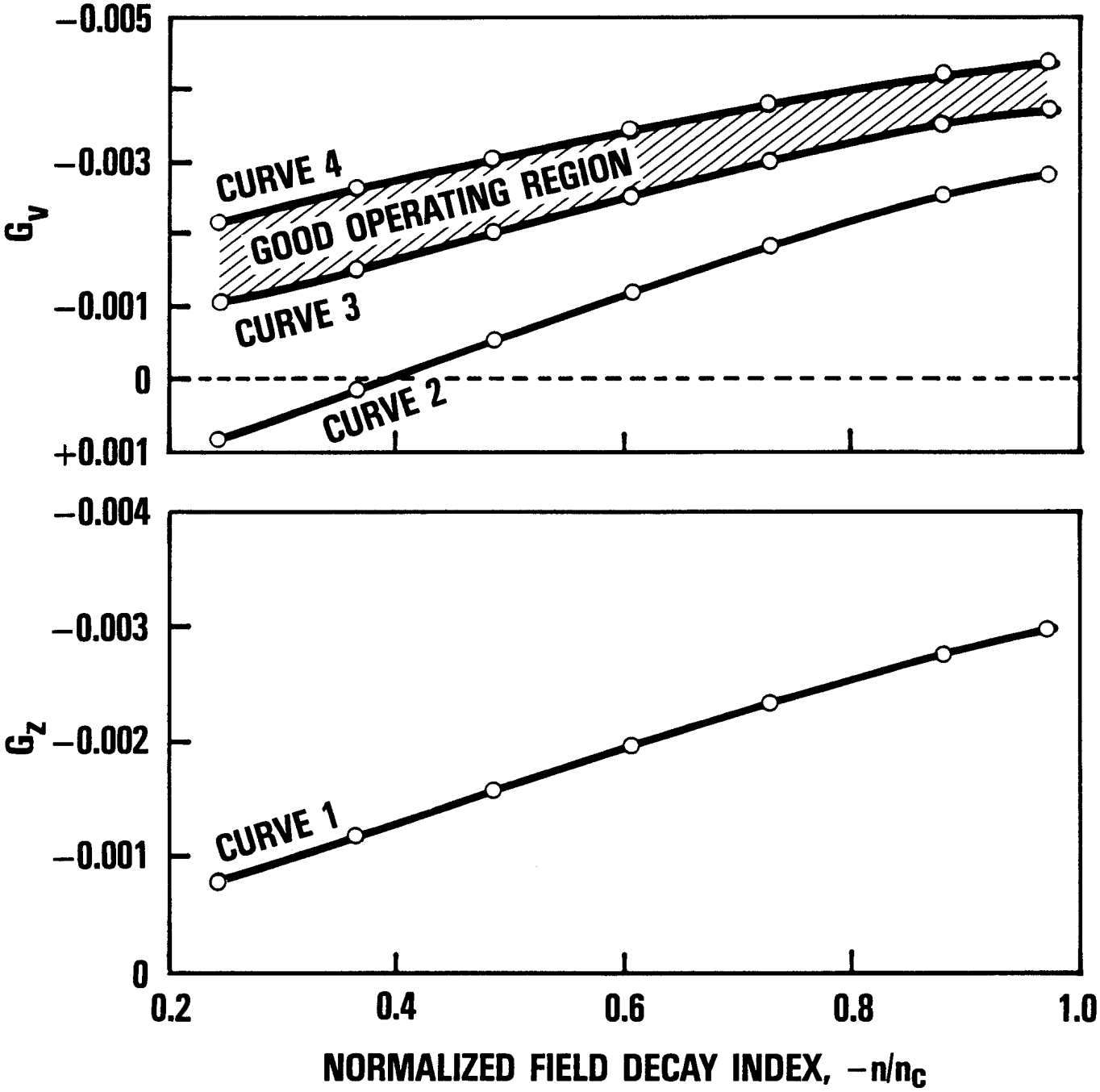

LAZARUS, et al. Fig. 1(

LAZARUS, et al. Fig. 1

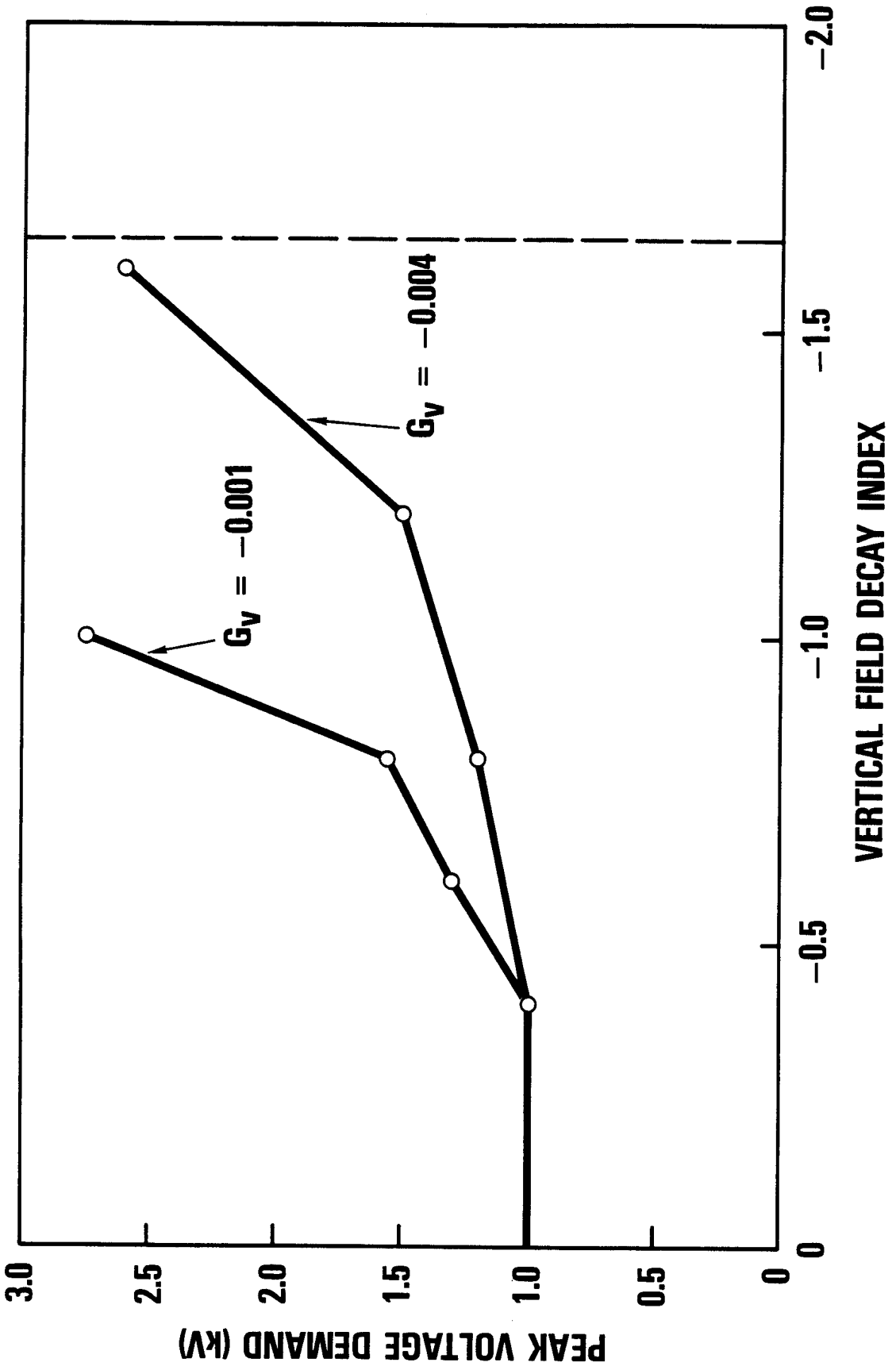

LAZARUS, et al. Fig. 12

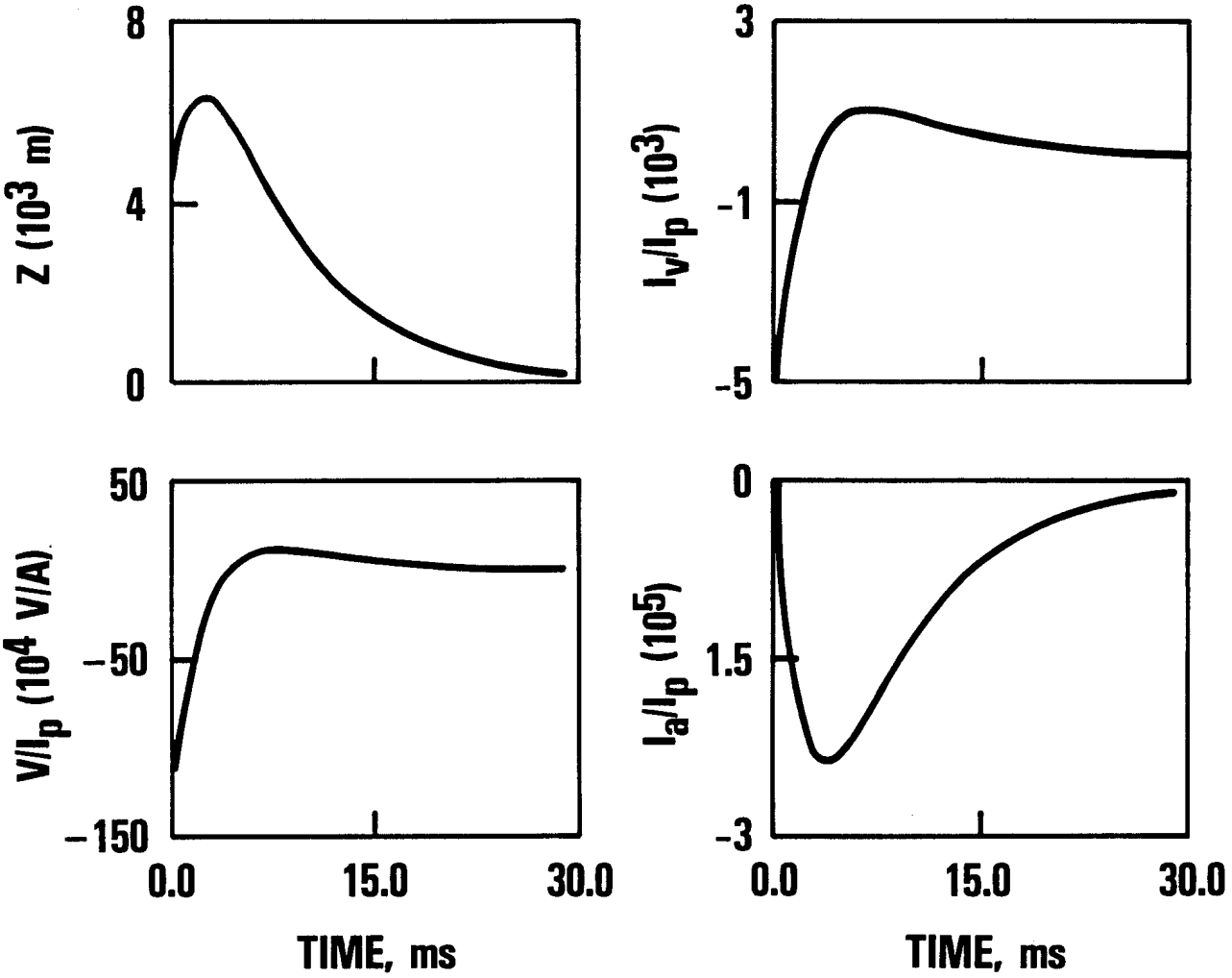

LAZARUS, et al. Fig. 13

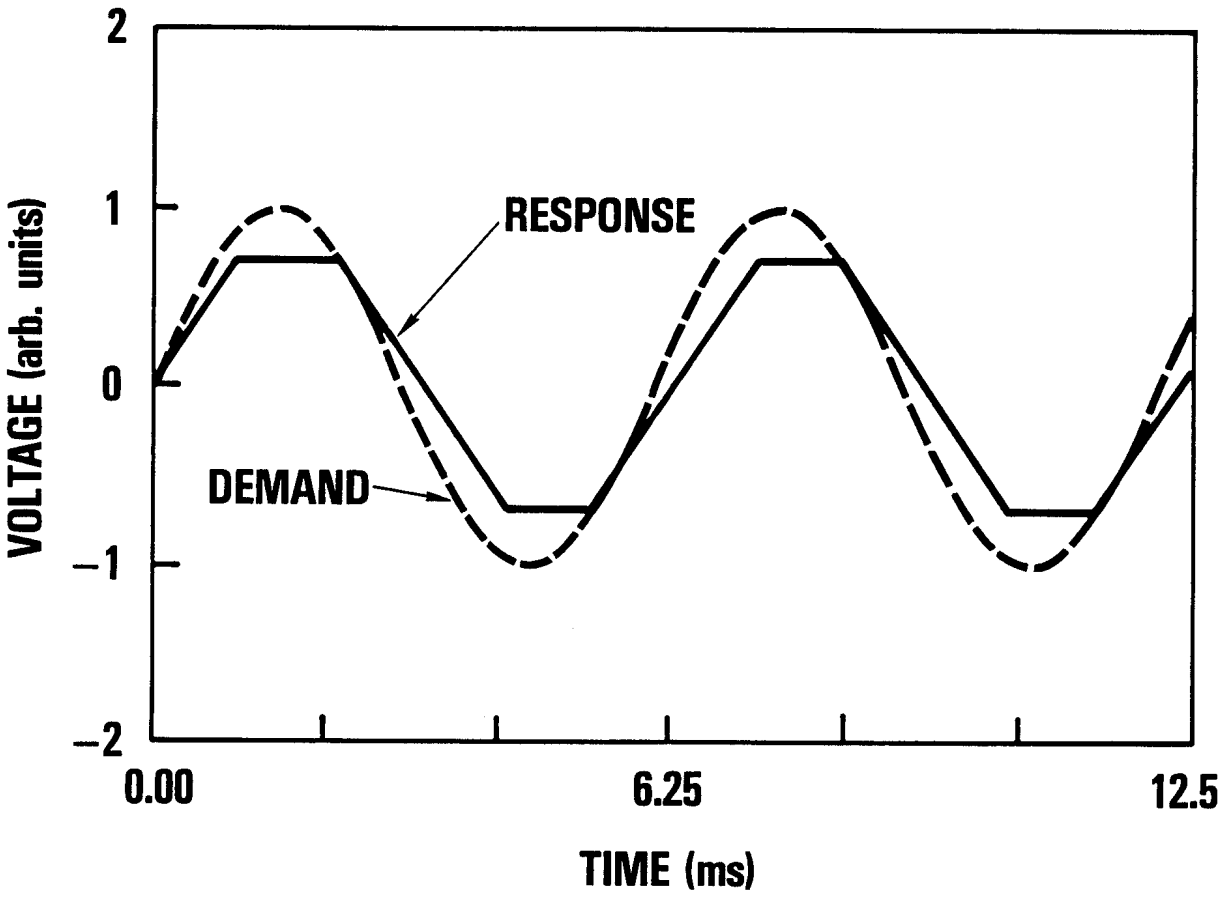

LAZARUS, et al. Fig. 14

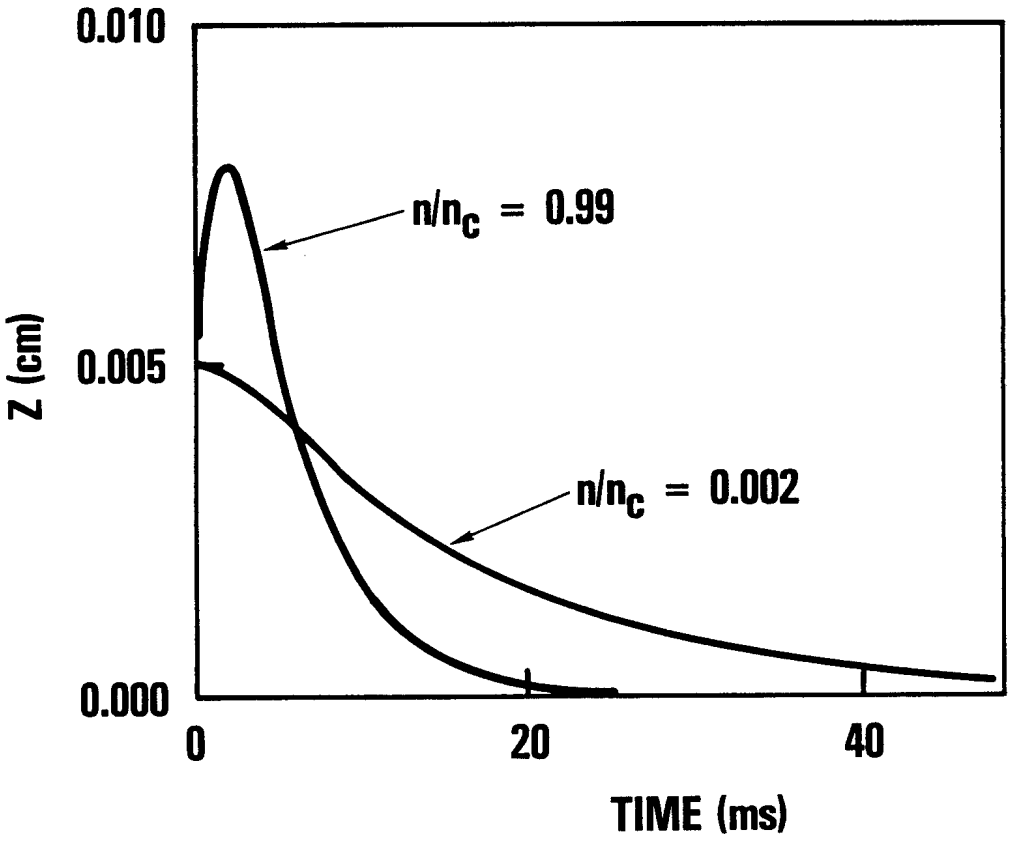

LAZARUS, et al. Fig. 15

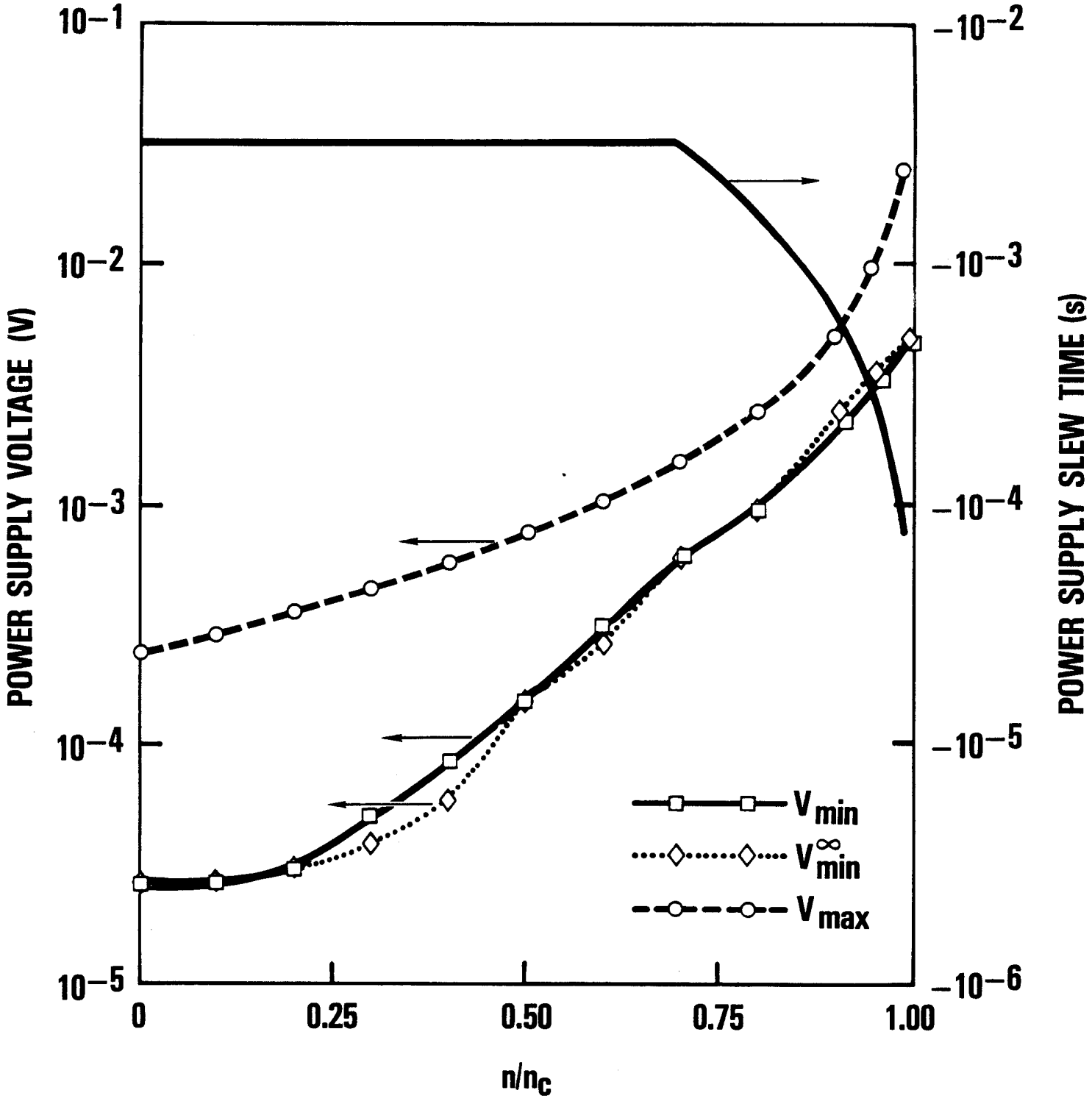

LAZARUS, et al. Fig. 16

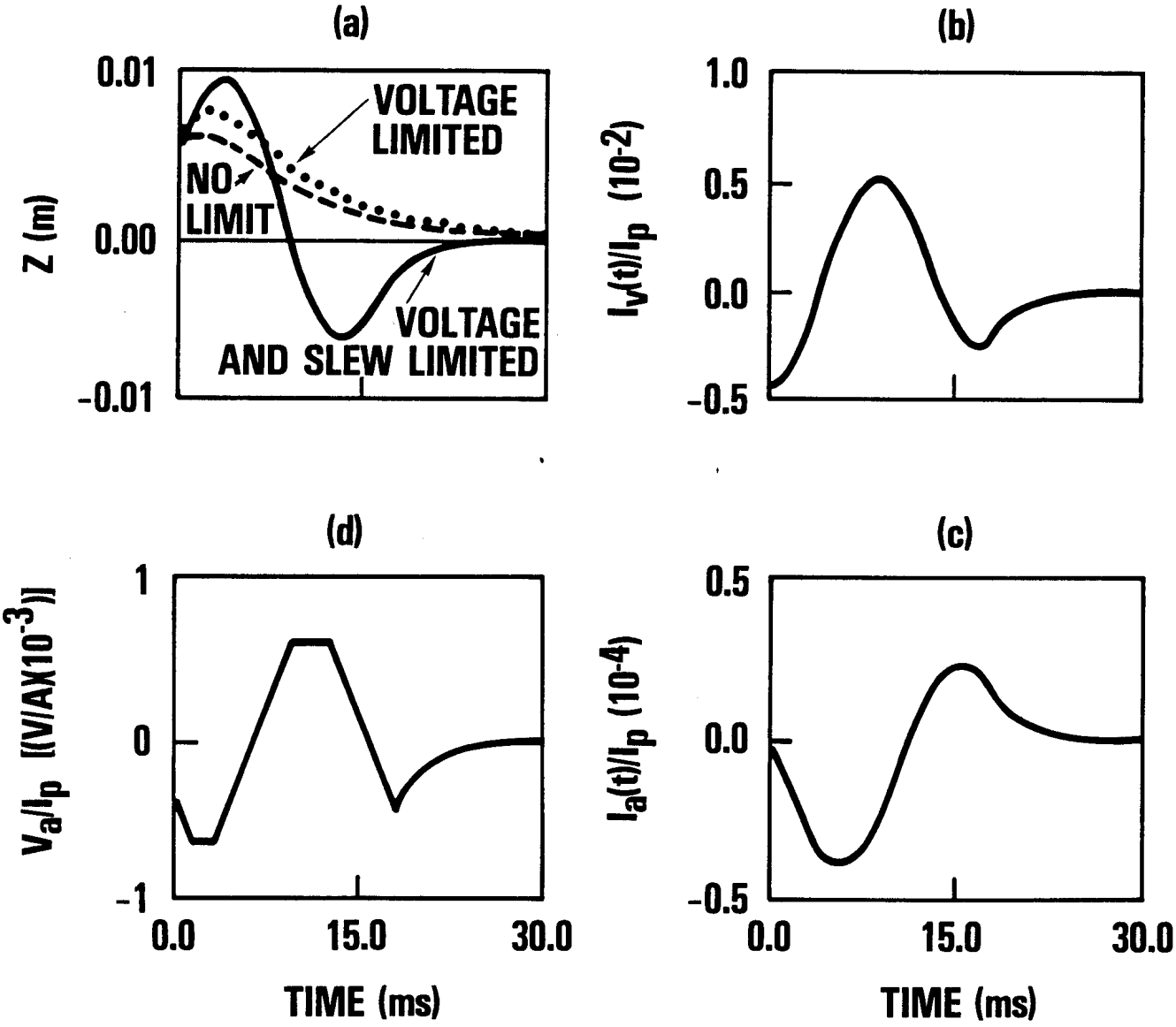

LAZARUS, et al. Fig. 17

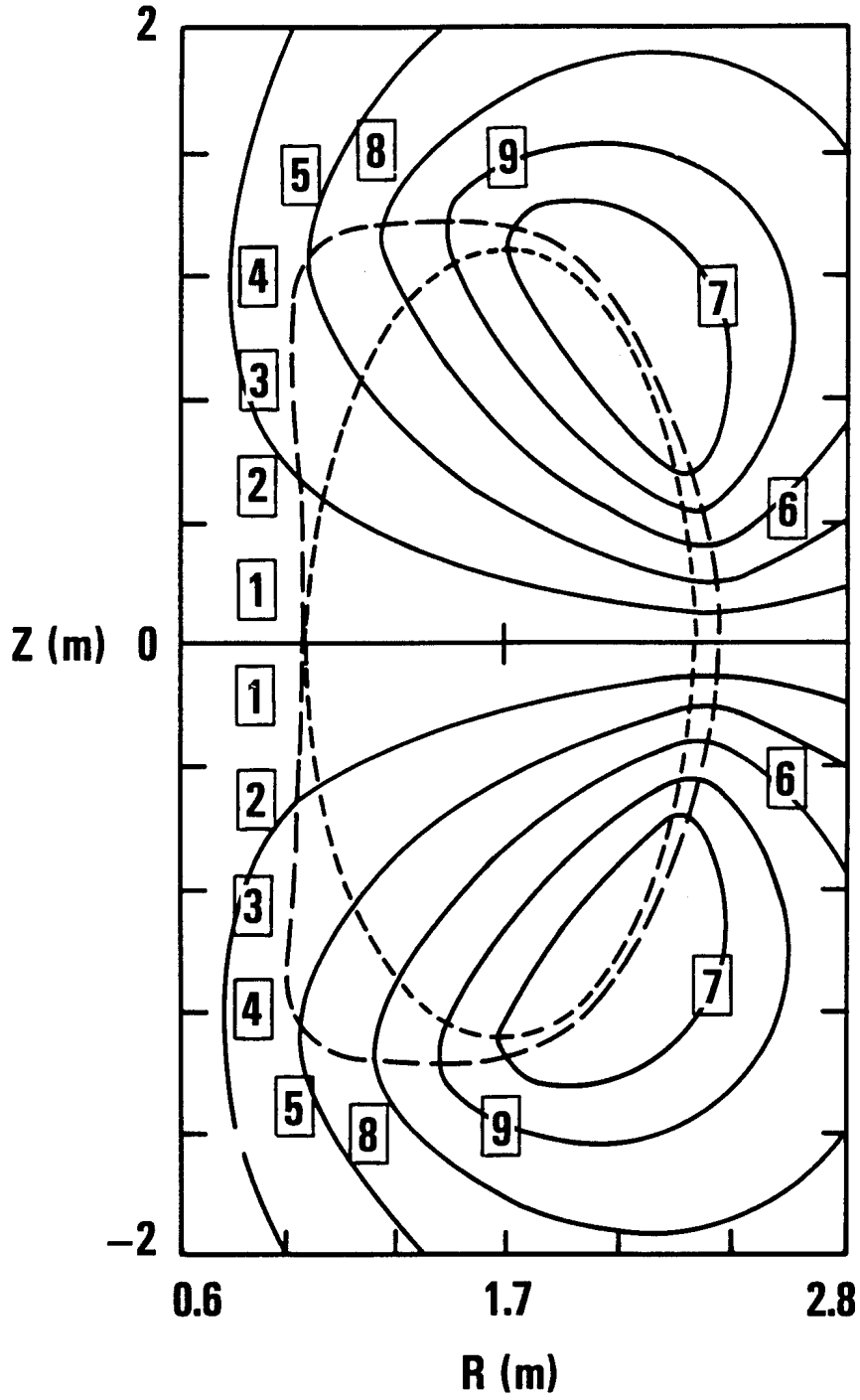

LAZARUS, et al. **Fig. 18**

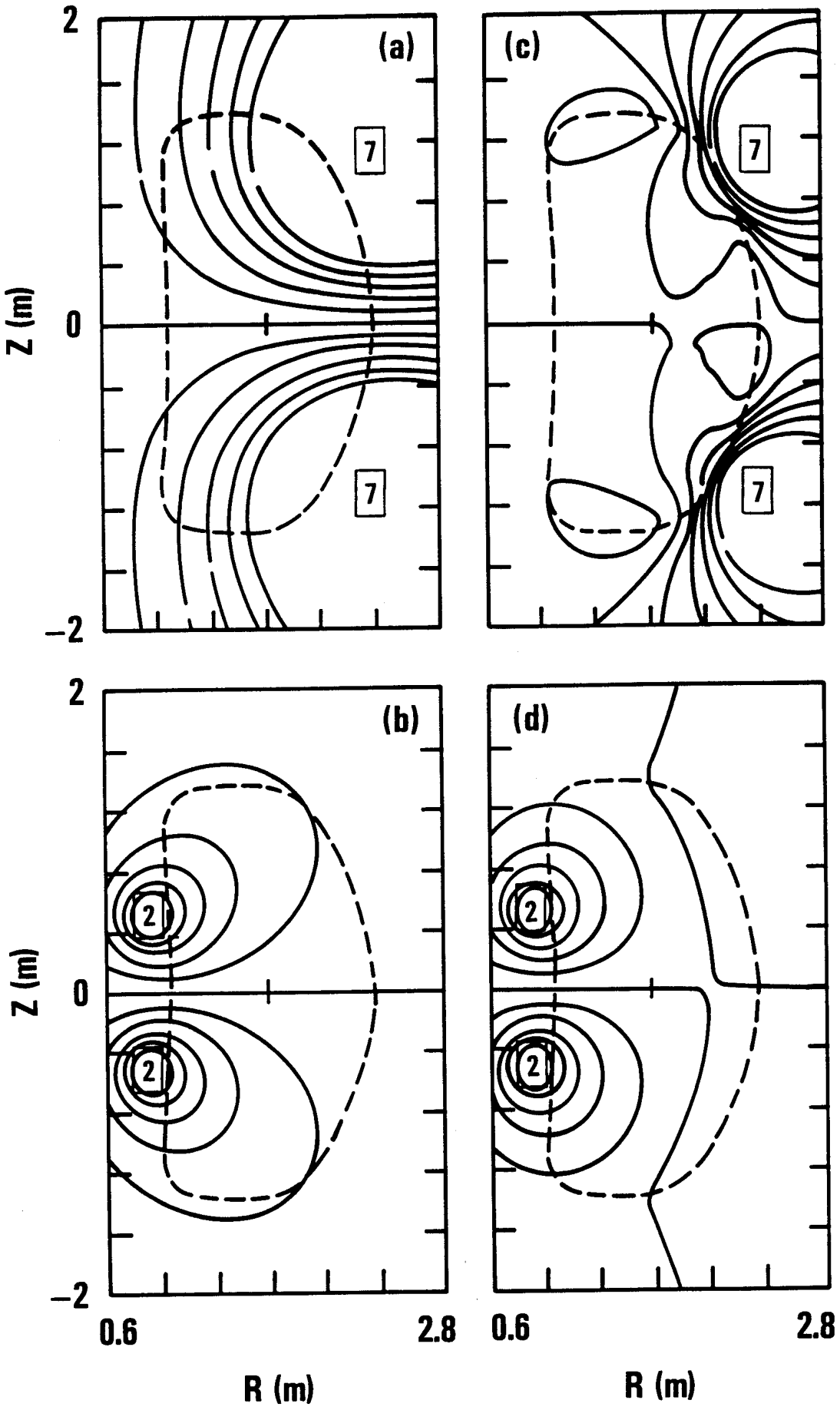

LAZARUS, et al. Fig. 19

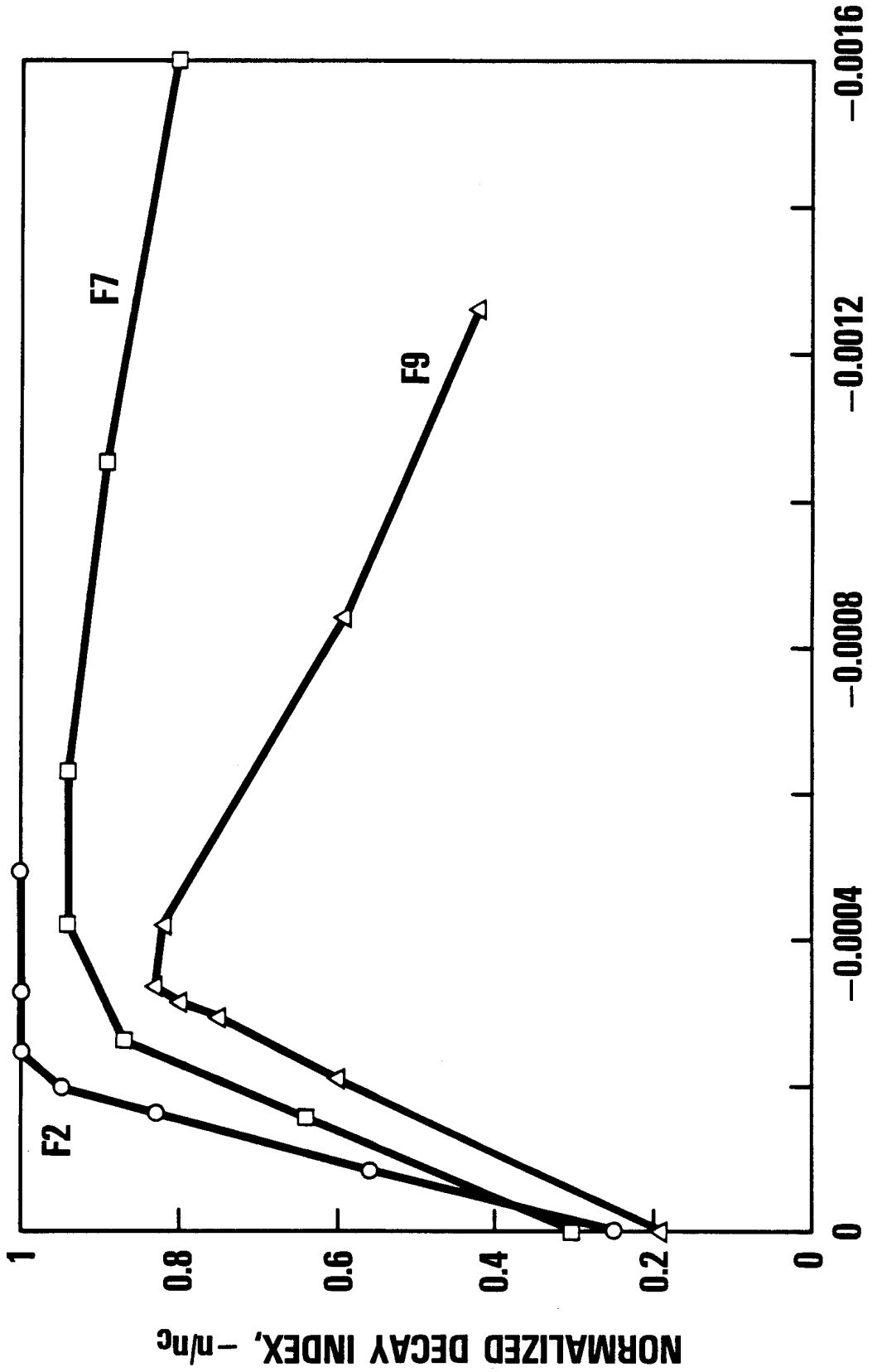

LAZARUS, et al. Fig. 20

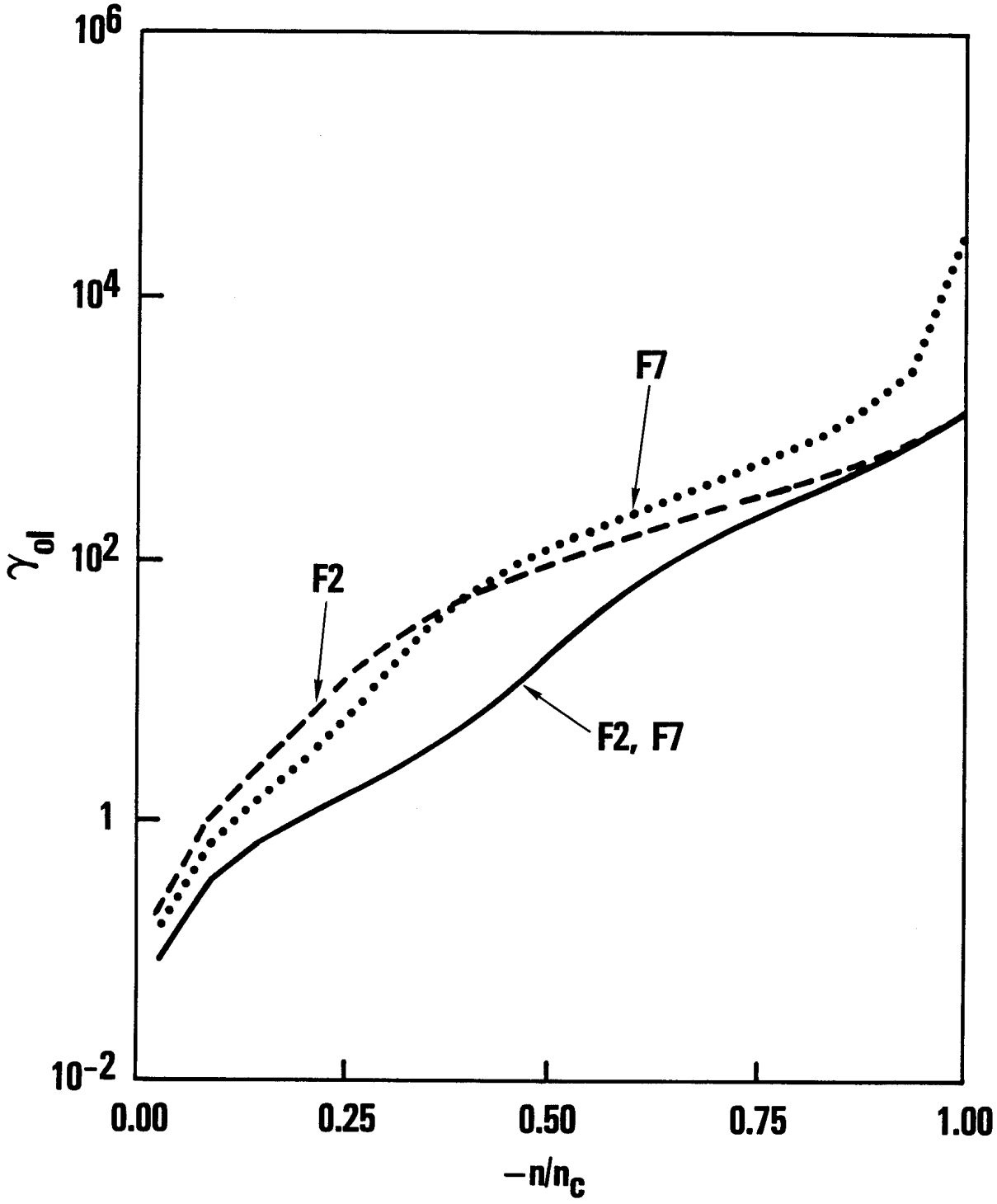

LAZARUS, et al. Fig. 21

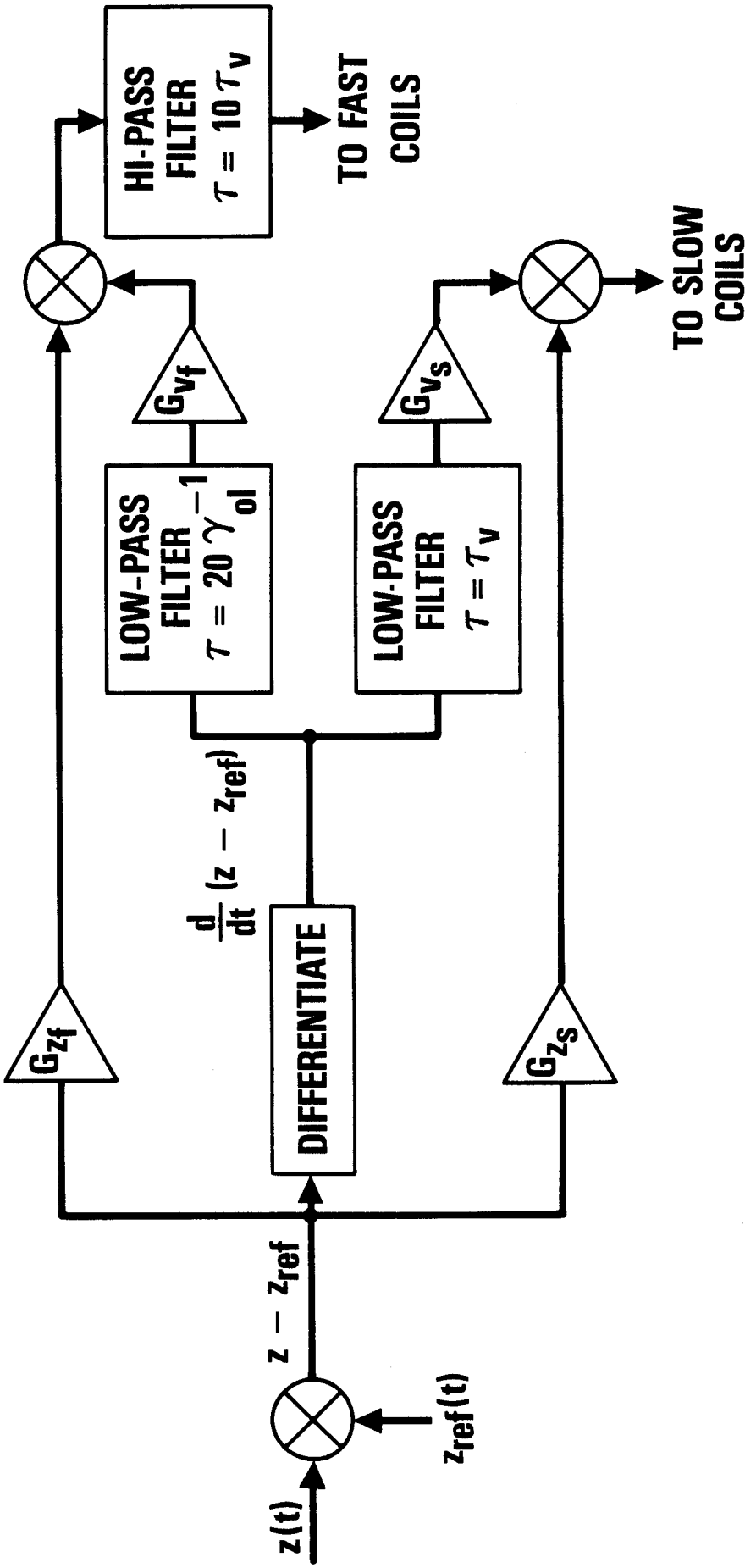

LAZARUS, et al. Fig. 22

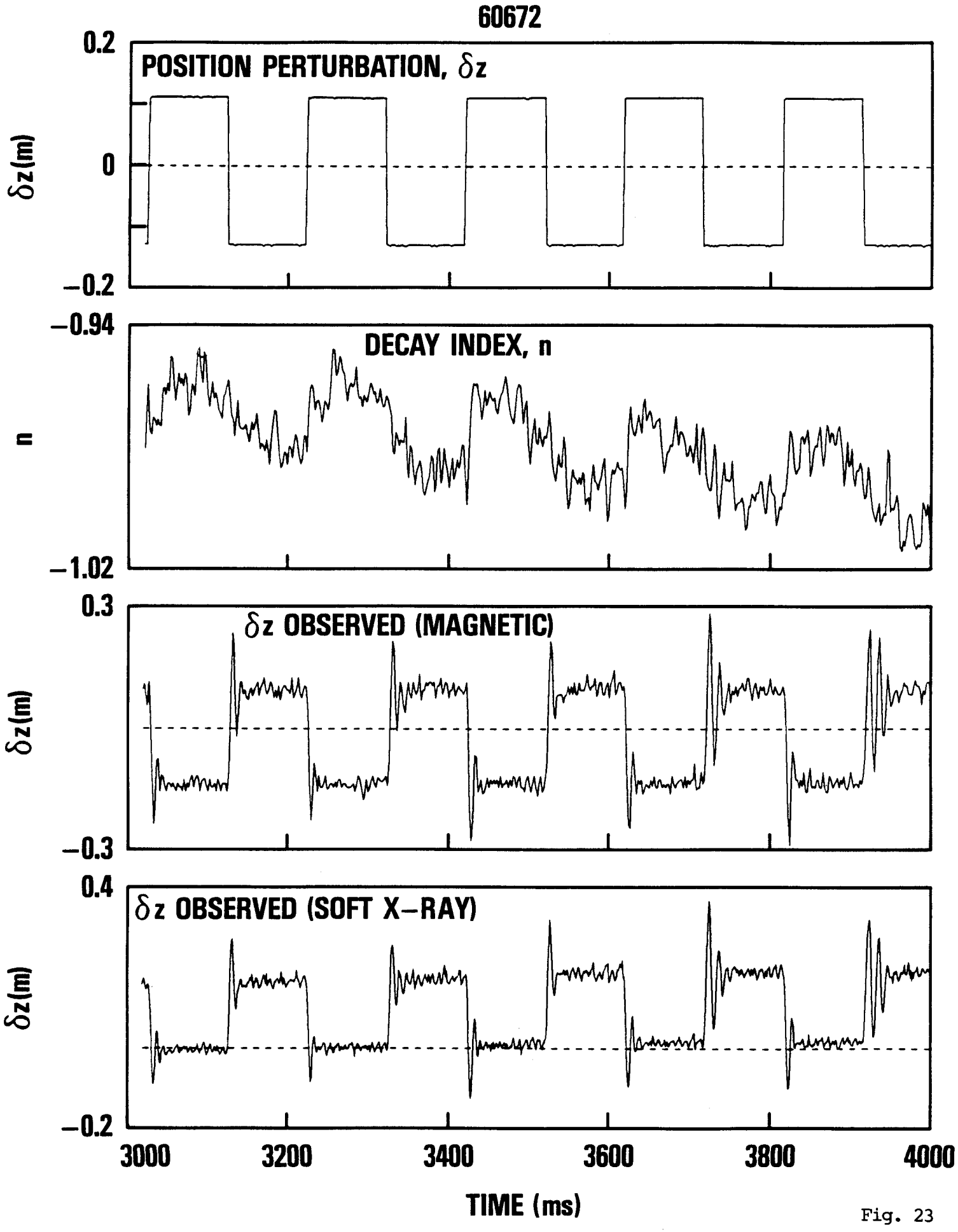
60672
POSITION PERTURBATION, δz
0.2
0
−0.2
δz(m)
DECAY INDEX, n
−0.94
−1.02
n
δz OBSERVED (MAGNETIC)
0.3
−0.3
δz(m)
δz OBSERVED (SOFT X−RAY)
0.4
−0.2
δz(m)
3000
3200
3400
3600
3800
4000
TIME (ms)

Fig. 23

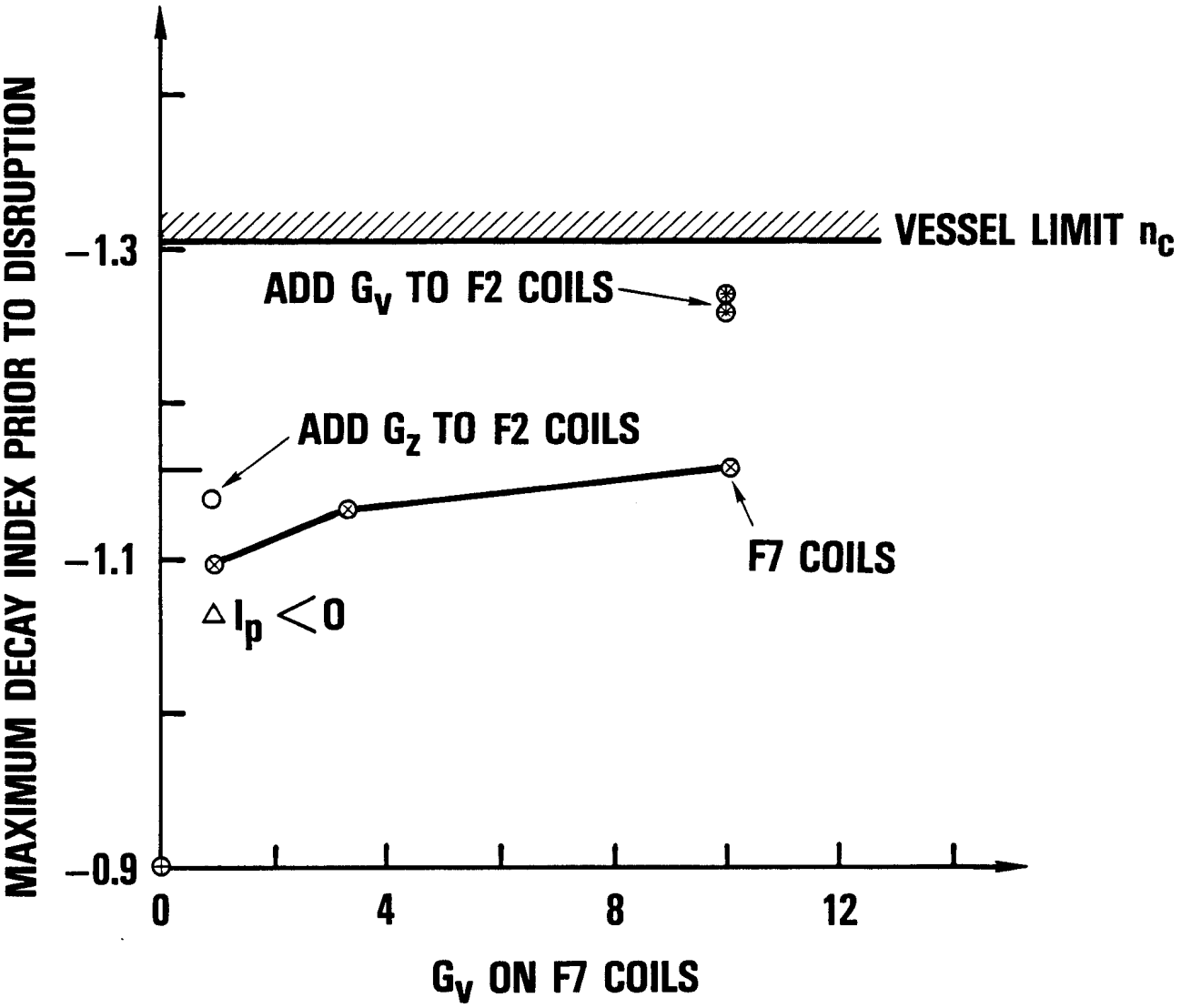

LAZARUS, et al. Fig. 24

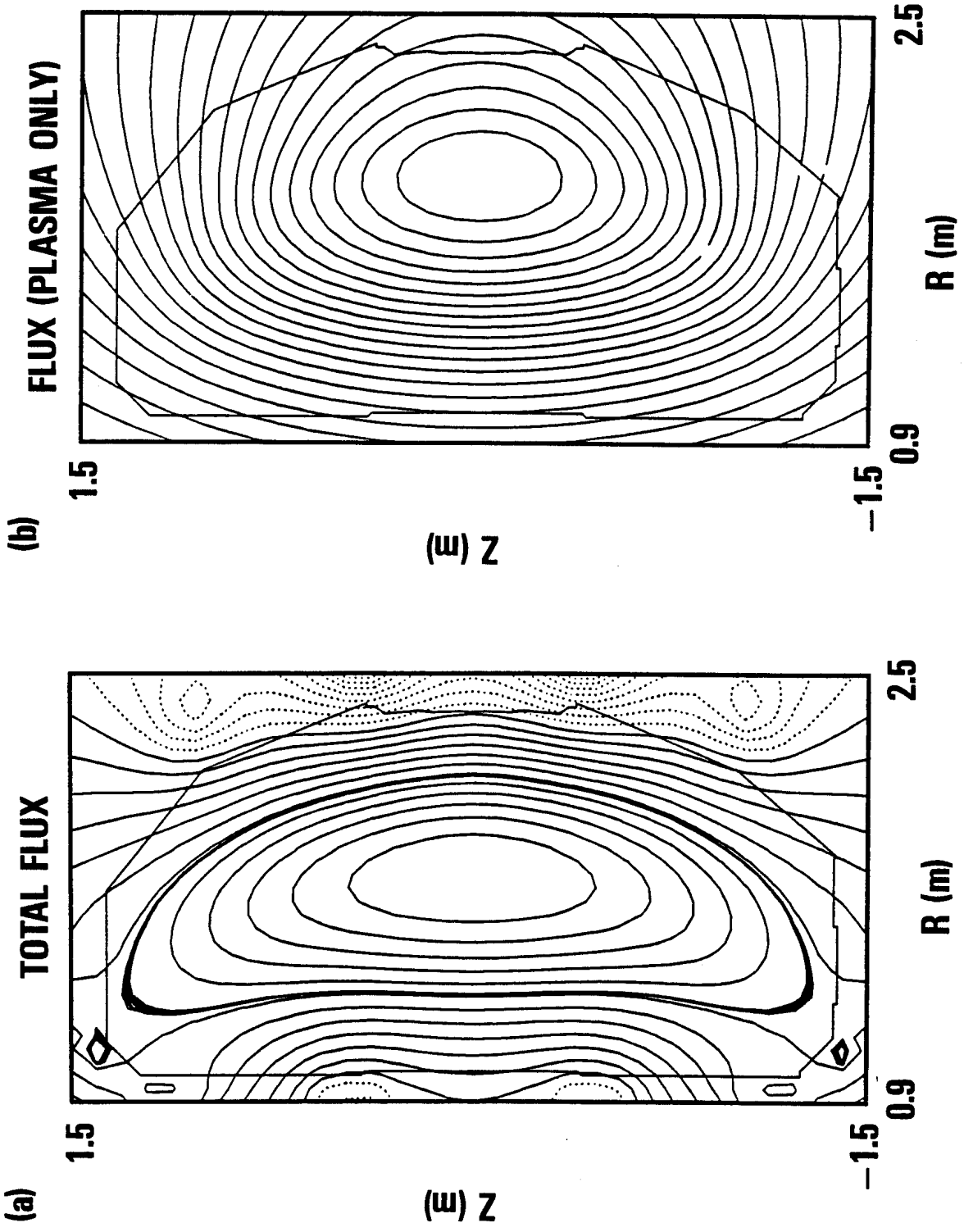

LAZARUS, et al. Fig. 25

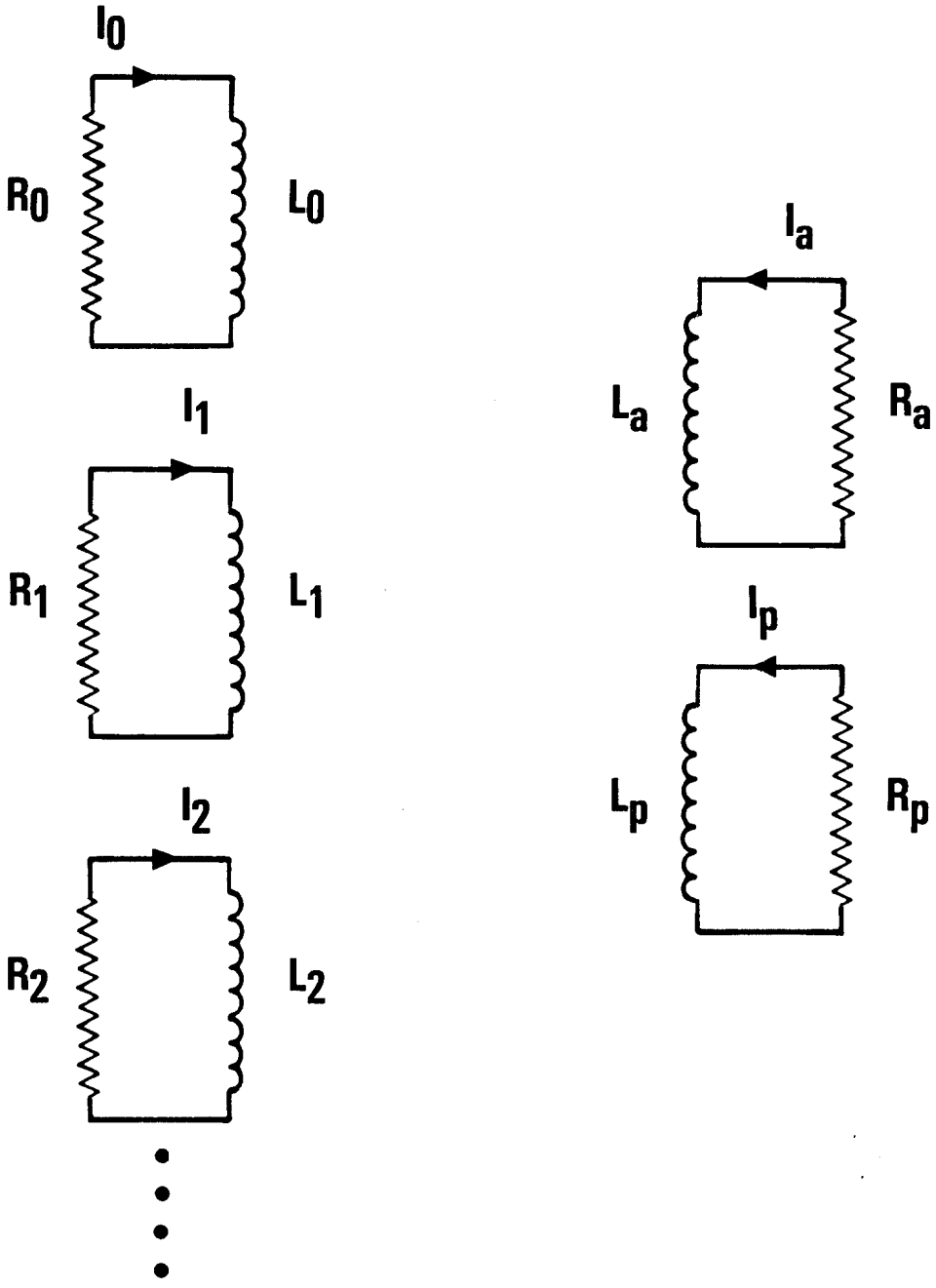

LAZARUS, et al. Fig. 26

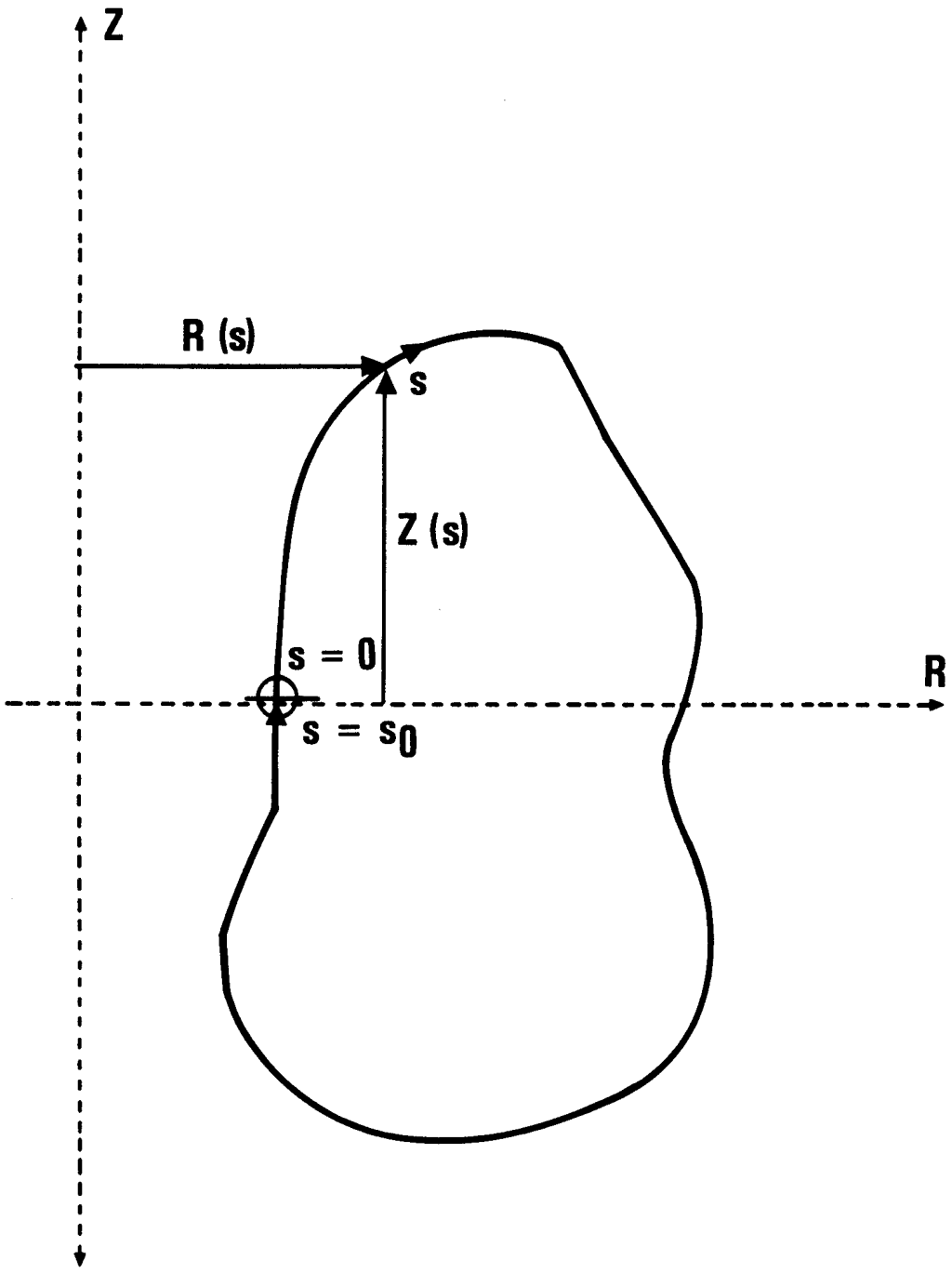

LAZARUS, et al. **Fig. 27**